STUDY OF THE REACTIVE DISTILLATION IN THE PRODUCTION OF ISOBUTYL ACETATE

Andrés Felipe Martínez Arias

Universidad Nacional de Colombia

Facultad de Ingeniería, Departamento de Ingeniería Química y Ambiental.

Bogota, Colombia

2020

STUDY OF THE REACTIVE DISTILLATION IN THE PRODUCTION OF ISOBUTYL ACETATE

Andrés Felipe Martínez Arias

Research Thesis Presented as a Partial Requirement to apply for the title of:

Master in Chemical Engineering

Director:

Ph.D. Gerardo Rodríguez Niño

Codirector:

Ph.D. Alvaro Orjuela Londoño

Area of research:

Biorefineries and Biofuels

Investigation Group:

Chemical and Biochemical Processes Group

Universidad Nacional de Colombia

Facultad de Ingeniería, Departamento de Ingeniería Química y Ambiental.

Bogota, Colombia

2020

ACKNOWLEDGMENTS

Special thanks to Professor Alvaro Orjuela, Professor Gerardo Rodrigues and Professor Cesar Sanchez for their constant support, their guidance and specially their friendship. Special thanks to all the members of the Chemical and Biochemical Processes Research Group for their advisor, especially to Dr. Ivan Gil and Dr. Julio Vargas and my partners Jesus Jaime, Sergio Lopez, Andres Herrera, Jesus Quintero, Sebastian Rodriguez and Andrea Suaza, and the chemical engineering laboratory staff specially laboratorist Ricardo Cortez.

This work is to my parents who teach me to work hard and to love the National University, the best university of Colombia.

ABSTRACT

This work presents a study of a reactive distillation process for the production of Isobutyl acetate, from the fundamentals of the operation like the phase equilibria and the reaction kinetics, to the conceptual design. Experimental phase equilibrium data was evaluated, and the quaternary mixture interactions were accurately described using an activity coefficients model for the liquid phase, and a viral equation of state for the vapor phase as described in Chapter one. In Chapter two a mole-based kinetic expression was adjusted to describe the esterification process using an heterogeneous catalyst. Then, a conceptual design of the reactive distillation process, coupling the phase equilibria and the reaction kinetics, was done in order to obtain a suitable configuration for an industrial scale process to produce Isobutyl acetate. Finally, rigorous simulations and optimization enabled to obtain the best operating conditions of the reactive distillation process for isobutyl acetate production at the industrial scale presented in Chapter three.

Resumen:

Este trabajo presenta un estudio del proceso de producción de Isobutil acetato por medio de destilación reactiva, desde los fundamentos de la operación como el equilibrio de fases y la cinética de reacción, hasta el diseño conceptual. Se evaluó información experimental del equilibrio de fases y las interacciones de la mezcla cuaternaria se describieron adecuadamente usando un modelo de coeficientes de actividad para la fase liquida y una ecuación de estado para la fase vapor. Una expresión cinética con base en fracciones molares fue desarrollada para describir el proceso de esterificación usando un catalizador heterogéneo. Posteriormente, se desarrolló el diseño conceptual del proceso de destilación reactiva empleando simultáneamente el equilibrio de fases y la cinética previamente obtenidos. Finalmente, con base en simulación rigurosa y optimización del proceso de destilación reactiva se obtuvieron las condiciones de operación masa adecuadas para la producción de Isobutil acetato por destilación reactiva a escala industria

Table of Content

List of Tables

List of Figures

INTRODUCTION

A new trend has being taking over the chemical industry during last years due to the need for substituting fossil resources as main feedstocks. This is driven by the scarcity and volatile prices of crude oil, and also by the public awareness about the non-renewable origin and environmental impacts of fossil-based consumer goods. This has pressured a global transition movement from traditional chemical products toward renewable ones. This pressure, also promoted by regulating policies implemented during last years (e.g. REACH in Europe and TSCA amended by Lautenberg Chemical Safety Act in USA), have boosted the implementation of the biorefinery production model. In some cases, this model has been developed around the production of certain platform molecules, and their subsequent transformation into a large variety of value added products.

Among the variety of fossil-based chemicals that have been severely scrutinized, the organic solvents standout because their large impacts. Solvents are used in massive volumes worldwide, in a variety of processes, and in numerous consumer products (e.g. paints, coatings, inks, household, personal care, and clean products, etc.). A large fraction of these chemicals is released to the environment during or after use, generating large economic and environmental impacts. Because of this, this industry segment has embraced the renewable trend introducing into the market a variety of green biobased alternative. Nowadays, green solvents have reached a production volume of nearly 20 million metrics tons in 2018 (i.e. $8 billion dollars), with a growing trend (International Trade Center, 2018).

In this direction, among the variety of industrial solvents, different biobased alcohols and esters has been successfully implemented as direct and functional substitutes of fossil-based ones. These types of compounds can be obtained from renewable resources by mean of different thermochemical, catalytic and microbial pathways. Within this group, isobutanol and isobutyl acetate stand out as main solvents of industrial interest, and they have been identified as potential platform molecules to be exploited in current and future biorefineries. Currently, isobutanol is mainly produced from petrochemical feedstock by using the “oxo” process. Also, it is known the presence of isobutanol as a main byproduct of the ethanolic fermentation of saccharides using *Saccharomyces cerevisiae*. In this case, isobutanol is obtained as a

main component of fusel oil; a side stream obtained during bioethanol distillation. Fusel oil is also an important source of other potential biobased molecules and platforms for biorefineries like Isoamyl alcohol. By 2018, the Isobutanol market was nearly 360 kt and it is mainly used in coatings, paints, fuels and as precursor for the production of commodity and specialty chemicals (Moncada et al. 2018). Among the most important isobutanol derivatives, biobased isobutyl acetate is considered a major green solvent for the chemical industry. This acetate is widely used in paintings, inks, coatings and cosmetics, and also as odor ingredient for the flavoring and fragrance industry. This isobutanol-derived solvent is highly desired because of its biodegradability, low water solubility, low surface tension, high electrical resistance, and because it complies with REACH regulations.

Isobutyl acetate is a product that belongs to the family of aliphatic esters produced from acetic acid, which are characterized by its fruity and natural aroma easily perceived, high volatility, by having a carboxylic functional group, and by not forming hydrogen bonds. Isobutyl acetate (IbAC) is generally produced via Fisher esterification between Acetic Acid (ACAC) and isobutanol (IbOH), generating water (W) as by product. Industrial isobutyl acetate is usually produced under batch operation, either using a reactor followed several distillation steps, or by using a reactor coupled to a distillation column with top decanter. These configurations intend to remove water during the process, to refine the acetate product, and to recover the excess of isobutanol used during reaction for further recycle. These approaches have the disadvantage of using less efficient batch operating policies, and it is also a highly energy intensive process.

Alternatively, different intensified processes have been tested to enhance reaction yields in Isobutyl acetate synthesis via esterification. These include extractive distillation, reactive distillation (i.e. via transesterification), pervaporation, pressure swinging distillation, and reactive dividing wall column. Particularly, reactive distillation has been successfully implemented in similar esterification systems for acetates production. In this regard, continuous reactive distillation (RD) seems suitable for a more cost-effective operation.

Disregarding the intensification approach, and for process design purposes, there is need for a comprehensive characterization and modeling of phase equilibria of the system. The IbOH+ACAC+W+IbAC mixture is highly non-ideal, exhibiting several azeotropes, partial miscibility in the liquid phase, and dimerization of the acid in the vapor phase, and an adequate phase equilibrium model is not available to model all these interactions. On the other hand, the esterification reaction is limited by the

chemical equilibrium, and it requires a catalyst to be economically feasible. Industrially, esterification of Isobutanol with acetic acid is mainly promoted by acid homogeneous catalysts such us sulfuric acid. Nevertheless, due to the potential of Isobutyl acetate for fragrance and flavor applications where a specific sensory profile is desired, heterogeneous catalysts such as ion exchange resins are preferred. This occurs because common mineral acids can affect the organoleptic properties of isobutyl acetate, promote equipment corrosion and its disposal is more complex. Therefore, it is also necessary to obtain a validated kinetic model to accurately describe reaction progression, and to develop an intensified process to enhance isobutyl acetate production.

Among the above-mentioned intensified processes for isobutyl acetate production via esterification, reactive distillation stands out as an energy efficient and less material-intensive alternative. This process couples reaction and separation stages into one single unit, thus reducing energy duty and improving reaction conversion. Among other reasons, this occurs by selective product removal, the harnessing of heat of reaction during distillation, and by reacting away the azeotropic mixtures. All these advantages turn into capital and operating costs reduction. Nevertheless, as this process has not been explored, it is necessary to assess its feasibility at the industrial scale. Also, there is need to stablish the best process configuration and operating conditions to ensure effective Isobutyl acetate in the RD process.

In this direction, this work focuses on the study of a reactive distillation process to obtain isobutyl acetate based upon a deep understanding the fundamentals of the operation. In the first part, a complete and adequate phase equilibrium model suitable for process modeling is developed. This is done based upon experimental evaluation of phase equilibria and from previously published data as presented in chapter 1. Afterwards, a validated kinetic model is developed using a heterogeneous commercial catalyst, and this is described in chapter 2. Finally, in chapter 3, a conceptual design is carried out by using shortcut design methods, and a further rigorous simulation and optimization is carried out to define RD processing conditions. Specifications of the process are defined according to commercial product requirements and the production capacity corresponds to an industrial scale facility. Results indicate that urethane-grade isobutyl acetate can be obtained as product from a reactive distillation column, and the process can be economically implemented at the industrial scale.

Specific and novel results of this work are:

- Experimental evaluation of liquid-liquid equilibrium data for the system: Acetic acid, isobutanol, Water at three different temperatures.
- Generation and validation of a complete set of parameters for an activity-based thermodynamic model combined with an equation of state, for the calculation of the phase equilibrium of the quaternary system IbOH+ACAC+W+IbAC.
- Development of a complete mole fraction based kinetic model suitable to describe the esterification reaction between acetic acid and isobutanol using an ion exchange resin as catalyst.
- A conceptual design and modeling of the reactive distillation process for the production of isobutyl acetate at the industrial scale.

Each chapter of this manuscript was edited following the structure of scientific papers, which were published or are under revision for publication in different journals.

CHAPTER 1.

PHASE EQUILIBRIUM AND TOPOLOGICAL ANALYSIS FOR THE NON-REACTIVE SYSTEM ACETIC ACID + ISOBUTANOL + ISOBUTYL ACETATE + WATER.

This section includes a copy of the paper: Martinez, A.F., Sanchez, C.A., Orjuela, A., Rodriguez, G. 2020. Isobutyl acetate production by reactive distillation. Non-reactive phase equilibrium and topological analysis. Fluid Phase Equilibria. 516: 112612. DOI: 10.1016/j.fluid.2020.112612

The paper is reformatted and figures and tables are enlarged to fulfill edition requirements for the dissertation document.

1. Phase equilibrium and topological analysis for the non-reactive system acetic acid + isobutanol + isobutyl acetate + water.

1.1. Summary

This work studies the non-reactive fluid phase equilibria for the quaternary system Acetic acid - Isobutanol - Isobutyl acetate – Water. Initially, available equilibrium data of binary (VLE and LLE) and ternary (LLE) mixtures involving the studied components were collected. Then, the experimental evaluation of the ternary liquid-liquid phase equilibriums for the mixture isobutanol, acetic acid and water, was carried out at 283.15; 293.25 and 303.15. K. Consistency of the LLE data was verified via the Othmer-Tobias correlation. The complete set of phase equilibrium data was used to correlate the corresponding binary parameters of the NRTL-HOC thermodynamic model. The adjusted model agrees well with experimental information, and it is able to model the different reported binary azeotropes of the system as illustrated in a topological diagram, and predict one binary azeotrope and two unreported ternary azeotropes consistent based on the azeotropic rule. These non-reported azeotropes were calculated and its temperature and composition established. Finally a reactive residue curve map was constructed using the transformed molar fractions. From the topological analysis of the diagrams presented, it is concluded that pure Isobutyl acetate cannot be obtained as pure product from a reactive distillation column as it is a saddle node.

Keywords: Isobutyl acetate; Isobutyl alcohol; Water; Acetic Acid; Liquid-Liquid Equilibrium; topology.

1.2. INTRODUCTION.

In recent years, a variety of biobased chemicals have been identified as potential platform molecules to be exploited in current and future biorefineries. Among these, isobutanol has emerged as alternative biofuel and also as precursor of different value-added derivatives [1, 2]. Currently, isobutanol is mainly produced from petrochemical feedstock by using the oxo process. In this process, propylene is subjected to hydroformylation with CO and H_2 to produce a mixture of butyraldehydes, followed by hydrogenation to generate a mixture of butyl alcohols (i.e. oxo-alcohols) [3]. Alternatively, Isobutanol can also be obtained from various renewable sources through different chemical and biochemical pathways. Historically, isobutanol was a main

byproduct obtained during ethanolic fermentation of different saccharides using Sacc*haromyces cerevisiae* [4]. In this case, isobutanol is obtained as a main component of fusel oil; a side stream obtained during bioethanol distillation [5, 6]. Also, numerous natural and metabolically engineered microbial strains have been used for the biological production of isobutanol using different substrates [7-13]. Using a different approach, ethanol/methanol mixtures can be catalytically converted into isobutanol through Guerbet reactions under alkaline conditions [14-18]. More recently, fermentation and Guerbet routes have been combined using water tolerant catalysts [19]. Also, isobutanol can be obtained from biobased glycerol and methanol via the methacroleine route [19], and via a catalytic pathway from biobased syngas [20].

While most of the research has been focused on isobutanol production, its incorporation into future biorefineries is meant to develop a variety of value added derivatives of commercial interest. Among these, bioderived isobutyl acetate can become a major green solvent for the chemical industry, considering that is widely used in paintings, inks, coatings and cosmetics, and as odour and flavor ingredient (i.e. fruity and floral smell) for the flavoring and fragrance industry [2]. This solvent is highly used because of its degradability, low water solubility, low surface tension, high electrical resistance, and because it comply with REACH guidelines [21, 22].

Isobutyl acetate (IbAC) is generally produced by the direct esterification between Acetic Acid (ACAC) and isobutanol (IsobOH), generating water (W) as by product. This reaction is limited strongly by the equilibrium and carried out using acid catalysts. The corresponding equilibrium conversion for the stoichiometric mixture is around 0.66 and 4 in the range of 318 to 368 K [23-26].

In this regard, several strategies have been proposed to improve the esterification process for isobutyl acetate production, being the use of isobutanol excess, and the continuous removal of products by distillation or pervaporation the most common methods [2, 5, 27-30]. In addition, subsequent separation of mixtures of unreacted isobutanol and isobutyl acetate via pressure swing distillation have been used to enhance the overall process [31].

Disregarding the intensification approach and continuing with the tendency of production of Esters like methyl acetate [32], ethyl acetate [33], and isoamyl acetate [34] by Reactive distillation, for process design purposes, there is need for a comprehensive characterization and modeling of phase equilibria of the system. The

IbOH+ACAC+W+IbAC mixture is highly non-ideal, exhibiting several azeotropes, partial miscibility in the liquid phase, and dimerization of the acid in the vapor phase.

Table 1.1 presents a compilation of reported azeotropic data and available studies on binary and ternary VLE and LLE involving components of the quaternary mixture, also Figures A2 to A12 in the annexes A present available graphical reported vapor-liquid, liquid-liquid, and vapor-liquid-liquid phase equilibrium data comprising components of the esterification mixture. The authors of the experimental information address that all the information reported passes different thermodynamic consistency tests.

Specials mentions must be done for the system IbOH-ACAC as it is a reactive mixture, requiring special considerations for measurement. The experimental data available in Aspen Plus was tested with the Herrington thermodynamic consistency test showing that the data is inconsistent with a final value of 16 where the maximum acceptable value is 10; and was also evaluated with the direct method that evaluates the Margules Equation with 2 terms where the Smith-Van Ness quality index show that the information pass the test. Still because of the lack of information, this experimental VLE for the system ACAC-IbOH was used.

Table 1.1. Available phase equilibrium Data for the involving components of the system.

Binary mixtures (VLE)

Components		**Azeotropes information**			
A	**B**	**P (Kpa)**	**T (K)**	**wt %A**	**Ref.**
W	IbBOH	---	336,07	66,8	[35][a]
		101,0	363,12	68,5	[36]
		101,3	362,35	67,0	[37]
W	ACAC	100,0	No Azeotropes		[38]
W	IbAC	---	360.6	19.5	[35][a]
ACAC	IbOH	101,3	391,42	80	[39]
ACAC	IbAC	---	353,15	---	[40]
		101,3	390,17	20,46	[41]
			389,7	58,27	
IbOH	IbAC	---	380,75	95	[35][a]
		2	339,13	50,9	[42]
		101,3	380,75	89,1	
Binary Mixtures (LLE)					

Comp A	Comp B	P	Temperature Range		Ref.
W	IBOH	101,0	307,6	362,2	[45]
W	IbAC	101,3	293,1	353,1	[46]
Ternary mixtures VLLE (101,3 Kpa)					
	Comp		**Azeotrope information**		
A	**B**	**C**	**T (K)**		**Ref.**
ACAC	IbAC	W	No azeotropes		[41]
Ternary mixtures LLE					
IbAC	ACAC	W	283,1 323,1		[47-48]
IbAC	IbOH	W	283,1 323,3		[49-50]

[a] only azeotropic data available. No pressure reported.

Many authors correlate the experimental data with a thermodynamic model, being NRTL the most used model [42, 47, 49] as in Montón et al., (2005), Cháfer et al., (2008) and Xu et al., (2014) but also other authors use different thermodynamic models as Wilson (Zong et al., 1983), Margules or UNIQUAC (Zhang et al., 2011), so there is not a unified set of parameters for a thermodynamic model to predict the phase equilibrium of the quaternary system. This modeling is a major challenge taking into account that most current phase equilibrium models have issues with the accurate simultaneous representation of the VLE, VLLE and LLE in multicomponent mixtures of highly polar compounds. In general, this occurs because current methods lack the ability to represent the change of hydrogen bonding interactions at different temperature [51].

Another observation is a phenomenon of multi-azeotropy in the binary mixture ACAC - IbAC [40, 41]. The binary system exhibits two azeotropes under certain pressure and temperature ranges, which is an infrequent behavior only observed in a few other cases [52].

In this regard, this chapter focuses in the acquisition of a global set of parameters for the NRTL-HOC thermodynamic model to represent the phase equilibrium of the reactive mixture for conceptual design of a reactive distillation process for isobutyl acetate production. To achieve this objective experimental determination of LLE of the mixture IbOH-ACAC-W at three different temperatures was done

The Non-Random Two Liquid Model (NRTL) thermodynamic model [53] was selected due to its ability to model highly non-ideal mixtures, meanwhile for the vapor phase it is required the Hayden-O'connell correlation [54] to represent adequately the vapor dimerization phenomenon.

1.3. Materials and methods

1.3.1. Materials

The list of components and their corresponding purity and grade are presented in Table 1.2.

Table 1.2. List of chemicals used during phase equilibrium experiments

Compound	CAS	Grade	Supplier	Water %*	Purity (% Wt.)*
Acetic acid	64-19-7	Glacial	PanReac	-	≥ 99.9
Isobutanol	78-83-1	Pure	PanReac	0.5	≥ 99
Isobutyl acetate	110-19-0	USP	PanReac	-	≥ 99
Acetone	67-64-1	Analysis	Sigma Aldrich	0.05	≥ 99.5
Dioxane	123-91-1	Analysis	Sigma Aldrich	0.05	≥ 99.9

*Reported by manufacturer.

The purity of chemicals was verified by gas chromatography, and they were used without further purification. Deionized water was obtained in the laboratory by treatment with two cationic and one anionic resin, and a conductivity below 0.4 µS was tracked with a Martinn CM-230 conductivity Monitor. Acetone and Dioxane were used as solvent and internal standard respectively during chromatographic analysis.

1.3.2. Apparatus and Procedure

1.3.2.1. LLE measurements

Liquid-liquid equilibrium measurements were performed at constant temperature at three different levels. Mixtures of W-IbOH-ACAC were gravimetrically prepared at a specific composition within the immiscibility region, and allowed to equilibrate at 283 K, 293 K and 303 K. Each mixture was placed inside a test tube that was filled to the top to reduce moles in the vapor phase. Subsequently, the tubes were introduced and maintained in an isothermal circulation bath for three days to allow equilibration. The tubes were intensely stirred every 1 hour during the first day to maximize contact between phases, and then allowed to decant until the two liquid phases were sampled for characterization. The time necessary for reaching the equilibrium condition was

stablished according to a previous report [47]. For the higher temperatures (293 K and 303 K) the decanting time was reduced to prevent the progression of the reaction. This time was verified by allowing the system to equilibrate at different times, checking for the presence of isobutyl acetate. Once the system equilibrated, samples were taken from both phases for further analysis.

1.3.2.2. Analysis method

The composition of samples from the two liquid phases was determined by gas chromatography using a Shimadzu 2010 plus, with a Flame ionization detector. The samples were prepared by dissolving 100 mg of sample in 700 mg of Acetone, and adding 40 mg of Dioxane as Internal standard. A SGE Analytical Science column of 30 m x 0.32 mm x 0.25 µm with stationary face BP-20 was used (SGE S/N 1270516). High purity chromatography grade Helium was used as carrier gas. Detector temperature was set on 523.15 K and injector port temperature was maintained at 523.15 K. Calibration was carried out by analyzing mixtures of known composition, prepared by a gravimetric method using a balance (± 0.001 g). As the FID detector is not suitable for water, its content was obtained by difference. This procedure was calibrated by analyzing samples of known composition, and it exhibited a maximum deviation of 3 % mass.

1.3.2.3. Data analysis and phase equilibrium modeling

Reliability of the LLE data was verified by using the Othmer-Tobias Correlation presented in equation 1.1. The linearity of the experimental data according to this correlation indicates reliability of the data [55].

$$\ln\left[\frac{1-a}{a}\right] = m * \ln\left[\frac{1-b}{b}\right] + C \qquad (1.1)$$

Here, a is the mass fraction of water in the aqueous phase, b is the mass fraction of the organic compound in the organic phase, and m and C and adjustable parameters.

After obtaining the LLE data, they were combined with reported binary and ternary VLE, LLE and VLLE data to correlate a suitable phase equilibrium model for the quaternary mixture. Taking into account the highly non-ideality of the mixtures, equilibrium data were correlated with the NRTL activity-based model for the liquid

phase [53], and the Hayden O'Connell equation for the vapor phase [54]. The NRTL model used to calculate the activity coefficient (γ_{ij}) is described in Equations 1.2 to 1.4, and the adjustable parameters ($A_{ij}, A_{ji}, B_{ij}, B_{ji}, \alpha_{ij}$) were used to calculate temperature dependence of energetic interactions (τ_{ij}) between molecules i and j. α_{ij} is the "non-randomness parameter" and it is used to calculate the Gibbs free energy G as presented in Equation 1.4. This parameter is symmetric ($\alpha_{ij} = \alpha_{ji}$) and has typical recommended values (e.g. 0.2, 0.3 or 0.48), but it can also be regressed from experimental information.

$$\ln(\gamma_{ij}) = \frac{\sum_{j=1}^{n} x_j \tau_{ji} G_{ij}}{\sum_{k=1}^{n} x_k G_{ki}} + \sum_{j=1}^{n} \frac{x_j G_{ij}}{\sum_{k=1}^{n} x_k G_{kj}} \left(\tau_{ij} - \frac{\sum_{m=1}^{n} x_m \tau_{mj} G_{mj}}{\sum_{k=1}^{n} x_k G_{kj}} \right) \quad (1.2)$$

$$\tau_{ij} = A_{ij} + \frac{B_{ij}}{T(K)} \quad (1.3)$$

$$G_{ij} = \exp(-\alpha_{ij} \tau_{ij}) \quad (1.4)$$

Vapor pressure of the pure components was modeled with Antoine equation, and the corresponding parameters are presented in Table A1 of the annexes A. The good fit of the vapor pressure model to reported experimental data for the pure components can be verified in Figure A1 in the annexes A. The corresponding solvation and association parameters of the Hayden O'Connell viral equation were obtained from literature [54, 56, 41], and they are summarized in Table A2, also in Annexes. The correlation of the corresponding NRTL binary interaction parameters was carried out by using the regression tool included in Aspen Plus V10. This tool uses a least square method applied to the differences between experimental and predicted equilibrium data considering the composition of liquids (*xL1*, *xL2*), vapor (*y*), and the corresponding equilibrium temperature (T) and pressure (P). The optimization during parameter regression was done using the maximum likelihood approach with the Britt-Luecke algorithm.

Special considerations were taken for the regression of the binary mixture IbAC-ACAC that exhibits double azeotropy. In this case, the available information was inserted in the software as different data sets with different weighting factors to enhance the adjustment around the azeotropic conditions. Finally, using the regressed set of parameters for the NRTL-HOC model, quaternary phase equilibria diagrams were obtained, and a non-reactive residue curve map was constructed for the quaternary mixture and using the measured chemical equilibrium constants of the esterification reaction, the reactive residue curve map was also constructed using transformed molar

fractions [58-60]. The chemical equilibrium constant used and its measurement are explained in more detail in chapter 2 of this work.

1.4. RESULTS

1.4.1. Experimental phase equilibria

Liquid-liquid phase equilibrium data for the ternary system IbOH (1) - ACAC (2) - Water (3) were obtained at 283 K, 293 K and 303 K, and at local atmospheric pressure (74.6 kPa). The obtained results are listed in Table 1.3, and in Figure 1.1 are presented the corresponding Othmer-Tobias correlations for the obtained LLE data at the different temperatures. Despite the liquid mixture is reactive, no isobutyl acetate was observed in the characterized samples from all experiments. This was expected taking into account the low temperatures, the large molar excess of water, and the low content of acetic acid. As observed, the obtained data are reliable as verified with the linearity of the correlation. The corresponding ternary diagrams at the different temperatures are presented in Figure 1.2. Similarly to other acetic acid esterification mixtures, the acid content in the liquid phase reduces the immiscibility region, enhancing the water uptake in the organic phase. This indicates that if unreacted acid is present in the effluents of a reactor, water removal cannot be readily done by decanting.

Table 1.3. Experimental LLE Data (mole fraction) for the mixture Isobutanol (IbOH) - Acetic Acid (ACAC) – Water (W) at 283, 293 and 303 K. Pressure 74.6 kPa.

	organic phase			aqueous phase		
T (K)	X_{IbOH}	X_{ACAC}	X_{H_2O}	X_{IbOH}	X_{ACAC}	X_{H_2O}
283.15	0.537	0.017	0.446	0.022	0.005	0.973
	0.510	0.030	0.460	0.023	0.010	0.968
	0.478	0.044	0.479	0.023	0.014	0.962
	0.440	0.056	0.504	0.024	0.019	0.957
	0.413	0.067	0.520	0.026	0.026	0.948
	0.368	0.080	0.553	0.028	0.031	0.942
	0.318	0.090	0.592	0.032	0.038	0.930
	0.261	0.092	0.648	0.039	0.046	0.915
	0.205	0.091	0.704	0.052	0.056	0.892
293.15	0.525	0.017	0.458	0.022	0.005	0.974

	0.498	0.032	0.470	0.022	0.009	0.969
	0.466	0.047	0.487	0.023	0.015	0.962
	0.416	0.062	0.522	0.024	0.020	0.956
	0.378	0.073	0.549	0.025	0.025	0.950
	0.337	0.083	0.580	0.028	0.032	0.940
	0.303	0.088	0.609	0.031	0.037	0.932
	0.263	0.089	0.649	0.038	0.045	0.917
	0.197	0.086	0.717	0.055	0.059	0.886
303.15	0.509	0.016	0.475	0.020	0.005	0.975
	0.489	0.032	0.479	0.021	0.009	0.970
	0.461	0.045	0.494	0.022	0.014	0.964
	0.412	0.057	0.531	0.023	0.019	0.958
	0.375	0.070	0.555	0.025	0.024	0.951
	0.340	0.080	0.580	0.028	0.030	0.942
	0.286	0.083	0.632	0.031	0.037	0.932
	0.206	0.080	0.709	0.034	0.042	0.924

Standard Uncertainties of X, P and T are: u(X) = 0.001, u(P) = 1.5 kPa, u(T) = 0.1 K.

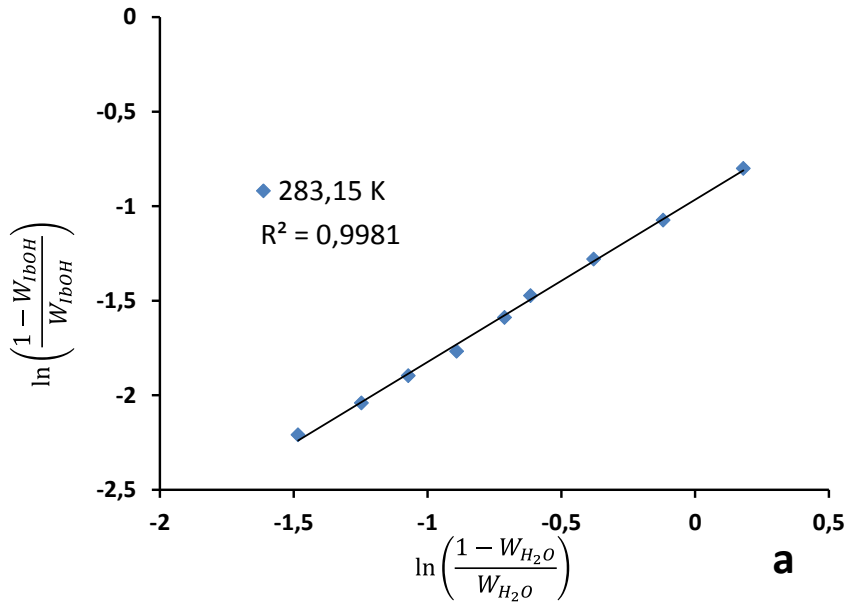

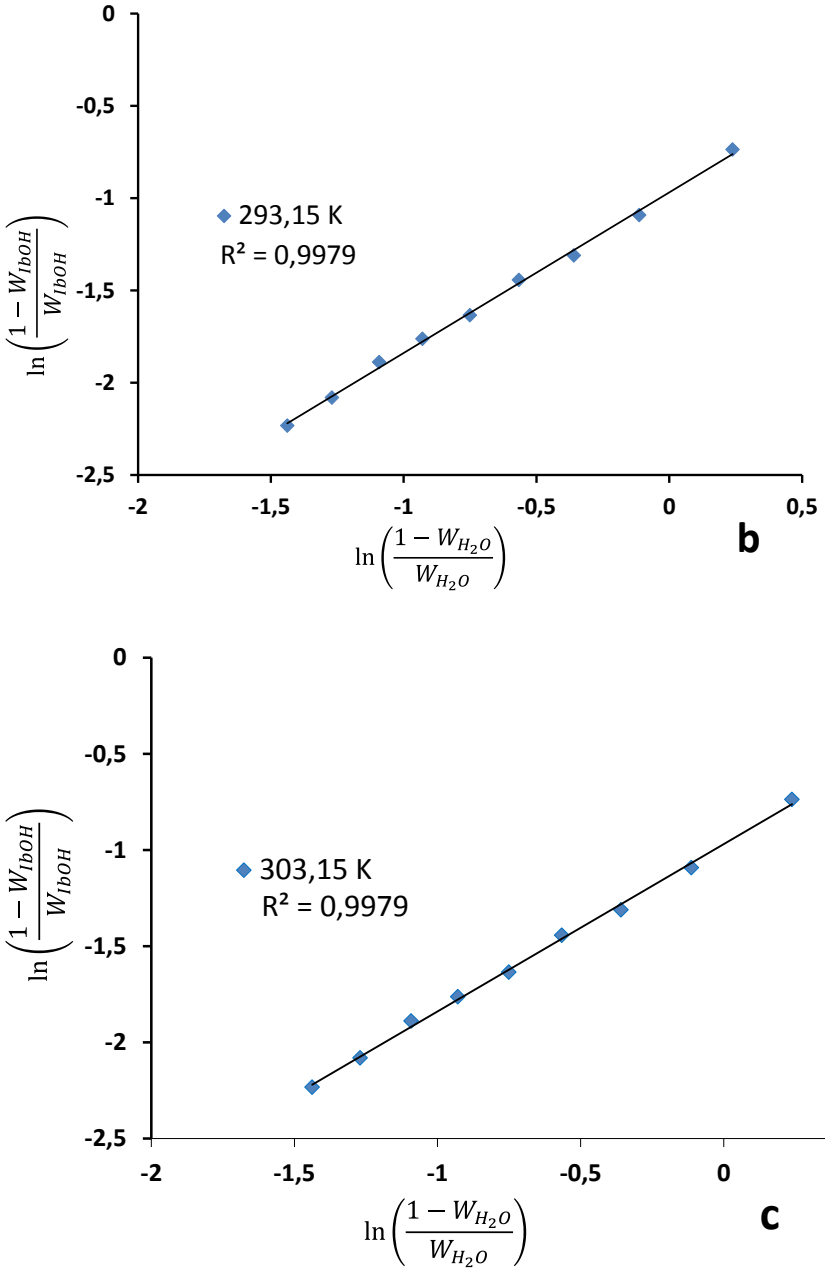

Figure 1.1. Othmer- Tobias correlation for the Liquid-liquid equilibrium data of mixtures IbOH+ACAC+W at constant temperature. (a) 283 K. (b) 293 K. (c) 303 K.

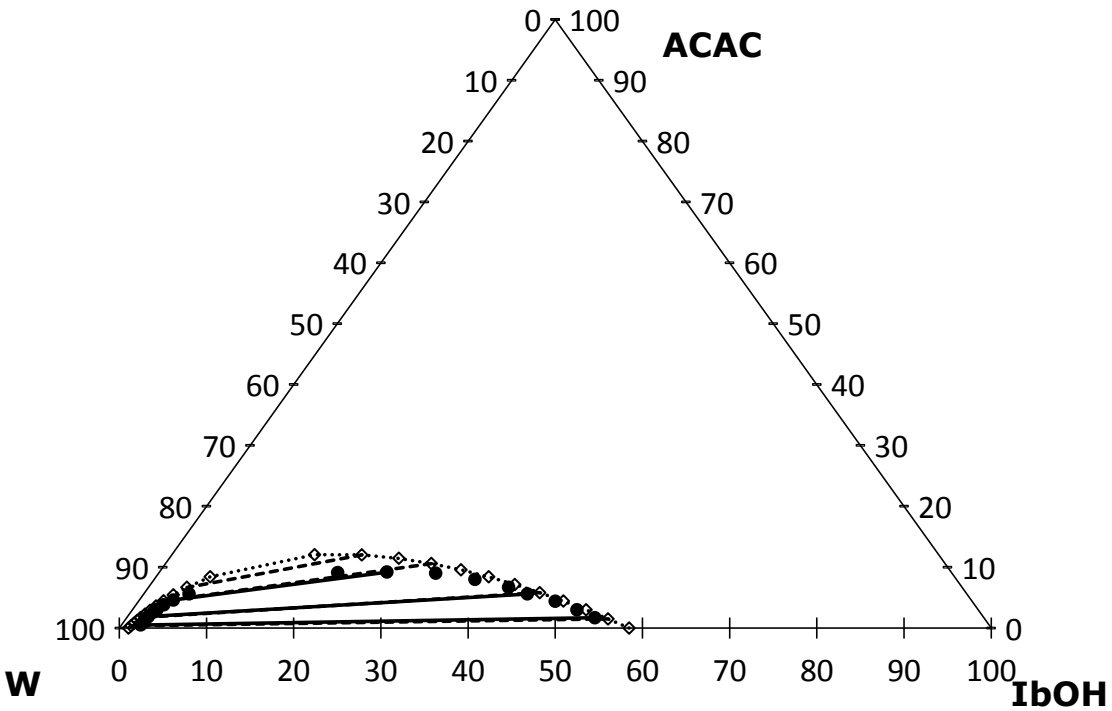

a) 283,15 K

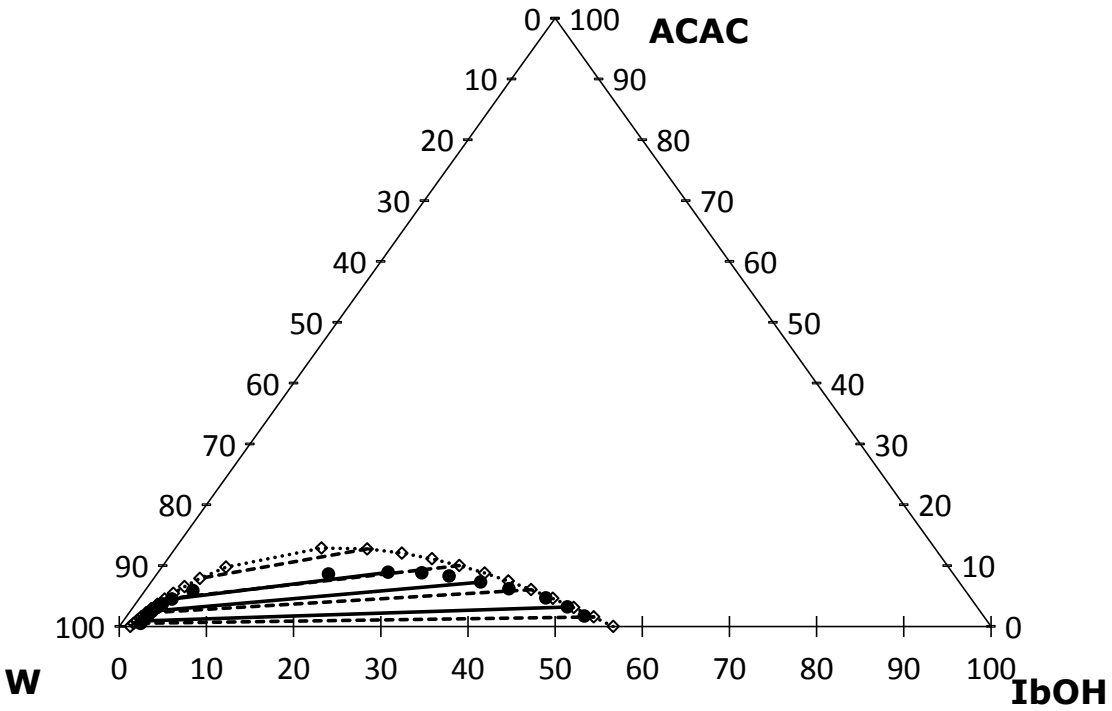

b) 293,15 K

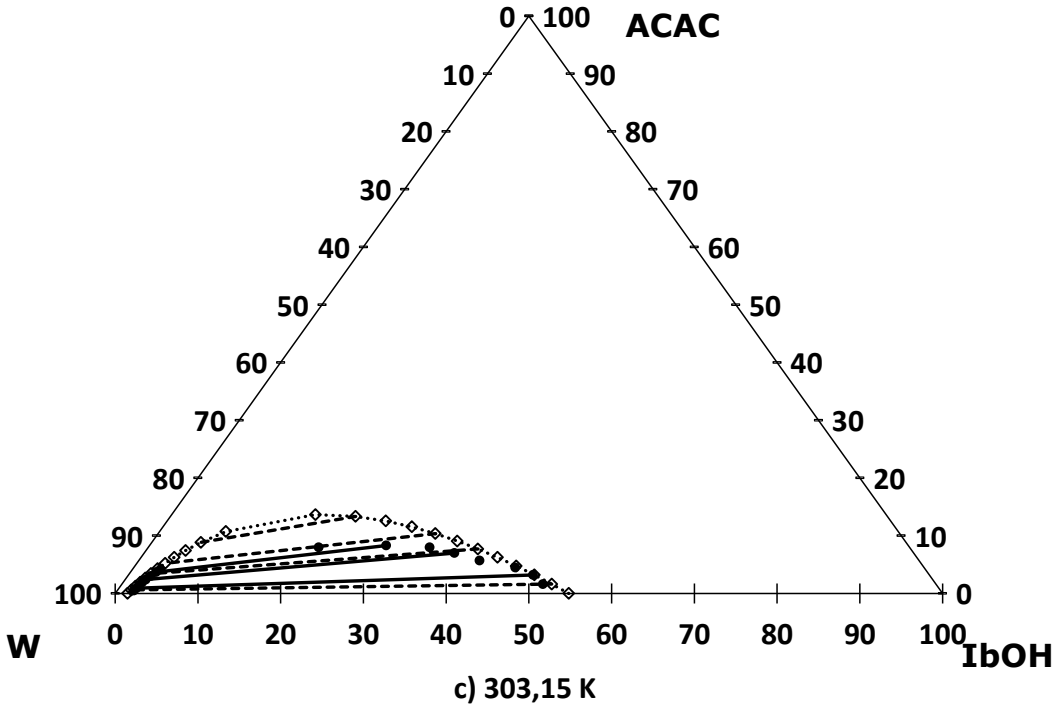

Figure 1.2. Ternary diagrams for mixtures of IbOH+ACAC+W at different temperatures. (a). 283,15 K; (b). 293,15 K; (c). 393,15 K. (•) experimental information; (—) experimental tie line; (◊) binodal curve; (---) model tie line.

1.4.2. Model adjustment

1.4.2.1. Hayden O'Connell Correlation

The Vapor phase is modeled by the Hayden O'Connell correlation, this is a viral equation that calculates the properties of the vapor phase of strongly associative compound like those involving acetic acid, by the incorporation of the dimerization theory as presented in Eq. 1.5.

$$Z_m = 1 + \frac{B}{RT} \tag{1.5.}$$

Were

$$B = \sum_i \sum_j x_i x_j B_{ij}\,(T) \tag{1.6.}$$

$$B_{ij} = \left(B_{free-nonpolar}\right)_{ij} + \left(B_{free-polar}\right)_{ij} + (B_{metastable})_{ij} + (B_{bound})_{ij} + (B_{chem})_{ij} \tag{1.7}$$

This correlation was developed for predicting the second virial coefficient based on critical properties and the molecular parameters Solvation and Association [54]. The parameters for the components Acetic Acid, isobutanol and water are available in the book: Computer calculations for multicomponent vapor-liquid equilibria [56] while the interaction parameters for Isobutyl acetate are taken from Zhang et al., 2011 [41]. Table 1.4 present the association and solvation parameters used in this work.

Table 1.4: Solvation and association parameters for Isobutyl acetate:

	Acetic Acid	**Water**	**Isobutyl acetate**	**Ref.**
Isobutyl Acetate	2.0	1.3	0,53	[41]

However, the solvation parameter between isobutyl acetate and isobutanol is not reported in the available literature, so it was estimated. For this, a compilation of the association and solvation parameters between alcohols and esters from different esterification system was searched and presented in table 1.5.

Table 1.5: Solvation and association parameters for different alcohols and its acetates:

Comp. i	**Comp. j**	**Comp. j**	**Comp. j**	**Comp. j**
	Methyl Acet.	Ethyl Acet.	n-butyl Acet.	Iso-butyl Acet.
Acetic Acid	2	2	2	2
Water	1.3	1.3	1.3	1.3
Methanol	1.3	1.3	1.3	N.R.
Ethanol	1.3	1.3	1.3	N.R.
n-Buthanol	1.3	1.3	1.3	N.R.
Iso-Buthanol	1.3	1.3	1.3	N.R.

N.R.: not reported.

As observed, the HOC parameters between different alcohols and their acetates are the same, so it is possible to deduce the missing parameter isobutyl acetate - isobutanol, with a value of 1.3.

1.4.2.2. NRTL parameters regression

The obtained LLE data, and the reported equilibrium information for the components of the quaternary mixture, were used to correlate binary parameters for the NRTL

equation. This unique set of parameters allows obtaining reliable predictions of all VLE, VLLE and LLE data. The obtained set of parameters is presented in Table 1.6.

Table 1.6. Regressed NRTL parameters for the mixture IbOH+ACAC+IbAC+W

			Model parameters				
	i	**j**	A_{ij}	A_{ji}	B_{ij} **(K)**	B_{ji} **(K)**	α_{ij}
Regressed	ACAC	IBOH[a]	7,20005	-4,43801	-2195,15	1366,33	0,47
	Standard deviation		0,1350	0,0615	997,0872	3012,0321	--
Regressed	ACAC	IBAC[a]	1,8059	-0,9455	-666,5556	584,0002	0,3
	Standard deviation		2,7164	0,0763	311,5627	642,1245	--
Regressed	IBOH	IBAC[a]	-2,7472	-0,0272	1099,7379	74,6936	0,3
	Standard deviation		3,1358	3,1687	1072,1766	1082,7280	--
Regressed	IBOH	W[a]	-1,74621	0,97442	667,127	875,726	0,357937
	Standard deviation		0,8017	1,0124	101,3013	201,5022	0,0192
Not regressed	IBAC	W[b]	-2,2213	8,8038	1012,1378	-866,8213	0,2
Not regressed	ACAC	W[b]	-1,9763	3,3293	609,8886	-723,8881	0,3

a: Regressed by Aspen Plus V.10.

b: Taken from Aspen Plus V.10.

The predicted and reported azeotropes of the different mixtures are presented in Table 1.7, the average deviation of the temperature and vapor composition between the experimental information and the model is presented in Table 1.8, and graphical comparison of the different LLE, VLE, and VLLE data with model predictions are presented in Figures A2 to A12 in the annexes A. It is observed that the regressed model is able to predict all azeotropes of the system, even the double azeotrope of the ACAC - IbAC mixture. As expected, there was a need for a compromise for the adjustment of the VLE and the LLE.

As observed in Table 1.6., the standard deviations of some parameters are larger than their corresponding value, indicating that they have minor importance in the fittings. Nevertheless, all the parameters were kept as regressed, and the predictions of the

obtained model were in good agreement with the whole set of experimental data. As verified in Table 1.7., reported azeotropes are reasonably well predicted with the obtained model, and there is a combined relative low average deviation between correlated and experimental data from the different sets. It is interesting to point out that the studied mixture turned to be extremely highly non-ideal, representing a major challenge for the phase equilibrium correlation with the evaluated model. Thus, this particular system could become a case study to evaluate the reliability and accuracy of novel activity or fugacity-based models for phase equilibria calculation.

In the obtained regressions, special considerations have to be made for the binary mixtures ACAC-IbOH and ACAC-IbAC. For the case ACAC-IbOH, the high deviation in the predicted azeotropic composition (Δy = 7.34%) can be associated to the difficulties of fitting the nearly constant bubble and dew temperatures in a broad range of compositions (0 < x_{IbOH} < 0.5). Also few points were collected near the reported azeotropic composition making difficult the adjustment of the VLE model in that region. The lack of VLE data near the azeotrope is understandable taking into account that this is a reactive mixture that requires special equipment and conditions to avoid ester formation during experiments. Further improvements could be done when collecting additional VLE data near the azeotropic conditions, preferably at different pressures.

In the other hand, and as already mentioned, in the case of the binary ACAC-IbAC, the system exhibits an uncommon double binary azeotrope that is difficult to correlate. In this case, larger deviations in the predicted compositions were expected because few data were available in the region surrounding one of the azeotropes. Also, the bubble and dew points of the mixture barely changed (< 0.3 K) almost in the entire range of compositions (i.e. 0 < x_{ACAC} < 0.8). This small change in the equilibrium temperature created difficulties during regression because the error hardly changed when modifying binary interaction parameters. Thus, most efforts during regression were put in adjusting VLE compositions, and the adjusted binary parameters were obtained after several attempts to fit the double azeotropic behavior. In this case it was necessary to establish a compromise between the prediction of the whole VLE diagram and that of the particular azeotropic conditions. As observed in Figure A6 and A7, a good fitting of the VLE data was obtained in the whole range of compositions.

Despite the difficulties on fitting these two binaries, average deviations from the model indicates a reasonably good agreement when considering the whole set of equilibrium data, as verified with the averaged deviations of Table 1.8. A graphical comparison of

the different LLE, VLE, and VLLE data with predictions from the regressed model are presented in Figures A2 to A11 in the annexes. As observed, the adjusted NRTL-HOC model is able to fit reasonably well the different phase equilibria, and to predict all azeotropes of the system, even the double azeotrope of the ACAC - IbAC mixture

Table 1.7. Predicted Azeotropes with regressed models and comparison with reported data of Table 1.1.

Component		**Reported Azeotrope**			**Predicted Azeotrope**		**Aver. Deviation**	
A	**B**	**T (K)**	**A%**[a]	**Ref.**	**T (K)**	**A%**[a]	ΔT[b] **(K)**	Δy[c] **(%)**
W	IbOH	363.12	68.5	[36]	363.85	69,76	0.73	1.17
		362.35	67.0	[37]	362.94	68.66	0.59	1.66
ACAC	IbOH	391.42	80.0	[39]	391.81	72.65	0.39	7.34
ACAC	IbAC	390.17	20.4	[41]	390.12	13.70	0.04	6.70
		389.72	58.2		389.77	55.00	0.05	3.20
IbOH	IbAC	339.13	50.8	[42]	339.23	49.10	0.10	1.76
		380.76	89.1		380.79	89.30	0.03	0.20

a. mole fraction.

b. $\Delta y = \left|y_{calcd} - y_{expermt}\right|$

c. $\Delta T = \left|T_{calcd} - T_{expermt}\right|$

Table 1.8. Calculated Temperature and composition average deviation with VLE reported data of Table 1.1.

Components			Aver. Deviation		
A	**B**	**Ref.**	Δy[b]	ΔT[a]	ΔP[c] **(Pa)**
W	ACAC	[38]	0.3	0.2	---
W	IbOH	[36]	2.19	0.86	---
		[37]	2.45	0.84	---
ACAC	IbOH	[39]	1.45	0.37	---
ACAC	IbAC	[40]	0. 43	Isothermal	66.9
		[41]	0.57	0.07	---
IbOH	IbAC	[42]	0.26	0.12	---
			0.46	0.11	---

a: $\Delta y = (1/N)\ \sum\left|y_{calcd} - y_{expermt}\right|$.

b: $\Delta T = (1/N)\ \sum\left|T_{calcd} - T_{expermt}\right|$.

c: $\Delta P\ (N/sqm) = (1/N)\sum\left|P_{calcd} - P_{expermt}\right|$.

As expected, and in order to get a good agreement of the VLE, VLLE and LLE simultaneously, there was a need for a compromise allowing larger deviations in some

cases. The main deviations occurred in the predictions of the ternary LLE, particularly in the immiscibility region where the model overestimates the size of the dome in all cases. Nevertheless, the composition of the aqueous phase is well predicted and the tie lines have the same slope as the experimental ones.

In spite of the deviations, the topological analysis can be performed taking into account that the azeotropes are reasonably well predicted, and they are required to verify if the azeotropic rule is fulfilled [61, 62].

1.4.3. Quaternary non-reactive phase equilibria diagram and residue curve analysis

Table 1.9., present all the singular points calculated for the reactive mixture with the adjusted parameters. Special considerations must be taken when using commercial simulation software like Aspen Plus, as it is not able to detect double binary azeotropes, incurring in errors establishing distillation regions.

Table 1.9. Complete set of singular points for the quaternary system IbOH+ACAC+IbAC+W. Compositions in mole fraction.

No.	Temp. (°C)	No. Comp.	ACAC	IbOH	IbAC	W
1	391.16	1	1	0	0	0
2	380.83	1	0	1	0	0
3	389.55	1	0	0	1	0
4	373.17	1	0	0	0	1
5	390.12	2	0,137	0	0,862	0
6	389.78	2	0,53	0	0,47	0
7	380.79	2	0	0,9314	0,0686	0
8	391.81	2	0,72	0,28	0	0
9	363.78	2	0	0,288	0	0,712
10	361.06	2	0	0	0,317	0,683
11	360.40	3	0	0,1325	0,2496	0,6179
12[a]	389.89	3	0,317	0,029	0,654	0

a. not reported by commercial simulation software.

Special attention must be put to the fact that most commercial simulation software (e.g. Aspen Plus) are not able to detect double binary azeotropes like in the case of the binary mixture ACAC - IbAC. This is a major challenge because the misprediction of

such azeotropic behavior will generate incorrect distillation regions, nodes, and feasible products within the residue curve maps. Because of this, the ternary azeotropes IbOH-IbAC-W and ACAC-IbOH-W were verified externally by solving Equations 1.8 to 1.10 simultaneously.

$$y_i \emptyset_i P = x_i \gamma_i \emptyset_i^{sat} P_i^{sat} \quad (1.8)$$

$$\sum y_i = 1 \quad (1.9)$$

$$\sum_{i=1}^{c} (y_i - x_i) = 0 \quad (1.10)$$

Here, P is the system preassure, T is the bubble point at P and the corresponding liquid composition, P_i^{sat} is the saturated vapor pressure of the component i, $\emptyset_i$ and $\emptyset_i^{sat}$ are the vapor phase and saturated vapor fugacity coefficients of the component i respectively, and γ_i is the activity coefficient of the component i.

The VLLE diagram for the quaternary mixture including the different non-reactive residue curves are presented in Figure 1.3a. The corresponding ternary diagrams are presented in Figure 1.3b., including the different non-reactive residue curves and the immiscibility region. According to the quaternary diagram, there is an unstable node at the ternary azeotrope IbOH-IbAC-W, and two stable nodes located at the binary azeotropes IbOH-ACAC and IbAC ACAC, respectively. All the remaining singular points correspond to saddle nodes forming several distillation regions visible in figure 1.3b. It was also verified that there are no quaternary azeotrope is the system. In Figure 1.3a., and 1.3b., it can be observed that in mixtures containing acetic acid, it is not possible to obtain pure isobutyl acetate as product of a distillation sequence because it becomes a saddle node. The ternary diagram for IbOH-IbAC-W, IbAC-ACAC-W, IbOH-ACAC-W and IbOH-IbAC-ACAC are presented in the annexes A (Figures A13 to A15). The different distillation regions and some residue curves are described there in more detail.

The reactive residue curve map in the transformed coordinates for the quaternary mixture is presented in Figure 1.4. This was calculated under the assumption of chemical equilibrium condition, and it is depicted in transformed coordinates. The slight changes in the azeotropic temperatures with respect to those of Table 1.9 are caused by numerical tolerance and convergence differences near the nodes when calculating the residue curve maps and due to the change in the composition of the azeotropes in chemical equilibrium condition. As observed no quaternary azeotropes are formed, and

the ternary saddle azeotrope ACAC-IbOH-IbAC is reacted away under the evaluated chemical equilibrium conditions (i.e. infinite Damköhler number).

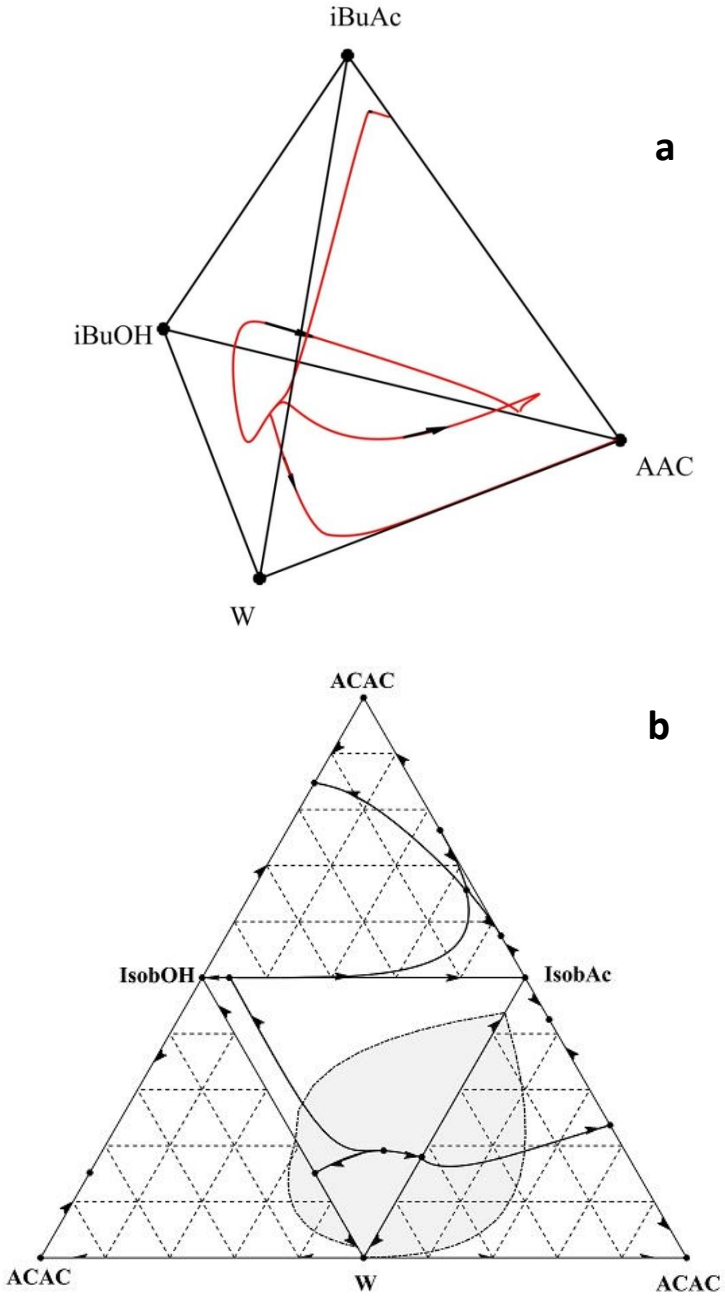

Figure 1.3. Non-reactive residue curves maps (Mole fraction basis) and phase equilibrium diagram for the quaternary system IbOH+ACAC+W+IbAC at P= 101.32 Kpa. (a) Quaternary diagram. (b) Unfold into the corresponding ternary diagrams. (–) Residue curves. (—) Immiscibility region. (—) Distillation boundaries. (•) Azeotropes.

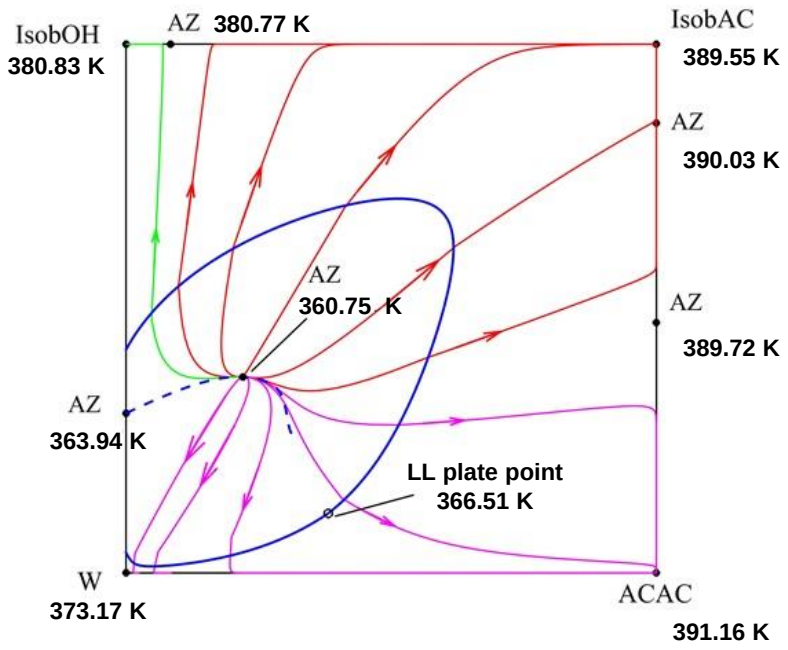

Figure 1.4. Transformed composition reactive residue curve map for the quaternary system at P= 101,32 Kpa. (Red, Green, Purple, ─) Residue curves. (─) Immiscibility reactive VLL region. (---) Reactive vapor line.

1.5. Analysis.

1.5.1. non-reactive topological structure validation

The consistency of the topological structure observed in Figure 1.3a and 1.3b and the azeotropes presented in Table 1.9, can be assessed by the azeotropic Rule proposed by Gurikov et al [61]. Different studies have verified the validity of such rule for multicomponent systems, even when they exhibit multiple azeotropes in the binary mixtures [63-68]. The general expression of this rule for *n* components is presented in Equation 1.11.

$$\sum_{K=1}^{n}[2^{K}(N_K^{+} + S_K^{+} - N_K^{-} - S_K^{-}) = 1 + (-1)^{n-1} \quad (1.11)$$

Here N_K is the number of k-components nodes, and S_K is the number of k-components saddles, *n* is the number of components. The corresponding positive and negative indices are explained by Kiva et al [69] (from the original works of Serafimov and coworkers), and they are based on the location of the node and the direction of increasing boiling temperature from each node.

For ternary mixtures containing isobutyl acetate, the presence of the double binary azeotropes generates ternary diagrams that are not listed in the ternary topological analysis performed by Hilmen et al. [69, 70] as these structures are uncommon and have not being studied. In this case, the topological consistency of the ternary structures can be assessed by using the following simplification of the azeotropic rule:

$$2N_3 + N_2 + N_1 = 2S_3 + S_2 + 2 \quad (1.12)$$

Here, N_3 are the numbers of ternary nodes (S_3 ternary Saddles nodes), N_2 are the numbers of binary nodes (S_2 binary saddles nodes), and N_1 is the number of pure components nodes.

The identification of the different node indices in the ternary mixture ACAC-IbAC-W are listed in Table 1.10, and for the system ACAC-IbAC-IbOH are listed in Table 1.11. Replacing indices of Table 1.10 and 1.11 in equation 1.12, the rule of azeotropy is fulfilled establishing that a topology with 3 binary azeotropes for the system ACAC-IbAC-W, and four binary azeotropes for the system ACAC-IbAC-IbOH, is consistent and feasible.

For the quaternary mixture, replacing on the equation 1.11, the derived 4 components Rule of Azeotropy (without quaternary azeotropes as it was demonstrated previously) results:

$$8(N_3^+ + S_3^+ - N_3^- - S_3^-) + 4(N_2^+ + S_2^+ - N_2^- - S_2^-) + 2(N_1^+ + S_1^+ - N_1^- - S_1^-) = 0 \quad (1.13)$$

As described before, the positive and negative index assignation was done according to Serafimov and coworkers, as reported by Kiva et al [69]. Table 1.12 present the index for the quaternary system. And replacing its values in equation 1.13, it is validated a topological configuration with six binary azeotropes and two ternary azeotropes.

Table 1.10 Topology indices for the ternary nodes in the system ACAC - IbAC - W based on [70].

Singular Point	**Type**	**Nomination**
Pure components		
W	Saddle	S_1
ACAC	Stable	N_1

IbAC	Saddle	S_1
Binary Azeotropes		
W-IbAC	Unstable	N_2
IbAC-ACAC (X_acac = 0,15)	Stable	N_2
IbAC-ACAC (x_acac = 0,53)	Saddle	S_2

Table 1.11. Singular points and Topological index for the system ACAC-IbAC-IbOH P=101,325Kpa.

Singular Point	Temperature	Type	Nomination
Pure components			
IbOH	107,68	Saddle	S_1
ACAC	118,01	Saddle	S_1
IbAC	116,4	Saddle	S_1
Binary Azeotropes			
IbOH-IbAC	107,64	Unstable	N_2
IbAC-ACAC (X_acac = 0,15)	116,97	Stable	N_2
IbAC-ACAC (x_acac = 0,53)	116,62	Unstable	N_2
IbOH-ACAC	118,23	Stable	N_2
Ternary Azeotropes			
IbAC-IbOH-ACAC	116,74	Saddle	S_3

Table 1.12. Singular points and Topological index for the quaternary system P=101,325Kpa.

Singular Point	Type	Topological Index	Nomination
Pure components			
W	Saddle	+1	S_1^+
ACAC	Saddle	+1	S_1^+
IbOH	Saddle	+1	S_1^+
IbAC	Saddle	+1	S_1^+
Binary Azeotropes			
W-IbAC	Saddle	-1	S_2^-
W-IbOH	Saddle	-1	S_2^-
IbOH-IbAC	Saddle	-1	S_2^-
ACAC-IbOH	Stable	-1	N_2^-
ACAC-IbAC ($X_{ACAC} = 0,15$)	Saddle	-1	N_2^-
ACAC-IbAC ($X_{ACAC} = 0,53$)	Saddle	-1	S_2^-
Ternary Azeotropes			
W-IbOH-IbAC	Unstable	+1	N_3^+
IbOH-IbAC-ACAC	Saddle	+1	S_3^+

1.6. CONCLUSIONS

This work focused on the description of the phase equilibria on the quaternary mixture: isobutanol, acetic acid, isobutyl acetate and water. Initially, this involved a comprehensive revision of VLE, VLLE and LLE phase equilibria data of mixtures containing the components of the reactive mixture. Afterwards, the evaluation of LLE for the mixture Isobutanol, Acetic Acid and water under isothermal conditions was carried out at three different temperatures. Then, these data together with reported phase equilibrium information (VLE, VLLE, and LLE), were used to regress a unique set of binary parameters for the NRTL-HOC thermodynamic model. This model allowed the accurate modeling of the quaternary mixture acetic acid - isobutanol - isobutyl acetate – water, with reasonably good prediction of reported azeotropes. Explorations with the regressed model indicates that the system does not exhibit quaternary azeotropes, and that there are two ternary azeotropes that have not been reported. The topological analysis allowed verifying that the predicted configuration with eight azeotropes is consistent and possible under the consideration of the azeotropic rule.
In addition, a reactive residue curve map for the quaternary mixture was calculated under chemical equilibrium condition, and depicted in transformed coordinates. According to the obtained map, there is a heterogeneous azeotrope of minimum boiling point that has not been reported before. These non-reported azeotropes are yet to be experimentally verified. Reactive residue curves indicate that isobutyl acetate cannot be obtained as pure product from the bottom stream of a reactive distillation column. Finally, the parameter presented here can be used with confidence for further process modeling, in particular in the design of a reactive distillation process for isobutyl acetate production.

1.7. References

1. Butamax, 2016. The Biofuel of the Future. https://www.butamax.com/the-bio-isobutanol-advantage/higher-value-biofuel/ (Consulted 23 Aug. 2019)

2. Moncada, J., Posada, J., Ramírez, A. Comparative early stage assessment of multiproduct biorefinery systems: An application to the isobutanol platform. Bioresour. Technol. **2017**, 241: 44–53.

3. Falcke, H., Holbrook, S., Clenahan, I., López, A., Sanalan, T., Brinkmann, T., Roth, J., Zerger, B., Roudier, S., Delgado, L. Best Available Techniques (BAT) Reference Document for the Production of Large Volume Organic Chemicals; EUR 28882 EN;

Publications Office of the European Union, Luxembourg, 2017, ISBN 978-92-79-76589-6, doi:10.2760/77304, JRC109279.

4. Ramli, N.A., Rahman, R.A., Ngadi, N., Samah, R.A. Optimisation of fermentation conditions for isobutanol production by saccharomyces cerevisiae using response surface methodology Chemical Engineering Transactions **2017**, 56: 301-306.

5. Patidar, P., Mahajani, S. Esterification of fusel oil using reactive distillation – Part I: Reaction kinetics. Chemical Engineering Journal. **2012**, 207–208: 377-387.

6. N. Montoya, J. Durán, F. Córdoba, I. Gil, C. Trujillo, G. Rodríguez, Colombian fusel oil, Ing. E Investig. **2016**, 36:21-27.doi:10.15446/ing.investig.v36n2.52369.

7. Atsumi S, Hanai T and Liao JC, Non-fermentative pathways for synthesis of branched-chain higher alcohols as biofuels. Nature **2008**, 451(7174):86–89.

8. Xiao, Y., Feng, X. Varman, A., He, L., Yu, H., Tang, Y. Kinetic Modeling and Isotopic Investigation of Isobutanol Fermentation by Two Engineered Escherichia coli Strains. Ind. Eng. Chem. Res. **2012**, 51(49): 15855-15863.

9. Lan, E.I., Liao, J.C. Microbial synthesis of n-butanol, isobutanol, and other higher alcohols from diverse resources. Bioresour. Technol. **2013**, 135, 339–349.

10. Minty, J.J., Singer, M.E., Scholz, S.A., Bae, C.-H., Ahn, J.-H., Foster, C.E., Liao, J.C., Lin, X. N. Design and characterization of synthetic fungal-bacterial consortia for direct production of isobutanol from cellulosic biomass. Proc. Natl. Acad. Sci. **2013**, 110, 14592–14597.

11. Gak, E., Tyurin, M., Kiriukhin, M. Genome tailoring powered production of isobutanol in continuous CO_2/H_2 blend fermentation using engineered acetogen biocatalyst. Journal of Industrial Microbiology and Biotechnology **2014**, 41(5): 763-781

12. Tao, L., Tan, E., McCormick, R., Zhang, M., Aden, A., He, X., Zigler, B. Techno-economic analysis and life-cycle assessment of cellulosic isobutanol and comparison with cellulosic ethanol and n-butanol. Biofuels, Bioproducts and Biorefining **2014**, 8:30–48.

13. Siripong, W., Wolf, P., Kusumoputri T. P., Downes J. J., Kocharin, K., Tanapongpipat, S., Runguphan, W. Metabolic engineering of Pichia pastoris for production of isobutanol and isobutyl acetate. *Biotechnol Biofuels*. **2018** 11:1-16.

14. Jordison, T.L., Lira, C.T., Miller, D. J. Condensed-Phase Ethanol Conversion to Higher Alcohols. Industrial and Engineering Chemistry Research. **2015**, 54 (44): 10991-11000.

15. Wingad, R.L., Bergström, E.J.E., Everett, M., Pellow, K.J., Wass, D.F. Catalytic conversion of methanol/ethanol to isobutanol - A highly selective route to an advanced biofuel. Chemical Communications **2016**, 52 (29): 5202-5204.

16. Pellow, K.J., Wingad, R.L., Wass, D.F. Towards the upgrading of fermentation broths to advanced biofuels: A water tolerant catalyst for the conversion of ethanol to isobutanol. Catalysis Science and Technology **2017**, 7(21): 5128-5134.

17. Nezam, I., Peereboom, L., Miller, D.J. Continuous condensed-phase ethanol conversion to higher alcohols: Experimental results and techno-economic analysis. Journal of Cleaner Production. **2019**, 209: 1365-1375.

18. Liu, Y., Shao, Z., Wang, Y., Xu, L., Yu, Z., Liu, Q. Manganese-Catalyzed Selective Upgrading of Ethanol with Methanol into Isobutanol. ChemSusChem **2019**, 12 (13) : 3069-3072.

19. Bauer, F., Hulteberg, C. Isobutanol from glycerine – A techno-economic evaluation of a new biofuel production process. *Appl. Energy* **2014**, 122: 261-268.

20. Subramanian, N., Adeyinka, A., Spivey, J.J. Catalytic conversion of syngas to i-butanol - Synthesis routes and catalyst developments: A review. Catalysis **2013**, 26:161-178.

21. Opdyke, D. L. J. Isobutyl acetate. Food and Cosmetics Toxicology **1978** 16: 795-796.

22. ECHA. Isobutyl Acetate. Substance Information. European Chemicals Agency. https://echa.europa.eu/substance-information/-/substanceinfo/100.003.406 (Consulted Sept. 18, 2019).

23. Altıokka, M., Çıtak, A. Kinetics study of esterification of acetic acid with isobutanol in the presence of amberlite catalyst. Applied Catalysis A: General, **2003**, 239 (1–2): 141-148.

24. Izci, A., Bodur, F. Liquid-phase esterification of acetic acid with isobutanol catalyzed by ion-exchange resins. *React. Funct. Polym.* **2007**, 67: 1458-1464.

25. Izci, A., Uyar, E., Izci, E. Determination of adsorption and kinetic parameters for synthesis of isobutyl acetate catalyzed by amberlite IR-122. *Chem. Eng. Commun.* **2009** 196: 56-67.

26. Çıtak A. Application of Ion Exchange Resins in the Synthesis of Isobutyl Acetate. In: Inamuddin D., Luqman M. (eds) *Ion Exchange Technology II*. Springer, Dordrecht. pp 137-148, **2012**.

27. Muñoz, R., Montón, J.B., Burguet, M.C., de la Torre, J. Separation of isobutyl alcohol and isobutyl acetate by extractive distillation and pressure-swing distillation: simulation and optimization. Sep. Purif. Technol. **2006**, 50, 175–183.

28. Korkmaz, S., Salt, Y., asanoglu, A., Ozkan, S., Salt, I., Dincer, S. Pervaporation membrane reactor study for the esterification of acetic acid and isobutanol using polydimethylsiloxane membrane. Applied Catalysis A: General **2009** 366 (1): 102-107.

29. Korkmaz, S., Salt, Y., Dincer, S. Esterification of acetic acid and isobutanol in a pervaporation membrane reactor using different membranes. *Ind Eng. Chem. Res.* **2011** 50: 11657-11666.

30. Patidar, P., Mahajani, S. Esterification of fusel oil using reactive distillation Part II: Process Alternatives. Ind. Eng. Chem. Res. **2013** 52, (47): 16637-16647.

31. Cho, S.J., Shin, J.S., Choi, S.H., Lee, E.S., Park, S.J. Optimization study for pressure swing distillation process for the mixture of isobutyl-acetate and isobutyl-alcohol system *Korean Chem. Eng. Res.* **2014** 52: 307-313.

32. V.H. Agreda, L.R. Partin, Reactive distillation process for the production of methyl acetate, US4435595A, 1984. https://patents.google.com/patent/US4435595A/en?q=%2b+methyl+acetate&assignee=eastman+kodak&oq=eastman+kodak+%2b+methyl+acetate.

33. M. Klöker, E.Y. Kenig, A. Górak, A.P. Markusse, G. Kwant, P. Moritz, Investigation of different column configurations for the ethyl acetate synthesis via reactive distillation, Chem. Eng. Process. Process Intensif. 43 (2004) 791–801. doi:10.1016/S0255-2701(03)00084-9.

34. W. Osorio-Viana, M. Duque-Bernal, J.D. Quintero-Arias, I. Dobrosz-Gómez, J. Fontalvo, M.Á. Gómez-García, Activity model and consistent thermodynamic features for acetic acid–isoamyl alcohol–isoamyl acetate–water reactive system, Fluid Phase Equilibria. 345 (2013) 68–80. doi:10.1016/j.fluid.2013.02.006.

35. Horsley, L.H. (ed.) Tables of Azeotropes and Nonazeotropes, in: *Azeotropic Data—III*, American Chemical Society, Washington, D. C., pp. 1–613. **1973**. doi:10.1021/ba-1973-0116.ch001.

36. Zong, Z. L., Yang, X. H., Zheng, X. Y. Determination and correlation of vapor-liquid of alcohol solutions J. Chem. Eng. Jpn. **1983** 16: 1–6. doi:10.1252/jcej.16.1.

37. Stockhardt, J. S., Hull, C.M. Vapor-liquid equilibria and boiling-point composition relations for systems n-butanol–water and isobutanol–water Ind. Eng. Chem. **1931** 23: 1438–1440. doi:10.1021/ie50264a034.

38. Yushu, C., Afef, A., Fabrice, M., Roland, S., Jeday, M. R. Thermodynamic Modeling of Mixtures Containing Carboxylic Acids Using the PC-SAFT Equation of State, Ind. Eng. Chem. Res. **2012** 51: 13846–13852. doi:10.1021/ie301930q.

39. Amezaga, S. A.; Biarge, J. F. Liquid-vapor equilibrium in systems formed by acetic acid and propyl, isopropyl, isobutyl, sec-butyl, and tert-butyl alcohols at 760 mm, An. Quim., 1973, 69, 587.

40. Burguet, M. C., Montón, J. B., Muñoz, R., Wisniak, J., Segura, H. Polyazeotropy in Associating Systems: The 2-Methylpropyl Ethanoate + Ethanoic Acid System, J. Chem. Eng. Data. **1996** 41: 1191–1195. doi:10.1021/je960159k.

41. Zhang, C., Wan, H., Xue, L., Guan, G. Investigation on isobaric vapor liquid equilibrium for acetic acid+water+(n-propyl acetate or iso-butyl acetate), Fluid Phase Equilibria. **2011** 305: 68–75. doi:10.1016/j.fluid.2011.03.006.

42. Montón, J. B., Muñoz, R., Burguet, M. C., de la Torre, J. Isobaric vapor–liquid equilibria for the binary systems isobutyl alcohol+isobutyl acetate and tert-butyl alcohol+tert-butyl acetate at 20 and 101.3kPa, Fluid Phase Equilibria. **2005** 227: 19–25. doi:10.1016/j.fluid.2004.10.022.

43. Linek, J. Vapour-liquid equilibrium in the isobutyl alcohol-isobutyl acetate binary system, Collect. Czechoslov. Chem. Commun. **1977** 42: 2469–2473.

44. Liu, H., Cui, X., Zhang, Y., Feng, T., Zhang, K. Isobaric Vapor–Liquid Equilibrium for the Binary and Ternary System with Isobutyl Alcohol, Isobutyl Acetate and Dimethyl Sulfoxide at 101.3 kPa, J. Chem. Eng. Data. **2017** 62: 1902–1909. doi:10.1021/acs.jced.7b00241.

45. Zhang, J.; Zhang, Y.; Fu, J.; Wang, X., Prediction of Partially Miscible System by VLE Data. Chemical Engineering (China), 1986, No. 4, 53-57.

46. Bomshtein, A. L.; Trofimov, A. N.; Gotlib, V. A.; Serafimov, L. A. Liquid-liquid phase equilibrium in isobutyl acetate-water and isobutyl acetate-water-acetic acid systems at normal temperature. Zh. Prikl. Khim. (Leningrad), 1978, 51, 440-442.

47. Cháfer, A., Lladosa, E., de la Torre, J., Burguet, M.C. Study of liquid–liquid equilibrium of the systems isobutyl acetate+acetic acid+water and isobutyl alcohol+acetic acid+water at different temperatures, Fluid Phase Equilibria. **2008** 271: 76–81. doi:10.1016/j.fluid.2008.07.001.

48. Procházka, J., Heyberger, A. Correlation of ternary liquid-liquid equilibria in system isobutyl acetate-acetic acid-water Chem. Eng. Sci. **1996** 51: 893-903

49. D. Xu, C. Wu, Q. Zhang, H. Zhang, Y. Wang, J. Gao, Liquid–liquid equilibrium for the ternary systems water+2-methyl-1-propanol+butyl acetate and water+2-methyl-2-propanol+butyl acetate at (298.15 and 323.15)K, Fluid Phase Equilibria. 381 (2014) 60–66. doi:10.1016/j.fluid.2014.08.014.

50. Cháfer, A., de la Torre, J., Monton, J.B., Lladosa, E. Liquid-liquid equilibria of the systems isobutyl acetate + isobutyl alcohol + water and isobutyl acetate + isobutyl alcohol + glycerol at different temperatures. Fluid Phase Equilibr. **2008** 265: 122-128

51. Killian, W., Bala, A., Peereboom, L., Stoner, J., Norfleet, A., Jackson, J. Lira, C. An Improved Spectroscopic Method for Determination of Association/Solvation Parameters Used in Process Models. AIChE Annual Meeting Nov. 10-15, Orlando, Fl. USA. **2019**

52. Christensen, S. P., Olson, J.D. Phase equilibria and multiple azeotropy of the acetic acid-isobutyl acetate system, Fluid Phase Equilibria. **1992** 79: 187–199. doi:10.1016/0378-3812(92)85129-V.

53. H. Renon, J.M. Prausnitz, Local compositions in thermodynamic excess functions for liquid mixtures, AIChE J. 14 (1968) 135–144. doi:10.1002/aic.690140124.

54. J.G. Hayden, J.P. O'Connell, A Generalized Method for Predicting Second Virial Coefficients, Ind. Eng. Chem. Process Des. Dev. 14 (1975) 209–216. doi:10.1021/i260055a003.

55. Othmer, D., Tobias, P. Liquid-Liquid Extraction Data - The Line Correlation, Ind. Eng. Chem. **1942** 34: 693–696. doi:10.1021/ie50390a600.

56. J. M. Prausnitz, C. A. Eckert, R. V. Orye, J. P. O'Connell, Computer calculations for multicomponent vapor-liquid equilibria, Prentice-Hall, Englewood Cliffs, New Jersey, 1962.

57. Zhang, C, Wan, H., Xue, L., Guan, G. Investigation on isobaric vapor liquid equilibrium for acetic acid+water+(n-propyl acetate or iso-butyl acetate), Fluid Phase Equilibria. **2011** 305: 68–75. doi:10.1016/j.fluid.2011.03.006.

58. M. Doherty, M. Malone, Conceptual design of distillation systems. McGraw–Hill, New York, 2001.

59 D. Barbosa, M. F. Doherty, Design and minimum reflux calculations for single-feed Multicomponent reactive distillation columns, Chem. Eng. Sci., 43 (1988a) 1523-1537. DOI: 10.1016/0009-2509(88)85144-3

60 D. Barbosa, M. F. Doherty, The simple distillation 782 of homogeneous reactive mixtures. Chem. Eng. Sci., 43 (1998b) 541-550. DOI: 10.1016/0009-
784 2509(88)87015-5

61 Y. V. Gurikov. Structure of the vapor–liquid equilibrium Diagrams of ternary homogeneous solutions. Russ. J. Phys. Chem. 32 (1958) 1980–1996.

62 L. A. Serafimov, V. T. Zharov, V. S. Timofeyev. Rectifcation of multicomponent mixtures I. Topological analysis of liquid–vapor phase equilibrium diagrams. Acta Chim. Acad. Sci. Hung. 69 (1971) 383–396.

63 L. A. Serafimov. Thermodynamic and Topological Analysis of Liquid-Vapor Phase Equilibrium Diagrams and Problems of Rectification of Multicomponent Mixtures. In: *Mathematical Methods in Contemporary Chemistry*, S.I. Kuchanov (Ed.) Gordon and Breach Publishers, Amsterdam pp. 557- 605. 1996.

64 L. A. Serafimov, A. Frolkova, T. V. Chelyuskina. Konovalov's First Law Validity for Multicomponent Azeotropic Mixtures. Theor. Found. Chem. Eng. 42 (2008) 171–178. DOI: 10.1134/S0040579508020097

65 L. A. Serafimov, O. B. Razova, A. Frolkova, T. V. Chelyuskina. The Gibbs–Konovalov Law at Simple Singular Points of Two-Phase Multicomponent System Diagrams. Russ. J. Phys. Chem. A. 82 (2008) 946–950. DOI: 10.1134/S0036024408060149

66 L. A. Serafimov, O. B. Razova, A. V. Frolkova, T. V. Chelyuskina. Observance of the Gibbs–Konovalov Law at Complex Singular Points of Two- Phase Multicomponent Systems. Theor. Found. Chem. Eng. 42 (2008) 415– 420. DOI: 10.1134/S004057950804009X

67 L. A. Serafimov, A. Frolkova. Determination of vapor–liquid equilibrium diagrams of multicomponent systems. Chem. Pap. 70 (2016) 1578–1589. DOI: 10.1515/chempap-2016-0091

68 V. Zhuchkov, A. Malyugin, A. Frolkova, F. 816 Alla. Double Ternary Azeotrope in the Benzene + Perfluorobenzene + Water System at 101 kPa. J. Chem. Eng Data 65 (2020) 2002-2007. DOI: 10.1021/acs.jced.9b01149

69. Kiva, V. N., Hilmen, E. K., Skogestad, S. Azeotropic phase equilibrium diagrams: a survey, Chem. Eng. Sci. **2003** 58: 1903–1953. doi:10.1016/S0009-2509(03)00018-6.

70.Hilmen, E.K., Kiva, V.N., Skogestad, S. Topology of ternary VLE diagrams: Elementary cells, AIChE J. **2002** 48: 752–759. doi:10.1002/aic.690480410.

CHAPTER 2.

KINETIC STUDY ON THE CATALYTIC ESTERIFICATION OF ACETIC ACID WITH ISOBUTANOL OVER AMBERLYST 15.

This section includes a copy of the paper: Martinez, A. F., Sanchez, C. A., Orjuela, A., Gil, I. D., Rodriguez, G. 2020. Kinetic study on the catalytic esterification of acetic acid with isobutanol over Amberlyst 15. Chem. Eng. Res. Des. Currently In revision

The paper is reformatted and figures and tables are enlarged to fulfill edition requirements for the dissertation document.

2. Kinetic study on the catalytic esterification of acetic acid with isobutanol over Amberlyst 15.

2.1. Summary

This work deals with kinetic modeling in the production of isobutyl acetate by liquid-phase esterification of isobutanol with acetic acid, in presence of the heterogeneous catalyst Amberlyst 15. Based upon a statistical experimental design, isothermal batch experiments were performed in the temperature range of 343.15-373.15 K, at three different catalyst loadings, and at different acid to alcohol mole ratios (1:1, 2:1 and 1:2). Preliminary experiments were run to assess the effects of internal and external mass transfer phenomena, and they were rule out based upon the Weisz−Prater criterion. Thus, further experiments were run at stirring rates of 800 RPM, and catalyst particle diameters under 300 μm to ensure a kinetic regime. Independent experiments were run to obtain the chemical equilibrium constant at different temperatures and by mean of a van't Hoff equation, a ΔH_R of 16.47 kJ/mol was obtained. Incorporating the equilibrium constant, the kinetic experimental data were regressed with a molar fraction-based pseudo homogeneous model. The obtained model accurately fits experiments and it can be used for further simulation of reactive distillation processes for isobutyl acetate production.

Keywords. Isobutyl acetate, Esterification, Chemical equilibrium, Kinetics, Amberlyst 15.

2.2. INTRODUCTION

Global environmental impacts caused by human activity have motivated changes in how people perceive and consume products, with a growing awareness about their origin and their impacts during final use and post-consumption. This new trend and the increasing environmental regulations and public policies have pressured a transition from fossil-based products toward biobased and renewable ones. This pressure has been particularly endured on the chemical industry, which has been urged to develop more sustainable products for the society. In particular, within the chemical industry, the solvents segment is under continuous scrutiny because they are used in massive volumes, in a wide variety of processes, and in numerous consumer products (e.g. paints, coatings, inks, household, personal care, and clean products, etc.). As they are

mostly released to the environment during or after use, regulations have been intensifying in recent years for their control, management and disposal. Consequently, different tools for the identification and selection of sustainable solvents for the chemical and pharmaceutical industry have been recently developed [1, 2].

Among the variety of alternative chemicals, medium and high molecular weight biobased alcohols and esters have been found suitable and more sustainable substitutes for most problematic solvents. Particularly, some of these components can be directly obtained via microbial pathways [3, 4], as side products from bioethanol production (e.g. fusel oils) followed by further esterification [5, 6], and also by catalytic processing of bioethanol (e.g. Guerbet reactions) [7]. Among the variety of biobased alcohol and esters, isobutanol and isobutyl acetate are considered main target green solvents because their biodegradability, low surface tension, and high electrical resistance. They are also desirable value-added ingredients for the fragrance and flavor industry, because their organoleptic and functional properties [8, 9]. Isobutanol (IbOH) can be produced by fermentation pathways [10-12], and further esterified to Isobutyl acetate (IbAC) by Fisher esterification with acetic acid (ACAC) as presented in Figure 2.1.

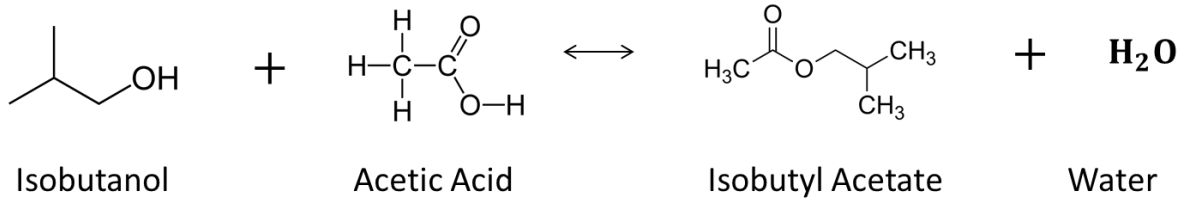

Figure 2.1. Esterification reaction of acetic acid with isobutanol.

Industrially, esterification of IbOH with ACAC is mainly promoted by acid homogeneous catalysts [13-15]. However, due to the required sensory profile for fragrance and flavor applications [16, 17], heterogeneous catalysts such as ion exchange resins are preferred [18]. While these catalysts normally exhibit less activity, they are more selective, less corrosive, they reduce side oxidation reactions and are easily removed avoiding neutralization or product contamination [18]. In addition to the reduced activity of heterogeneous catalysts, a main challenge to obtain high purity IbAC is the chemical equilibrium limitation [13-15]. In order to overcome these issues, esterification could be carried out via reactive distillation, enabling higher conversions and energy savings [19]. Despite this process has been successfully applied in different esterification process, there is need to assess if this technology is suitable for the specific case of

IbAC production. This is particularly important because the quaternary esterification mixture (ACAC+IbOH+IbAC+H_2O) exhibits a highly non-ideal behavior with multiple azeotropes, immiscibility in the liquid phase, and un-common mutiazeotropy phenomena [20]. In this case it is necessary to assess if reaction and distillation can work effectively under the same range of conditions, thus avoiding very large equipment (i.e. slow kinetics) or separation difficulties.

In order to explore the feasibility of a reactive distillation process for IbAC production, there is need to develop a conceptual design of the operation based upon a validated kinetic model. In this direction, this chapter focuses on the kinetic study of the Fisher esterification between isobutanol and acetic acid using Amberlyst 15 as catalyst. Preliminary experiments helped to rule out mass transfer limitations during experiments, and the Weiss-prater criteria was used as surrogate for ensuring kinetic regime. Experiments were carried out based upon a suitable experimental design considering temperature, catalyst loading and reactant molar ratio, as main variables to adjust a kinetic model of the reaction. Additional experiments were carried out to explore the chemical equilibrium condition at different temperatures. The whole set of experimental data were correlated with mole fraction-based kinetic expression.

2.3. Experimental Details

2.3.1. Materials

The list of chemicals used during experiments and their corresponding purity and grade are summarized in Table 2.1. The purity of chemicals was verified by gas chromatography, and they were used without additional purification. Deionized water was obtained in situ and a conductivity below 0.4 µS was verified with a Martinn CM-230 conductivity Monitor. Acetone and Dioxane were used as solvent and internal standard respectively, during chromatographic analysis. Amberlyst 15 catalysts was supplied by Dow-Dupond, and Table 2.2 lists main characteristics [21].

Table 2.1. List of chemicals used during kinetic experiments

Compound	CAS	Grade	Supplier	Purity (% Wt.)*
Acetic acid	64-19-7	Glacial	PanReac	≥ 99.9
Isobutanol	78-83-1	Pure	PanReac	≥ 99
Isobutyl acetate	110-19-0	USP	PanReac	≥ 99

Acetone	67-64-1	Analysis	Sigma Aldrich	≥ 99.5
Dioxane	123-91-1	Analysis	Sigma Aldrich	≥ 99.9

*Reported by manufacturer.

Table 2.2. Physicochemical properties of Amberlyst 15 catalysts

Parameter	Value
Presentation	Amber spherical beads
Matrix	Styrene-divinylbenzene, macrcoporous
Functional group	Sulfonic Acid
Ionic form	H^+
Acid sites concentration (H^+/Kg of dry solid)	≥4.95
Surface area (m^2/g)	53
Average pore diameter (A)	300
Dry solid effective size (µm)	650-800
Pore Volume (cc/g)	0.40
Water retention capacity	52-57%
Maximum operating temperature (K)	393

2.3.2. Catalyst pretreatment

Amberlyst 15 was pre-treated by washing several times in a stirred container for 2 hours with deionized water with a volumetric ratio of 1:4. This process was conducted until the conductivity of the rinsing water was that of the deionized water. Afterwards, it was washed three times with anhydrous ethanol with a solid:liquid volumetric ratio of 1:4 for 2 hour, in order to remove remaining water or any other organic compound in the porous media. Subsequently, the solid was subjected to drying in a vacuum oven at 50°C and absolute pressure of 41 kPa until the mass of the resin remained constant. Once dried, the catalysts was sieved and separated in the following fractions of different particle sizes (in µm): $\varphi<250$; $250<\varphi<300$; $300<\varphi<425$; $425<\varphi<500$; $400<\varphi<500$. These particle sizes corresponded to the standard Tyler series of mesh sieves No. 100, 60, 50, 40 and 30, respectively. Finally the resin was stored in a hermetic container within a vacuum oven until final use. The ion exchange capacity of the resin was measured after the pre-treatment process to ensure its stability using a standard method previously described [22], and the concentration of acid sites was 4.90 ± 0.12 eq/dry kg.

2.3.3. Reaction equipment setting and experimental procedures

Kinetic experiments were carried out under isothermal conditions using three 150 ml stainless steel batch jacketed reactors. A scheme of the experimental set up is presented in Figure 2.2.

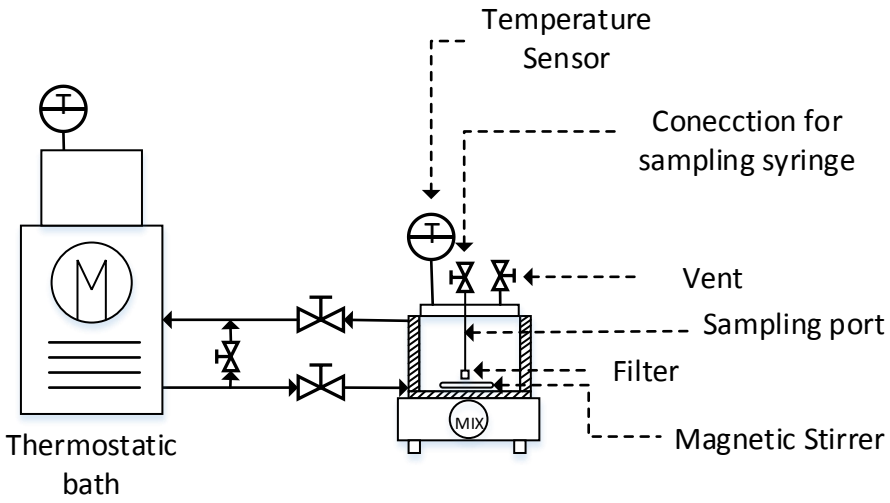

Figure 2.2. Scheme of batch reaction system used for kinetic experiments

The operating temperature was controlled by oil circulation from a controlled thermal bath. Each reactor was positioned over a stirring plate for magnetic stirring, and the temperature was monitored with a thermocouple inserted in a submerged thermowell. The reactor had a vent valve and a submerged sampling port with valve and a stainless steel filter at the end to avoid catalyst removal. Samples from reactors were withdrawn with disposable syringes, transferred into hermetic glass containers, and stored under refrigerated conditions at 269 K prior to chromatography quantification.

The experimental procedure for every kinetic experiments involved different stages. Initially, one reactant and the defined amount of catalyst were loaded in the reactor, the thermostatic bath was started and set at 10 K below the desired reaction temperature, and the magnetic stirring was started. In parallel, the other reactant was loaded in a jacketed syringe to adjust the temperature 5 K above the desired reaction temperature. Then, when both reactants were at the specified conditions, the reactant in the syringe was loaded into the reactor through the vent valve; at this point the reaction time was initiated. Samples from reaction were taken at the following times: 10, 20, 30, 45, 60, 75, 105, 135, 165, 225, 285 and 345 minutes. Each sample was collected and

immediately stored in a fridge to quench reaction until chromatography characterization.

2.3.4. Analysis

Liquid samples withdrawn from the reactors during kinetic experiments were analyzed by gas chromatography using a Shimadzu 2010 plus with a flame ionization detector. The samples were prepared by dissolving 100 mg of sample in 700 mg of Acetone, and adding 40 mg of Dioxane as Internal standard. A SGE Analytical Science column of 30 m x 0.32 mm x 0.25 µm with stationary phase BP-20 was used (SGE S/N 1270516). High purity chromatography grade Helium was used as carrier gas. Detector temperature was set on 523.15 K and injector port temperature was maintained at 523.15 K. Calibration was carried out by analyzing mixtures of known composition, prepared by a gravimetric method using a balance (± 0.001 g). As the FID detector is not suitable for water determination, its content was obtained by stoichiometry. This procedure was calibrated by analyzing samples of known composition, and maximum deviation of 3 % were observed.

2.3.5. Experimental planning

2.3.5.1. Preliminary tests

Before performing the kinetic study, the absence of mass transfer limitations at the experimental conditions was verified. Intra-particle and extra-particle limitations were evaluated by performing reactions under different catalyst particle sizes, and different stirring rates, respectively. For the exploration of external mass transfer limitations, three different reactions were performed using the same amount of catalyst, temperature and reactant ratio, varying the stirring rate at 600, 800 and 1000 RPM. The detailed experimental conditions are summarized in Table B1 in the annexes B. For the assessment of internal mass-transfer effects on the reaction rate, the reaction experiments were performed with different catalyst particle sizes (MESH 30, 40, 50, 60 and 100). Experimental conditions during these experiments are reported in Table B2 in the annexes B. To assure that the intra-particle mass transfer limitations where negligible, the Weisz-Prater module (Φ_W) was analyzed. According to this criterion, the intraparticle mass transfer limitations can be neglected when the module is considerably less than 1 [23, 24].

2.3.5.2. Chemical equilibrium condition

The chemical equilibrium constant for the esterification reaction was determined experimentally at three different temperatures. In this case, reaction experiments were run as above described, but without catalyst and for several days (minimum 10 days). Reaction media was monitored until no variation in composition was observed. Once the equilibrium condition was reached, liquid media was analyzed, and Equation 2.1 was used to calculate the value of the molar fraction-based equilibrium constant ($K_{eq,x}$).

$$K_{eq,x} = \prod_{i=1}^{4} x_i^{v_i} \quad (2.1)$$

Here, x_i is to the molar fraction of each component *i*, and v_i is the corresponding stoichiometric coefficient.

2.3.5.3. Kinetic experimental design

A suitable experimental design was planned in a similar way to other kinetic studies on esterification reactions [13, 15, 25, 26]. This involved a central composite design (i.e. Box-Behnken) with three variables at three levels. The design considered the catalyst loading, reaction temperature, and reactants molar ratio. Reaction temperature was evaluated at 343.15, 353.15 and 363.15 K, and the assessed levels of acid:alcohol molar ratio were 1:1, 1:2 and 2:1. The catalyst loading was based upon the same acid equivalents corresponding to sulfuric acid loading of 0.25%, 0.75% and 1.5% wt. with respect to the total weight of the reactive mixture. The complete set of experiments and the corresponding conditions are summarized in the Table B3 from the annexes B.

2.3.6. Kinetic model description and regression procedure

Esterification kinetics was described with a pseudo-homogeneous power law kinetic model, assuming a first order for each reactant, and employing an Arrhenius-type temperature dependence. Once the absence of mass transfer limitations was verified, the kinetic expression was considered linearly dependent on the catalysts loading. Thus, the corresponding molar fraction-based kinetic model is described in Equation 2.2.

$$r = C_{cat} k_{cat} \left(x_{ACAC} x_{IbOH} - \frac{x_{IbAC} x_{water}}{K_{EQ}} \right) \quad (2.2)$$

Here r is the reaction rate per volume of liquid mixture (kmol/m^3.s), $k_{cat,i}$ is the kinetic constant (kmol/kg$_{CAT}$.s), C_{cat} is the catalyst concentration with respect to the liquid phase (kg$_{CAT}$/m^3), and K_{EQ} is the molar fraction-based equilibrium constant. The kinetic constant can be represented by the Arrhenius equation as in Equation 2.3.

$$k_{Cat} = k_{o,Cat} \exp\left[\frac{-Ea_{cat}}{RT}\right] \quad (2.3)$$

As usual, Ea_{cat} is the energy of activation (kJ/mol) and $k_{o,Cat}$ is the pre-exponential factor (kmol/m^3.s). The mole balance of every component *i* in a batch reaction along time can be described as follows:

$$\frac{dn_i}{dt} = Vr \quad (2.4)$$

Here, n_i is the number of moles of component i, and V the volume of the reactive media. As the total number of moles of the reactive system is constant, and assuming a constant liquid volume, Equation 2.4 can be calculated in terms of the total molar concentration of the liquid phase C_T as:

$$\frac{dx_i}{dt} = -\frac{r_i}{C_T} \quad (2.5)$$

Integrating Equation 2.5 for every component at the corresponding conditions of the kinetic experiments (Table B3), it was possible to adjust the kinetic parameters of Equation 2.2. Model regression was done using the *fmincon* function from Matlab R2018a. This function attempts to minimize the squares differences between the measured and predicted compositions of all components along time during batch reactions. Integration of Equation 2.5 was done using a fourth grade Runge-Kutta method implemented in the "*ode45*" integrator. In this case, the minimization was done varying the energy of activation and the pre-exponential factor.

2.4. RESULTS AND DISCUSSION

2.4.1. External and Internal Mass Transfer Resistances

Results from the preliminary experiments indicate that the external mass-transfer resistance was negligible when the stirring rate is above 800 rpm. In Figures 2.3., are presented the corresponding kinetic profiles along time for reaction experiments run under different stirring rates. The corresponding rates of reactions are plotted in Figure B1 in the annexes B. Experimentally it was observed that when using higher stirring rates (>900 RPM), the catalyst got pulverized and it was partially removed through the filter of the sampling port during samples withdrawal. Thus, further reactions were performed at 800 rpm.

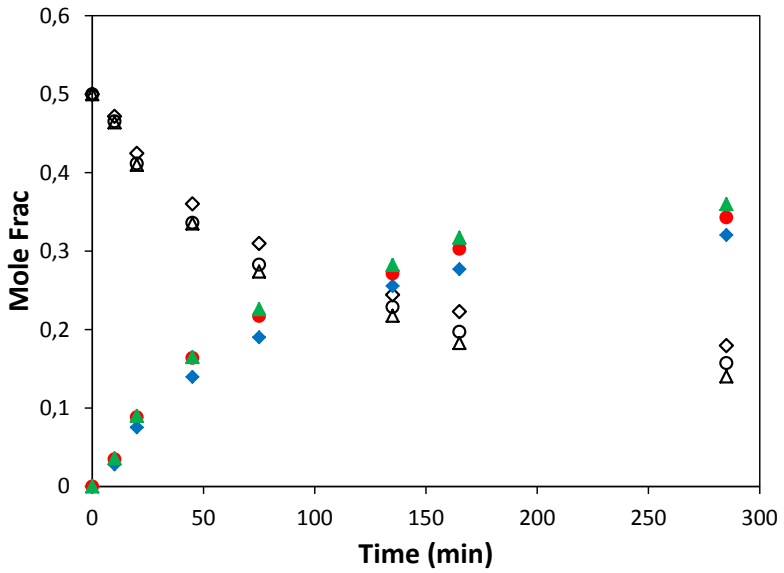

Figure 2.3. Esterification of acetic acid with Isobutanol using Amberlyst 15 as Catalyst, at three different stirring velocity (600, 800 ad 1000 RPM's). Feed molar ratio, 1:1; Temperature, 363.15 K; Catalyst loading equivalent to Sulfuric Acid at 0.75% wt. Filled markers ACAC at (♦) 600 RPM. (●) 800 RPM. (▲) ACAC - 1000 RPM. Void markers IbAC at (◊) 600 RPM. (○) 800 RPM. (Δ) 1000 RPM.

The kinetic profiles obtained during experiments run with different catalyst particle sizes are presented in Figure 2.4. As observed, there was no significant changes in the rate of reaction among the different experiments when using particle sizes below 300 µm. Thus, as the internal mass-transfers limitations could be neglected when operating with catalyst particle sizes below this level, further kinetic experiments were run with particle sizes below 50 MESH. For confirmation, the Weisz-Prater module was calculated for experiments run with different catalysts particle sizes.

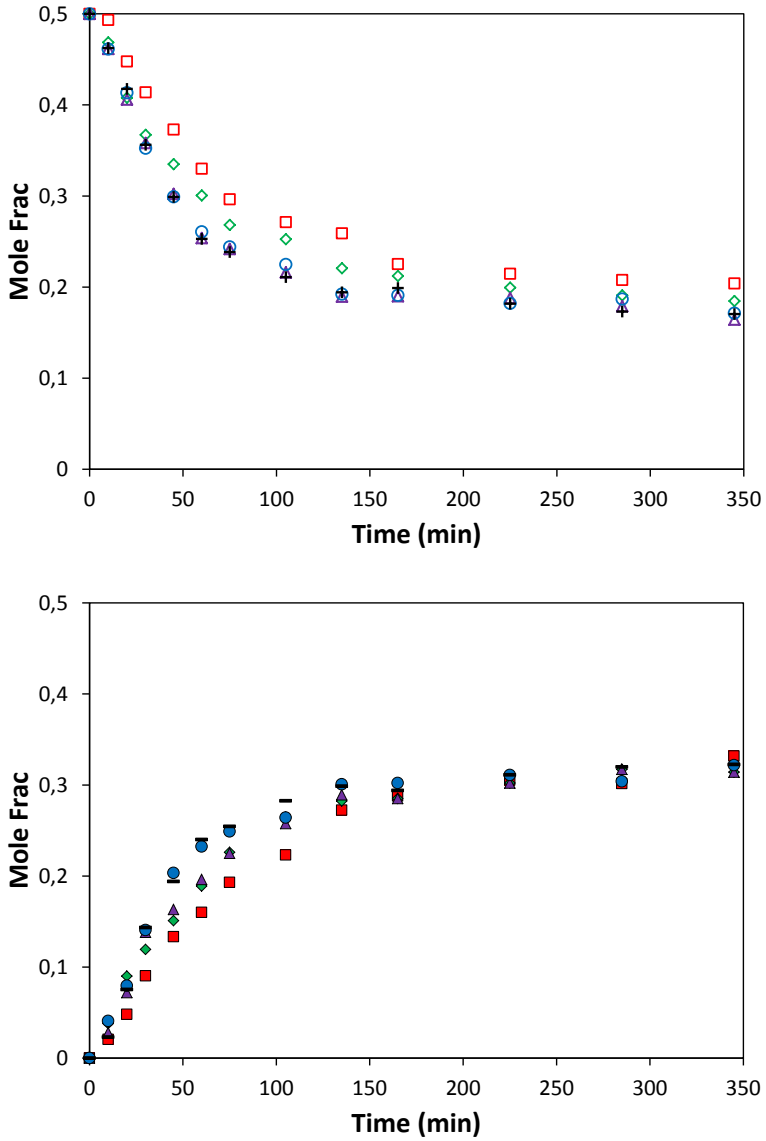

Figure 2.4. Esterification of acetic acid with Isobutanol using Amberlyst 15 as Catalyzer, at five different catalyst particle diameter (30, 40, 50, 60 and 100 MESH size). Feed molar ratio, 1:1; Temperature, 363.15 K; Catalyst loading 0.75% wt. equivalent to Sulfuric Acid. (□) ACAC - 30 MESH. (◊) ACAC -40 MESH. (Δ) ACAC - 50 MESH. (○) ACAC - 60 MESH. (**+**) ACAC - 100 MESH. (■) IbAC - 30 MESH. (♦) IbAC - 40 MESH. (▲) ACAC - 50 MESH. (●) ACAC - 60 MESH. (**-**) ACAC - 100 MESH.

Equation 2.6 presents the corresponding Weisz-Prater module for spherical particles.

$$\Phi_W = \frac{r'_{obs}\ \rho_{Cat}}{D_e\ C_{CAo}} * \left(\frac{d_p}{6}\right)^2 \qquad (2.6)$$

Here, r'_{obs} is the observed rate of reaction per mass of catalyst, d_p is the catalyst particle diameter, ρ_{Cat} is the density of the catalyst, C_{CAo} is the initial concentration of

acetic acid in the liquid bulk, and D_e is the effective diffusivity of the acid calculated by the Wilke-Chang model [27, 28]. Here r'_{obs} is the ratio between the reaction rate per unit of volume of reaction liquid (r_{obs}) and the catalyst loading w'_{cat}, and the density of the liquid phase (ρ_{sol}):

$$r'_{obs} = \frac{r_{obs}}{w'_{cat}\ \rho_{sol}} \tag{2.7}$$

The particle diameter could be calculated using Equation 2.8, based on the diameter and volume of the dry particle (d_{pdry}, V_{dry}), and diameter and volume of the swollen particle ($d_p, V_{Pswollen}$). Different reports indicate that Amberlyst 15 can swell up to two times the volume of the dry particle when being in contact with an alcohol. Thus, the swollen catalyst density has been reported to be around 1000 kg/m^3 [29].

$$\frac{d_p}{d_{pdry}} = \sqrt[3]{\frac{V_{Pswollen}}{V_{dry}}} \tag{2.8}$$

A summary of the properties and parameters used for calculating the Weisz-Prater criterion are presented in Table 2.3.

Table 2.3. Weisz-Prater criteria evaluation for mass transfer resistance at initial reaction conditions.

Parameter	**Value**	
$\rho_{cat}(Kg/m^3)\ (swollen)$	1000	
$d_p\ (\mu m)$ (swollen)	377	
C_{ACAC_0} (Kmol/m^3)	0.6699	
$w_{cat}\ (Kg_{cat}/Kg_{sol})$	0.0308	
IbOH association factor - Wilke-Chang	1.5	
ε	0.57	
Experimental Run	T90°C	T100°C
T(K)	363.15	373.15
r_{obs} (Kmol ACAC/m^3) (1/s)	1.293 x 10^{-6}	2,624 x 10^{-6}
ρ_{sol} (Kg/m^3)[a]	841.7	828.8
μ_{liq} (cP)[a]	0.574	0.497
D_{ACAC} (m^2/s)	1.479 x 10^{-5}	1.752 x 10^{-5}
D_{eff} (m^2/s)	4.806 x 10^{-6}	5.693 x 10^{-6}

Φ_w	0.1404	0.145
ϕ	0.383	0.391
η	0.953	0.961

[a] Calculated in Aspen Plus® v.10.3

As observed, the effectiveness factor are 0.953 and 0.961 for 363.15K and 373.15 K, respectively, and in both cases, the Weisz-Prater value are well below the unity. This confirms the absence of intra-particle mass transfer limitations observed in the kinetic profiles of Figure 2.4. Based on this result, further kinetic experiments were performed with catalysts particle sizes below 0.3 mm.

2.4.2. Effect of reactants molar ratio and catalyst loading

Kinetic profiles from experiments run with different initial molar ratio of reactants (Alcohol to Acid 2:1, 1:1 and 1:2) are presented in Figure B3 (i.e. IbAC mol fraction) and Figure B4 (i.e. Extent of reaction). Similarly to the synthesis of acetates of different alcohols [18, 21, 25, 26], as well as for isobutanol [13-15], the reaction order of each component is one. It was also observed that the autocatalytic effect of the reaction is very small compared with the catalyzed reaction and it can be neglected. The effect of the catalyst concentration in the reaction can be observed in kinetic profiles of Figure B5 in the annexes B. From these data, the initial rate of reaction was obtained as the slope of the concentration of the limiting reactant with time at the beginning of each experiment. The corresponding linear dependence of the rate of reaction with the catalyst loading can be verified in Figure B6, confirming that experiments were run under a kinetic regime.

2.4.3. Chemical equilibrium Constant.

The molar fraction based equilibrium constant ($K_{eq,x}$) was calculated using Equation 2.4, and the obtained values were in the range of 3.5 to 4.8. The obtained data were correlated with a van't Hoff type expression, and the obtained profile is presented in Figure 2.5. The linear tendency of the obtained plot is consistent with a slightly endothermic reaction, and the corresponding heat of reaction was 16.47 KJ/mol, which is similar to the reported for esterification reactions [13-15, 21].

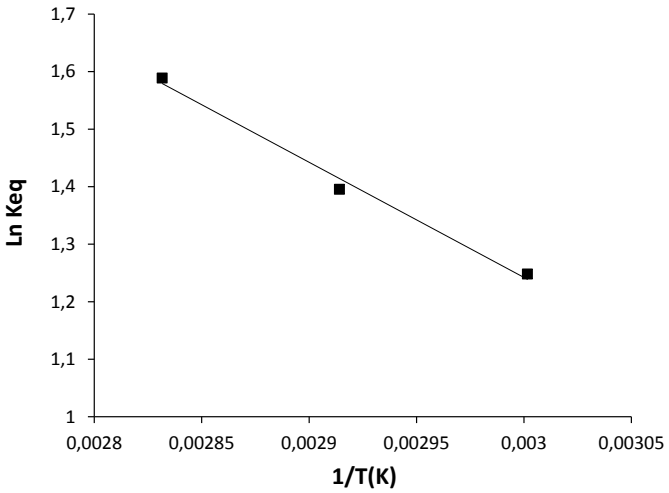

Figure 2.5. Chemical equilibrium constant for the esterification of acetic acid with Isobutanol, at three different temperatures (333.15 K; 343.15 K; 353.15 K) using equimolar feed.

2.4.4. Kinetic experiments and parameters regression

As expected and observed in Figure 2.6, temperature was the variable with the major impact over the reaction rate and the final conversion. The rate of reaction increases more than double with a 30 K increase in temperature, and the equilibrium condition is achieved is shorter times when operating at the highest temperature. The kinetic profiles of the whole set of experiments of Table B3 are presented in Figures B8 to B15 of the annexes B. Using these data, the corresponding kinetic parameters of Equation 2.3 were obtained, and they are presented in Table 2.4. The obtained activation energy was lower to that observed for the self-catalytic reaction (59.3 kJ/mol) [13, 14], and still lower than that of a similar ion exchange resin catalysts Amberlite IR-120 (49 kJ/mol, [14]). This indicates that Amberlyst 15 exhibits a better performance for the esterification reaction.

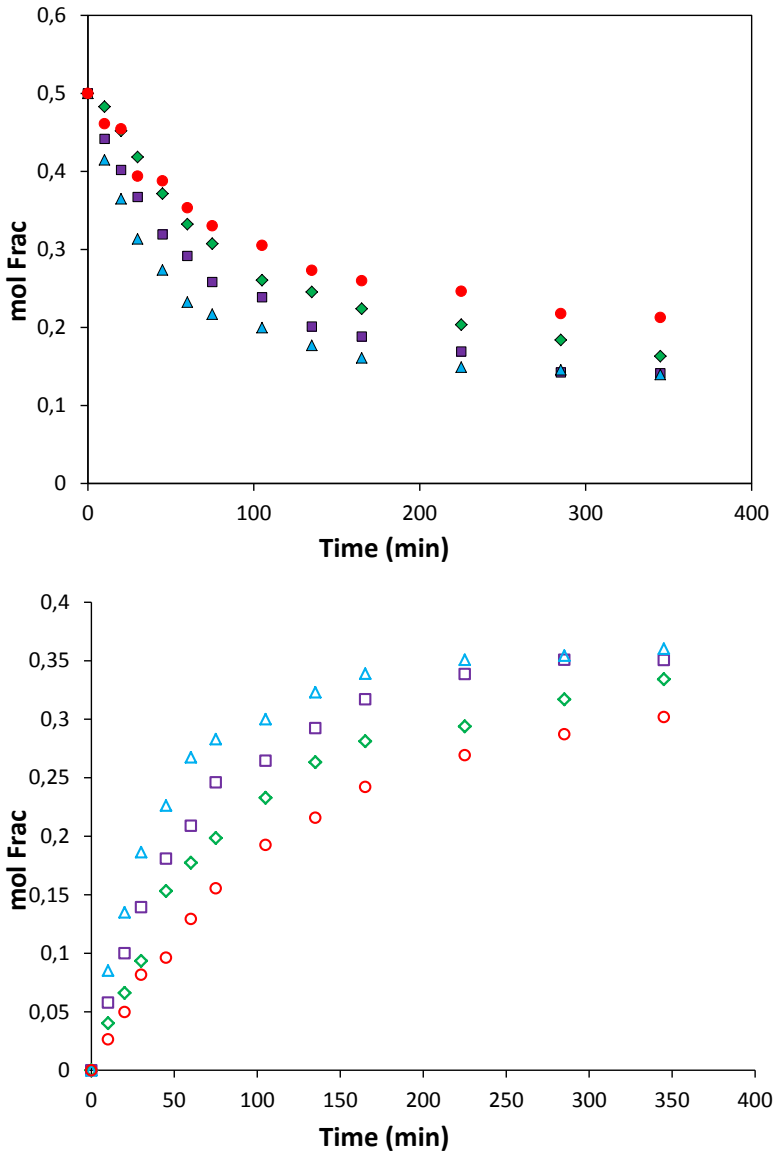

Figure 2.6. Esterification of acetic acid with Isobutanol using Amberlyst 15 as catalyst, at four different Temperatures (343.15 K; 353.15 K; 363.15 K; 373.15 K). Feed molar ratio 1:1; Catalyst loading equivalent to sulfuric acid at 0.75% wt.; Filled markers ACAC at (●) 343.15K; (♦) 353.15 K; (■) 363.15 K; (▲) 373.15 K. Void markers IbAC at (○) 343.25 K; (◊) 353.15 K; (□) 363.15 K; (Δ) 373.15 K.

Table 2.4. Regressed kinetic parameters of Equation 2.3.

Parameters	Units	Value
$k_{o,Cat}$	Kmol/kg$_{CAT}$·s	87.3161
Ea_{cat}	kJ/mol	41.5063

The good agreement between the obtained kinetic profiles and the regressed model can be verified in Figures B8 to B15. For a concise presentation of those results, a Pareto plot of the experimental and calculated concentrations of the characterized species in all kinetic experiments are presented in Figure 2.7.

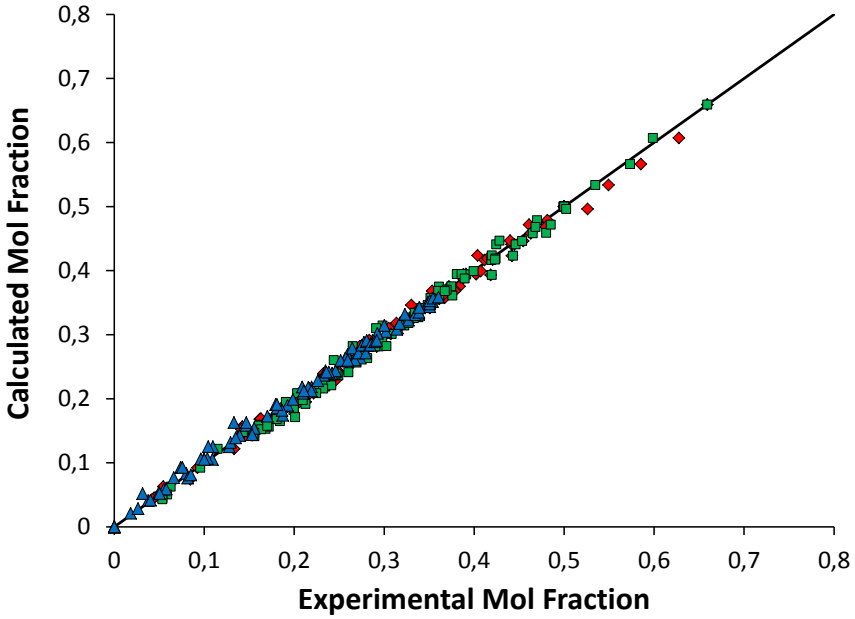

Figure 2.7. Pareto plot of experimental and calculated concentrations of characterized species during the whole set of kinetic tests. (♦) ACAC; (■) IbOH; (▲) IbAC.

As observed the regressed model accurately predicts reaction kinetics under the different operating condition. Remarkably, this simplified model was suitable to adjust the experimental data without the need for a more complex model such as those reported for similar esterification reactions (e.g. Eley-Rideal, LHHW) [13, 14]. This facilitates its incorporation in the default formats of commercial process design software. Also, it is particularly important that the model is able to accurately predict reaction kinetics at temperatures near the bubble point of the reactive quaternary mixture. Thus, the obtained model can be confidently used for further process development, in particular for the conceptual design a reactive distillation process in the production of Isobutyl acetate.

2.5. Conclusions

A kinetic study of the liquid phase esterification of isobutanol with acetic acid for the production of isobutyl acetate was carried out. A heterogeneous ion exchange resin (Amberlyst 15) was used as catalyst, with loadings equivalent to sulfuric acid between 0.25 and 1.5 % wt. During the kinetic tests, reaction temperature was varied between

343.15 K and 373.15 K, and the initial feed molar ratios were 2:1, 1:1 and 1:2. Preliminary experiments allowed to verify the absence of mass transfer limitation during experiments when using stirring rates of 800 RPM and catalyst particle diameters of 300 μm. The observed molar-based chemical equilibrium constant was in between 3.5 to 4.8, and the reaction exhibited and endothermic behavior with a heat of reaction of 16.47 KJ/mol. Finally, a kinetic model was regressed and accurately fitted the experimental data. This model can be used near to the bubble points of the quaternary mixture, so it is suitable for further process design. In particular, this can be used for conceptual design of a reactive distillation process under the assumption that chemical reaction occurs in the liquid phase during the distillation process.

2.6. References

1. Alder, C.; Hayler, D.; Henderson, R.; Redman, A.; Shukla, L.; Shuster L.; Sneddon, H. Updating and further expanding GSK's solvent sustainability guide. *Green Chem.;* **2016**, 18, 3879-3890. DOI: 10.1039/C6GC00611F

2. Byrne, F.; Jin, S.; Paggiola, G.; Petchey, T.; Clark, J.; Farmer, T.; Hunt, A.; McElroy, R.; Sherwood, J. Tools and techniques for solvent selection: green solvent selection guides. Sustain Chem Process **2016**, 4 (7), 1-24. DOI: 10.1186/s40508-016-0051-z

3. Lan, E.I.; Liao, J.C. Microbial synthesis of n-butanol, isobutanol, and other higher alcohols from diverse resources. *Bioresour. Technol.* **2013**, 135, 339–349. DOI: 10.1016/j.biortech.2012.09.104

4. Atsumi, S.; Hanai, T.; Liao, J. C. Non-fermentative pathways for synthesis of branched-chain higher alcohols as biofuels. *Nature* **2008**, 451(7174), 86–89. DOI: 10.1038/nature06450

5. Patidar, P.; Mahajani, S. Esterification of fusel oil using reactive distillation – Part I: Reaction kinetics. *Chem. Eng. J.* **2012**, 207–208, 377-387. DOI: 10.1016/j.cej.2012.06.139

6. Montoya, N.; Durán, J.; Córdoba, F.; Gil, I.; Trujillo, C.; Rodríguez, G. Colombian fusel oil, *Ing. Invest.* **2016**, 36, 21–27. DOI: 10.15446/ing.investig.v36n2.52369

7. Jordison, T. L.; Lira, C. T.; Miller, D. J. Condensed-Phase Ethanol Conversion to Higher Alcohols. *Ind. Eng. Chem. Res*. **2015**, 54 (44), 10991-11000. DOI: 10.1021/acs.iecr.5b02409

8. Moncada, J.; Posada, J.; Ramírez, A. Comparative early stage assessment of multiproduct biorefinery systems: An application to the isobutanol platform. *Bioresour. Technol*. **2017**, 241, 44–53. DOI: 10.1016/j.biortech.2017.05.074

9. Butamax, 2016. The Biofuel of the Future. https://www.butamax.com/the-bio-isobutanol-advantage/higher-value-biofuel/ (Consulted 23 Aug. 2019).

10. Sizov, A. Krupnov, L.; Meledina, T. Intensification of Higher Alcohols Biosynthesis – An Advanced Feedstock for Biofuel Production. *Energy Procedia* **2017**, 113, 333–338. DOI: 10.1016/j.egypro.2017.04.074

11. Yoshizawa, K. On Various Factors Affecting Formation of Isobutanol and Isoamyl Alcohol during Alcoholic Fermentation. *Agric. Biol. Chem.* **1966**, 30, 634–641. DOI: 10.1080/00021369.1966.10858659

12. Ramli, N.A.; Rahman, R.A.; Ngadi, N.; Samah, R.A. Optimisation of fermentation conditions for isobutanol production by saccharomyces cerevisiae using response surface methodology, *Chem. Eng. Trans.* **2017**, 56, 301-306. DOI: 10.3303/CET1756051

13. Izci, A.; Bodur, F. Liquid-phase esterification of acetic acid with isobutanol catalyzed by ion-exchange resins. *React. Funct. Polym.* **2007**, 67, 1458–1464. DOI: 10.1016/j.reactfunctpolym.2007.07.019

14. Altıokka, M. R.; Çıtak, A. Kinetics study of esterification of acetic acid with isobutanol in the presence of amberlite catalyst. *Appl. Catal. Gen.* **2003**, 239, 141–148. DOI: 10.1016/S0926-860X(02)00381-2

15. Izci, A.; Uyar, E.; Izci, E. Determination of Adsorption and Kinetic Parameters for Synthesis of Isobutyl Acetate Catalyzed by Amberlite IR-122. *Chem. Eng. Commun.* ***2008***, 196, 56–67. DOI: 10.1080/00986440802303293

16. Opdyke, D. L. J. Isobutyl acetate. *Food Cosmet. Toxicol.* **1978**, 16, 795-796. DOI: 10.1016/S0015-6264(78)80119-9

17. ECHA. Isobutyl Acetate. Substance Information. European Chemicals Agency. https://echa.europa.eu/substance-information/-/substanceinfo/100.003.406 (Consulted Sept. 18, 2019)

18. Yadav, G. D.; Mujeebur, M. S. M. Synthesis of fragrance and flavour grade esters: activities of different ion exchange resins and kinetic studies. *Clean Technol. Environ. Policy* **2003**, 5, 128–135. DOI: 10.1007/s10098-003-0196-9

19. Luyben, W. L.; Yu, C. C. *Reactive Distillation Design and Control*. John Wiley & Sons, Inc.; Hoboken, New Jersey. 2008.

20. Martínez, A. F.; Sánchez, C. A.; Orjuela, A.; Rodríguez, G. Isobutyl acetate by reactive distillation. Part I. Phase equilibrium and topological analysis. Submitted for publication. *Fluid Phase Equilibr.* **2020**.

21. Calvar, N.; González, B.; Dominguez, A. Esterification of acetic acid with ethanol: Reaction kinetics and operation in a packed bed reactive distillation column. *Chem. Eng. Process. Process Intensif.* **2007**, 46, 1317–1323. DOI: 10.1016/j.cep.2006.10.007

22. Helfferich, F. *Ion Exchange*; McGraw Hill: New York, 1962.

23. Froment, G. F.; Bischoff, K. B. *Chemical reactor analysis and design*. Wiley, 1990.

24. Weisz, P. B. & Prater, C. D. Interpretation of Measurements in Experimental Catalysis. in *Advances in Catalysis* (eds. Frankenburg, W. G.; Komarewsky, V. I. & Rideal, E. K.), Academic Press, 6, 143–196, 1954.

25. Sanz, M. T.; Gmehling, J. Esterification of acetic acid with isopropanol coupled with pervaporation: Part I: Kinetics and pervaporation studies. *Chem. Eng. J.* **2006**, 123, 1–8. DOI: 10.1016/j.cej.2006.06.006

26. Duque-Bernal, M.; Quintero-Arias, J. D.; Osorio-Viana, W.; Dobrosz-Gómez, I.; Fontalvo, J.; Gómez-García, M. Á. Kinetic study on the homogeneous esterification of

acetic acid with isoamyl alcohol. *Int. J. Chem. Kinet.* **2013**, 45, 10–18. DOI: 10.1002/kin.20737

27. Wilke, C. R.; Chang, P. Correlation of diffusion coefficients in dilute solutions. *AIChE J.* **1955**, 1, 264–270. DOI: 10.1002/aic.690010222

28. Orjuela, A.; Yanez, A. J.; Santhanakrishnan, A.; Lira, C. T.; Miller, D. J. Kinetics of mixed succinic acid/acetic acid esterification with Amberlyst 70 ion exchange resin as catalyst. *Chem. Eng. J.* **2012**, 188, 98–107. DOI: 10.1016/j.cej.2012.01.103

29. Osorio-Pascuas, O. M.; Santaella, M. A.; Rodriguez, G.; Orjuela, A. Esterification Kinetics of Tributyl Citrate Production Using Homogeneous and Heterogeneous Catalysts. *Ind. Eng. Chem. Res.* **2015**, 54, 12534–12542. DOI: 10.1021/acs.iecr.5b03608

CHAPTER 3.

ISOBUTYL ACETATE BY REACTIVE DISTILLATION. CONCEPTUAL DESIGN AND SIMULATION

This section includes a copy of the paper: Martinez, A. F., Rodríguez, J.S., Sanchez, C. A., Orjuela, A., Rodriguez, G. 2020. **Isobutyl acetate by reactive distillation. Conceptual design and simulation**. Eng. Res. Des. Currently In revision

The paper is reformatted and figures and tables are enlarged to fulfill edition requirements for the dissertation document.

3. Isobutyl acetate by reactive distillation. Conceptual design and simulation

3.1. Summary

This work studies the conceptual design of a reactive distillation (RD) process for isobutyl acetate production by esterification of acetic acid and isobutanol. A reactive residue curve map analysis was used to assess RD feasibility and to identify suitable operating conditions for industrial implementation. The maps were obtained using validated phase equilibria and reaction kinetic models, by coupling Aspen plus V.10 and Python, Afterwards, conceptual design outputs were used for a rigorous simulation and optimization of the process. The obtained results indicate that pure isobutyl acetate can't be obtained as pure product from the RD column as it is a saddle node. However, Isobutyl acetate can be obtained as bottom product at enough purity to fulfil urethane grade specifications. A final reactive distillation configuration was developed enabling to obtain almost complete reactants conversion, with a molar composition of isobutyl acetate of 0.99 at the bottoms of the column. According to the optimal operating conditions, isobutyl acetate via RD can be produced under an energy intensity of 0.77 kW/kg_{IbAC}, a mass intensity of 1.16 $kg_{reactants}/kg_{IbAC}$, a productivity of 328.7 kg_{IbAC}/m^3h, and a production cost of 0.98 USD/ kg_{IbAC}.

Keywords. Isobutyl acetate, esterification, reactive distillation, Conceptual design

3.2. Introduction

The increasing number of regulating policies that have been implemented during last years for the production, management and use of chemical compounds (e.g. REACH in Europe [1], TSCA amended by Lautenberg Chemical Safety Act in USA [2]) have boosted the transition from traditional fossil-based products towards safer, biobased, renewable and more sustainable chemicals. Aligned with the compliance with this kind of policies, pursuing sustainable development goals, and also following market trends, different chemical industries have embraced the biorefinery production model. Similarly to the traditional petroleum refineries, in biorefineries the biomass is transformed into a conglomerate of fuels, materials, chemicals, energy and even food/feed products. In

particular, some biorefineries have been developed around the production of certain platform molecules, and their subsequent transformation into a large variety of value added products [3-7].

Among the different target products suitable for biorefineries, biobased solvents are of paramount importance due to their ubiquitous use as processing materials in different industries, and because they are main ingredients in a wide variety of end goods (e.g. paints and coatings, inks, resins, cosmetics, pharmaceuticals, polymers, cleaning and household products, etc.). As a consequence of their massive consumption, and from a life cycle perspective, typical solvents generate large environmental impacts, reason why greener alternatives are urgently required [8, 9]. In this direction, among many chemicals, a multiplicity of biobased alcohols and esters have been successfully implemented as direct and functional substitutes of many petrochemical solvents. These type of compounds can be obtained from biobased resources by mean of different thermochemical, catalytic and microbial pathways [10-16].

Amid the variety of biobased alcohols and esters of commercial interest, isobutanol and isobutyl acetate stand out as main platform for chemicals and solvents of industrial interest [17-20]. They are characterized for their biodegradability, low surface tension, viscosity-modifying action, low water solubility (i.e. the ester), high electrical resistance, and because they comply with REACH regulations [19, 21]. Currently, these components are mainly used in the coatings industry as solvents, and in the flavor and fragrance industry for their pleasant organoleptic properties [17, 22]. Isobutanol is traditionally produced from petrochemical feedstock by the “oxo” process, involving hydroformylation to butyraldehydes and further hydrogenation to the butyl alcohols [23]. Nonetheless, it can be obtained from various renewable sources via different chemical and biological routes [11, 20, 24-33].

On the other hand, isobutyl acetate can be produced by fermentation pathways [31], but it is mainly produced by esterification of Isobutanol (IbOH) with Acetic Acid (ACAC) as described in Chapter 2. As the ester has a higher added value, this work focuses on the production of isobutyl acetate.

For Industrial applications, the esterification of IbOH with ACAC is carried out under acid catalysis, mainly using homogeneous promoting agents (e.g. methanesulfonic, *p*-toluene sulfonic, sulfuric, or phosphoric acid) [34, 35]. While the heterogeneous catalysts (e.g. ion exchange resins) have demonstrated lower yields, they have

exhibited enhanced selectivity, less corrosiveness, and enabling better sensory properties of the product (i.e. for fragrance and flavor industry) [36, 37]. As presented in Figure 1, the esterification reaction in the production of isobutyl acetate is limited by chemical equilibrium, therefore the use of an IbOH excess is a normal practice to enable high conversions [38-40]. Also, different intensified processes have been tested to enhance reaction yields in Isobutyl acetate synthesis via esterification or transesterification. These include extractive distillation [41], reactive distillation [10, 42], pervaporation [43, 44], pressure swinging distillation [41, 45], and reactive dividing wall column [46]. Particularly, reactive distillation has been successfully implemented in similar esterification systems for acetates production [47-49].

Nowadays, industrial isobutyl acetate is usually produced under batch operation, either using a reactor followed several distillation steps, or by using a reactor coupled to a distillation column with top decanter. These configurations intend to remove water during the process, to refine the acetate product, and to recover the excess of isobutanol used during reaction for further recycle. These approaches have the disadvantage of using less efficient batch operating policies. Also, as the reactive mixture is highly non-ideal, exhibiting several multicomponent azeotropes and limited miscibility [50], product purification and isobutanol recovery and recycle are rather cumbersome, and highly energy intensive. In this regard, continuous reactive distillation (RD) seems suitable for a more cost-effective operation [51].

Taking into account that the production of isobutyl acetate via esterification using continuous RD has not been explored in the open literature, there is need to assess its feasibility. For this purpose, it is required to stablish the process configurations and operating conditions that enable to obtain high yields under the required product specifications. In this regard, this work focuses on the conceptual design of a continuous RD process for the production of isobutyl acetate. This task was addressed based upon a validated quaternary phase equilibrium model [50] and an experimentally verified kinetics [52], using a reactive residue curve maps methodology (RRCMs) [53, 54]. Once a preliminary process configuration is obtained, a rigorous simulation is accomplished using a commercial process design software. A further sensitivity analysis allowed to identify key operational variables required to maximize conversion and purity of the final product, and an optimization of these variables was performed. Finally, a suitable RD configuration under continuous operation was assessed for the production for isobutyl acetate at the industrial scale.

3.3. Methods

This work was carried out at three stages. Firstly, the conceptual design of the RD process was carried out using RRCMs, secondly, a rigorous simulation of the RD process was done using Aspen Plus V.10 enabling to identify the key operating variables of the process using conversion and purity as the main output criteria. Finally, an optimization was performed using a stochastic method to obtain a suitable RD column configuration that fulfilled product specifications under high conversions and low energy consumption. The methodology of these stages is detailed described in the following sections.

3.3.1. Conceptual design

3.3.1.1. Reaction kinetics and catalysis

As above stated, Isobutyl acetate (IbAC) is produced by Fisher esterification between acetic acid (ACAC) and isobutanol (IbOH), generating water (W) as byproduct. This reaction is limited by the chemical equilibrium, reaching maximum conversions around 70%, and it requires the use of an acid catalyst for cost-effective implementation [38-40, 52]. Then, catalyst loading becomes a key parameter for the implementation of the reaction in a RD column. If the process operates with an homogeneous catalysts (i.e. liquid), the entry stage must be stablished and it will determine the number and location of the reactive and non-reactive stages within the column. If the catalyst is non-volatile, the non-reactive stages would be located above the feed point of the catalyst. Correspondingly, the reactive sections would be those located below the catalysts entry stage, including the reboiler. Most certainly, some operating constrains would have to be implemented in this case to avoid product decomposition at the reboiler conditions. Those might involve certain maximum temperature limits or a reduced residence time at the reboiler. Also, the use of a homogeneous catalyst will make necessary to purify the bottoms product in subsequent processes for its removal.

Comparatively, if the RD operates with a heterogeneous catalyst, the particle size of the catalyst and its loading within the stages must be defined in concordance with the internals type and geometry, and their liquid hold-up. In this case, the catalyst loading and the location of the reactive sections within the column become key variables of the process. Despite the use of a heterogeneous catalyst reduces the need for its removal from the product, other considerations have to be included in the conceptual design. In

this case, thermal stability of the catalysts would establish constrains regarding the operating pressure of the column and the location of the reactive stages. Also, as the activity of the heterogeneous catalysts is lower, large loadings would be required. Then, hydraulic constrains would have to be considered during the conceptual design stage as this might lead to the need for special RD configurations (e.g. side reactors).

Taking into account the above considerations, and bearing in mind that a target high value added market for IbAC is the fragrance and flavor industry, it was decided to assess the RD feasibility using a heterogeneous catalyst. In this case, Amberlyst 15 was assumed as catalyst for its high acid sites concentration, and the corresponding validated kinetic model [52] in a mole fraction basis is described in the following equations:

$$r\left(\mathrm{kmol}/_{m^3\ \cdot \mathrm{s}}\right) = C_{cat}k\left(x_{ACAC}x_{IbOH} - \frac{x_{IbAC}x_{water}}{K_{EQ}}\right) \quad (3.1)$$

$$k\left(\mathrm{kmol}/_{kg_{cat}\ \cdot \mathrm{s}}\right) = 87.3161\exp\left[\frac{-41.506\ kJ/mol}{RT}\right] \quad (3.2)$$

$$\ln K_{EQ} = -1981.1 * \frac{1}{T(K)} + 7.1927 \quad (3.3)$$

In these expressions, x_i is the mole fraction of component i, k is the kinetic constant, and K_{EQ} is the temperature ($T(K)$) dependent equilibrium constant. The catalyst loading per volume of reactive liquid (C_{cat}) was assumed as 780 Kg_{cat}/m^3_{liq} taking into account reported liquid hold-up in similar RD systems using ion exchange resins as catalysts [55]. This parameter corresponded to a Katapak sp-11 structured packing that has a volumetric hold-up of ~0.1 m^3_{liq}/m^3_{col}, and a catalyst packing density (ρ_{cat}) of 78 Kg_{cat}/m^3_{col}. It was assumed that the reaction only occurred in the liquid phase and the autocatalytic effect was neglected.

3.3.1.2. Phase equilibria

Regarding phase equilibria, the IbOH + ACAC + W + IbAC mixture is highly non-ideal, exhibiting several binary and ternary azeotropes, partial miscibility, and association of the acid in the vapor phase. Even, there is a non-common biazeotropic behavior in the binary IbAC-ACAC [50,56,57]. To accurately describe the phase equilibria behavior of

this complex system, a validated thermodynamic model was recently developed [50]. This model corresponds to an activity-fugacity approach described by the NRTL activity coefficient model for the liquid phase, and the Hayden O'Connell equation of state for the fugacity coefficients of the vapor phase. Vapor pressure of the pure components were calculated using the Antoine equation. The corresponding parameters of these equations are summarized in Tables C1 to C3 in the Annexes C.

3.3.1.3. Reactive residue curve maps

Similarly to the traditional non-reactive residue curve map analysis for conventional distillation sequencing, the reactive residue curve map (RRCM) analysis is based upon the model of a differential still considering a reaction in the liquid phase only, as presented in figure 3.1.

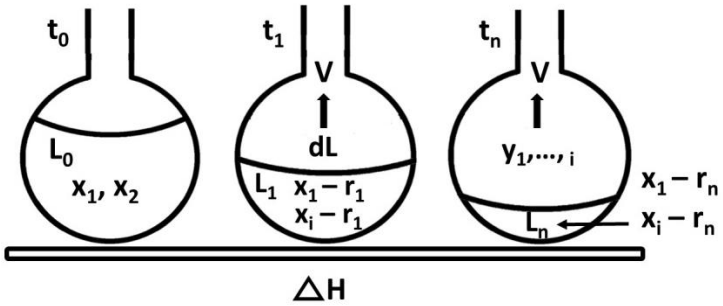

Figure 3.1. Differential distillation model.

The material balance of the global system is presented in Eq. 3.4.

$$-V = \frac{d}{dt}(L) \tag{3.4}$$

The balance per component is equal to:

$$Vy_i + \frac{d}{dt}(Lx_i) = r_i L \tag{3.5}$$

Here, V is the molar flow rate of vapor, L is the total number of moles in the liquid phase, y_i and x_i are the phase equilibrium vapor and liquid mole fractions of component i.

Replacing Eq.3.4 in Eq.3.5:

$$Vy_i + (-V)x_i + L\frac{d}{dt}(x_i) = v_i RL \tag{3.6}$$

v_i is the stoichiometric coefficient of component i in the reaction, R is the rate of reaction at the corresponding bubble point condition.
Rearranging this expression and dividing by V:

$$\frac{L}{V}\frac{d}{dt}(x_i) = \frac{V}{V}(x_i - y_i) + \frac{L}{V}v_i R \tag{3.7}$$

And transforming the time variable in a dimensionless variable as presented in Eq. 3.8, Ee. 3.7 turns into Eq.3.9:

$$\frac{L}{Vdt} = \frac{d}{d\xi} \tag{3.8}$$

$$\frac{dx_i}{d\xi} = x_i - y_i + \frac{L}{V}v_i R \tag{3.9}$$

The ratio $\frac{L}{V}$ is related with the distillation policy, indicating the amount of liquid remaining (i.e. residue) with respect to the vapor flow rate abandoning the differential still. In Eq. 3.9 the system already considers the phase equilibria and the reaction simultaneously, with a new grade of freedom for the distillation policy, however it is possible to establish a direct relation between the phase equilibrium and the reaction, for this, a reference reaction rate R^{ref} at a reference condition (i.e. T^{ref}, x^{ref}) can be added to the second term of the right side of Eq. 3.9 Multiplying and dividing by R^{ref}:

$$\frac{dx_i}{d\xi} = x_i - y_i + \frac{L}{V} * R^{ref} * \frac{v_i R}{R^{ref}} \tag{3.10}$$

Where:

$$\frac{L}{V} * R^{ref} = Da \tag{3.11}$$

Da is the Damköhler number, a useful relation for determining whether the diffusion rate (phase equilibrium) or the reaction rate represents the mayor contribution on establishing the state of the chemical distribution of the system.

$$\frac{dx_i}{d\xi} = x_i - y_i + Da * \frac{v_i R}{R^{ref}} \tag{3.12}$$

Small Da values are related to distillation driven operations behaving similarly to a short residence time reactor with fast separation. In comparison, at large Da values slow vapor removal is achieved, and large residence times are observed; in this last case the process is reaction or kinetically controlled. When Da is very large, the separation process occurs at the chemical equilibrium condition [58]. The residue curves turns into the conventional non-reactive ones when $Da = 0$.

Based upon the phase equilibrium and the reaction kinetic models, different reactive residue curves were constructed by solving Equation 4 (i.e form –∞ to +∞) from random liquid compositions at 101.3 kPa. The integration of the Eq. 3.12 to obtain the reactive residue curves was carried out by coupling Aspen Plus for phase equilibria calculation, and Python where kinetics was calculated and the differential equations were solved. The integration was performed using the method Cash and Karp (1990). This method uses six function evaluations to calculate a fifth and fourth order function approximations [59] as presented next:

$$k_1 = f(x_i, y_i) \tag{3.13}$$

$$k_2 = f\left(x_i + \frac{1}{5}h, y_i + \frac{1}{5}k_1 h\right) \tag{3.14}$$

$$k_3 = f\left(x_i + \frac{3}{10}h, y_i + \left(\frac{3}{40}k_1 + \frac{9}{40}k_2\right)h\right) \tag{3.15}$$

$$k_4 = f\left(x_i + \frac{3}{5}h, y_i + \left(\frac{3}{10}k_1 - \frac{9}{10}k_2 + \frac{6}{5}k_3\right)h\right) \tag{3.16}$$

$$k_5 = f\left(x_i + h, y_i + \left(-\frac{11}{54}k_1 + \frac{5}{2}k_2 - \frac{70}{27}k_3 + \frac{35}{27}k_4\right)h\right) \tag{3.17}$$

$$k_6 = f\left(x_i + \frac{7}{8}h, y_i + \left(\frac{1631}{55296}k_1 + \frac{175}{512}k_2 + \frac{575}{13824}k_3 + \frac{44275}{110592}k_4 + \frac{253}{4096}k_5\right)h\right) \tag{3.18}$$

$$y_{i,4^{th}} = y_{i-1,RK4} + \left(\frac{37}{378}k_1 + \frac{250}{621}k_3 + \frac{125}{594}k_4 + \frac{512}{1771}k_6\right)h \tag{3.19}$$

$$y_{i,5^{th}} = y_{i-1,RK5} + \left(\frac{2825}{27648}k_1 + \frac{18575}{48384}k_3 + \frac{13525}{55296}k_4 + \frac{277}{14336}k_5 + \frac{1}{4}k_6\right) \tag{3.20}$$

To minimize de approximation error due the numerical integration, the step size was modified in each step using an adaptation of the strategy presented by Press and cols. (1992) [60]. First an estimator of the method precision was calculated using the norm of

the difference vector between the fifth and fourth order values. Next, the step size was modified proportional to the ratio of the required and calculated precision. The required precision was fixed in the value as presented in Equation 3.22, so each composition had at least this precision. The alpha value was 0.2 if $\Delta_{calc} \geq \Delta_{req}$ and 0.25 in other case so it is easier to increase precision.

$$\Delta_{calc} = \left\| y_{i,4^{th}} - y_{i,5^{th}} \right\| \quad (3.21)$$

$$\Delta_{req} = 5 \times 10^{-5} \quad (3.22)$$

$$h_i = h_{i-1} \left| \frac{\Delta_{calc}}{\Delta_{req}} \right|^{\alpha} \quad (3.23)$$

The behavior of the reactive residue curves and the structure of maps obtained at different Da values are unique for every reactive mixture, as result, it has been observed particular cases where azeotropes appear, disappear or change their composition when increasing Da [61]. In order to facilitate RRCM interpretation and analysis, they are preferably presented in transformed (or reduced) composition diagrams [53] This transformed compositions scale is superior to normal mole fraction composition as in here the non-reactive limits are well defined, the equilibrium surfaces are tangent at azeotropic states and the number of linearly independent transformed composition variables is equal to the number of independent variables describing the chemical equilibrium state [53]. This transformed composition are based on a key component K and equations 3.24 and 3.25 present the generalized equations to convert the general composition to the new transformed composition for systems with one reaction and 4 components with no inert substances. For this case, choosing IbAC as key component and solving equation 3.24 and 3.25, the new transformed compositions for ACAC and IbOH defined in Equations 3.26 and 3.27, can be used to construct the transformed RRCM diagram.

$$X_i = \frac{x_i/v_i - x_k/v_k}{v_k - v_T x_k} \quad (3.24)$$

$$Y_i = \frac{y/v_i - y_k/v_k}{v_k - v_T y_k} \quad (3.25)$$

When:

$i = 1, \ldots, c$ and $i \neq k$.

$$X_{ACAC} = x_{ACAC} + x_{ibAC} \quad (3.26)$$

$$X_{IbOH} = x_{IbOH} + x_{ibAC} \quad (3.27)$$

These transformed compositions reduces the number of variables from $c-1$ to $c-2$ which coincide exactly with ne number of independent variables of new transformed compositions X_i and Y_i, conserving all the generalities and rules of normal compositions diagrams for residue curves maps.

Several RRCM for different Da have to be constructed and the location of the stable, unstable and saddles nodes within the RRCMs maps would help to identify potentially feasible product streams of the RD column. The preferably situation would occur when azeotropes are reacted away, and the unstable and stable nodes corresponds to the pure products of reaction. The selection of a suitable operating policy (i.e. specific Da value), requires a trade-off between the catalyst amount per stage, the number of stages and the boil-up ratio. However, high Da values are generally recommended to ensure high conversions and small equipment. Once Da value is selected, feasible products streams can be estimated by using material balances and the reactive residue curves.

Special considerations must be taken when working with mixtures that exhibit partial liquid miscibility. If liquid phase splitting occurs inside the column, the different phases could have different reaction rates due to the uneven components distribution. Also, when immiscibility occurs at low temperature, liquid splitting might occur after condensing the distillate. In this case, the distillate collection tank acts as a decanter, and there is need to define if only one or the two phases are returned as reflux, and the corresponding flowrates. In the particular case of the studied esterification mixture, there is partial miscibility in mixtures containing water, isobutanol and isobutyl acetate. Generally, the aqueous phase contains minor amounts of the organic compounds, so aqueous phase removal would enhance reaction conversion. Nevertheless, acetic acid reduces immiscibility in the quaternary mixture, meaning that feed molar ratio will have a major impact in the process, and this have to be further analyzed.

3.3.2. Simulation and optimization

Once a basic configuration of the RD process for isobutyl acetate production was developed from the RRCM analysis, a rigorous model was implemented in Aspen Plus V.10. A phase equilibrium stage approach with reaction kinetics was used in the modeling, and as previously mentioned, the corresponding hold-up of the reactive stages was defined as the 10% of the stage volume [55, 62, 63]. The model was constructed assuming an IbAC production of 30,000 t/yr that corresponds to reported

throughput in an isobutanol biorefinery [17]. Afterwards, the impact of different key operating parameters (i.e. Reflux composition, feed-to-bottom ratio, feed-to-distillate ratio and reactants molar ratio) on the conversion and product purity was assessed.

Finally, the key operating parameters were tuned to maximize IbAC conversion and purity in the bottom stream while reducing capital and operational costs. This was done via optimization using a genetic algorithm coupling Aspen Plus V.10 and Python. The objective function was a preliminary economic potential based upon the total annual cost (TAC) including capital and operating costs, and it is presented in Equation 3.28.

$$f_{objective} = F_{prod} * P_{prod} - \left[\frac{1}{T_{payback}} * \sum C_i^{equip} + \sum \left(C_i^{Utility}\right)_{year} + \sum F_{react,i} * P_{react,i} + F_{des}^{prod} * P_{prod} + W_{cat} * P_{cat}\right] \quad (3.28)$$

Here, F_{prod} is flow of IbAC in the bottom stream, and C_i^{equip} are the purchase and installation costs of the equipment i (i.e. distillation column, reboiler, condenser, decanter) with the corresponding annualization period ($T_{payback}$). $C_i^{utility}$ are the total utilities costs (i.e. reboiler and condenser duties). F_{react} is the amount of unconverted reactants in outlet streams and P_{react} is the corresponding purchase price of the i reactant. F_{des}^{prod} is the amount of IbAC lost in the distillate product and P_{prod} is the corresponding selling price of the IbAC (i.e. Urethane grade). W_{cat} and P_{cat} are the amount and purchase price of required catalyst. While it is expected that the operating life of the catalysts can be larger than a year (i.e. 2 to 5), this cost was assumed per year taking into account that the replacement costs of the catalysts within the structured packing can be substantial.

As presented in equations 3.29 to 3.31, the Marshall and Swift (*M&S*) index was used for costs updating (1593.7 for 2017).

$$C_{vessel} = \left(\frac{M\&S}{280}\right) * (957.9 * D^{1.066} * H^{0.802}) * (2.18 * F_c) \quad (3.29)$$

$$C_{column\ tray} = \left(\frac{M\&S}{280}\right) * (97.2 * D^{1.55} * H) * (F_c) \quad (3.30)$$

$$C_{heat\ exchanger} = \left(\frac{M\&S}{280}\right) * (474.4 * A^{0.65}) * (2.29 + F_C) \quad (3.31)$$

The payback time $T_{payback}$ was set ten years, D and H are the vessel diameter and Height in meters, respectively. A is the heat exchanger area in m^2 and the F_C factor

considers the construction material factor (F_m) and the pressure (P in Pa) correction factor (F_P) as presented in Equation 3.32.

$$F_C = F_m * F_P \tag{3.32}$$

$$F_P = 1 + 0.0074(P - 3.48) + 0.00023(P - 3.48)^2 \tag{3.33}$$

The optimization was done using the particle swarm metaheuristic method [64]. The adjusted variables were the feed molar ratio, the bottom to feed ratio, the number of stages, the number and location of the reactive stages within the column, and the location of the feed inlets.

3.4. Results and Discussion

Next are described the principal results generated from the conceptual design analysis and simulation.

3.4.1. Conceptual design

3.4.1.1. Non-reactive residue curve maps

Based upon the validated phase equilibria model, a quaternary non-reactive residue curve map for the mixture IbOH + ACAC + W + IbAC was calculated at 101.3 kPa, and presented in Figure 3.2. As observed, the system exhibits eight azeotropes and a partial miscibility region around the IbOH + W and IbAC + W edges (calculated at the corresponding bubble temperatures). There are six binary and two ternary azeotropes, and no quaternary singular points. According to results, the highest temperature node is the binary azeotrope between IbOH + ACAC (i.e. 391.75 K) but this node would be reacted away as the esterification is considered. The second highest temperature node corresponds to pure ACAC (391.16 K), but this would be reached only under large excess of acid, which would not be an expected operating condition. The followings nodes in descendent order correspond to three azeotropes and pure IbAC, all having similar temperatures: the biazeotropic ACAC + IbAC (390.1 K and 389.8 K), the ternary ACAC + IbOH + IbAC (389.9 K) and pure IbAC (389.5 K). This indicates that the use of IbOH excess would be preferable to ensure complete conversion of ACAC, and to avoid any high boiling azeotrope containing the acid. Then, IbAC would be a feasible

bottoms product as long as the column operates under an IbOH excess and with high conversions.

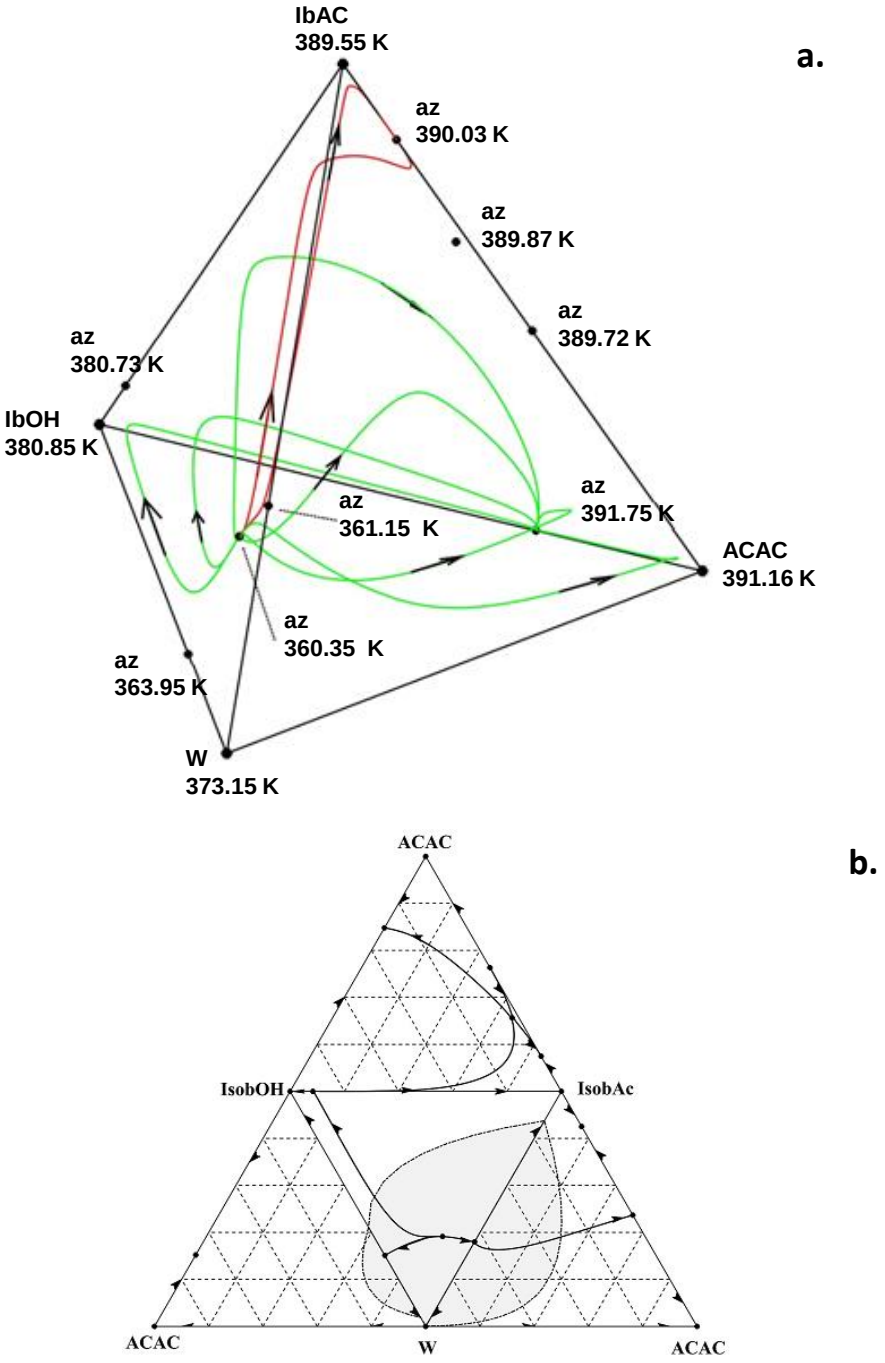

Figure 3.2. Non-reactive residue curves maps (Mole fraction basis) phase equilibrium diagram for the quaternary system IbOH+ACAC+W+IbAC at P= 101.32 Kpa. (a) Quaternary diagram. (b) corresponding ternary diagrams. (→) Residue curves. (─) Immiscibility region. (═) distillation boundaries. (●) Azeotropes.

According to Figure 3.2, the lowest temperatures among the obtained nodes correspond to the ternary azeotrope IbOH + IbAC + W (360.4 K), and the binary azeotropes IbAC + W (361.1 K) and IbOH + W (363.8 K). All these are heterogeneous azeotropes, and when IbAC is present the content of organics in the aqueous phase is decreased. This is a valuable result because indicates that the unstable node of the map would correspond to the ternary heterogeneous azeotrope, and almost pure water could be removed by implementing a top decanter. Also, the organic phase could be used as reflux to avoid any IbOH and IbAC losses, but further exploration would be required as there is significant water in this phase that will affect reaction performance. Additional analysis is required to evaluate if it is possible to simultaneously obtain the highly pure isobutyl acetate and water nodes as product streams from a single column. It is important to point out that the selected catalyst is stable when operating below 393 K [65], which matches the highest bubble temperatures of the quaternary system at 101.3 kPa. Therefore, to ensure catalyst integrity, highly efficient and reduced pressure drop internals might be required to avoid higher temperatures in the lower reactive sections within the column.

The above mentioned findings were obtained from the analysis of a non-reactive residue curve map, thus there is need of a further exploration involving the reaction. However, this information can be useful to identify the advantages of implementing the esterification process in a RD column.

3.4.1.2. Reactive residue curve map analysis

A set of RRCMs were constructed at different Da values, from the non-reactive condition (i.e. Da = 0) to the kinetically controlled regimes (i.e. Large Da values). Figure 3.3 presents different RRCMs in transformed concentrations (i.e. Eqs. 3.26 and 3.27) obtained for Da values of 0, 0.05, 0.1, 0.5, 1, 2, 10 and 100. As usual, the vertices of the two-dimension square diagram represent the pure components. Initially, the corresponding RRCM for a distillation driven operation with no reaction (i.e. Da = 0) exhibits all the non-reactive azeotropes (Figure 3.3a). Then as expected, when including reaction (increasing Da values), the binary ACAC + IbOH azeotrope located in the imaginary line between ACAC and IbOH vertex, disappears of the diagram. Interestingly, disregarding of the operating regime (i.e. distillation of kinetically controlled) there is only one unstable node in all diagrams that corresponds to the ternary azeotrope IbOH + IbAC + W (x_{IBOH} = 0.1325, x_{IbAC} = 0.2496, x_W = 0.6179, T = 360.35 K). Comparatively, different stable nodes are identified at low Da values (i.e.

slow reaction) that would corresponds to low catalysts loadings or very high boil-up ratios (i.e. low residence time in reactive stages). Initially, in the non-reactive RRCM four distillation regions are formed, all sharing the same unstable node but with different stable nodes. Once reaction is considered, only three stable nodes remain, pure ACAC, pure IbOH and one of the binary azeotropes between IbAC + ACAC (i.e. x_{IbAC} = 0.862, x_{ACAC} = 0.137, T = 390.03 K), forming three distillation regions. One of these regions corresponds to mixtures with large acid concentration, where the ACAC node would be the bottoms product of a distillation column.

As observed in all maps, the pure isobutyl acetate vertex is a saddle node, indicating that is not possible to obtain pure isobutyl acetate as a product of a RD column. Nevertheless, as the Da becomes larger, the residue curves in one of the regions closely approach to the IbAC corner by the IbOH + IbAC edge. This suggests that the use of an excess of IbOH would help to reduce ACAC concentration, ensuring high conversions, and enabling to reach a high IbAC content in the bottom product. Nonetheless, if the RD column is operated with an excess of isobutanol, this variable must be adequately defined. An alcohol excess would involve large energy consumption, and also as the binary IbOH + IbAC can form an azeotropic mixture, this might generate challenges for IbAC recovery.

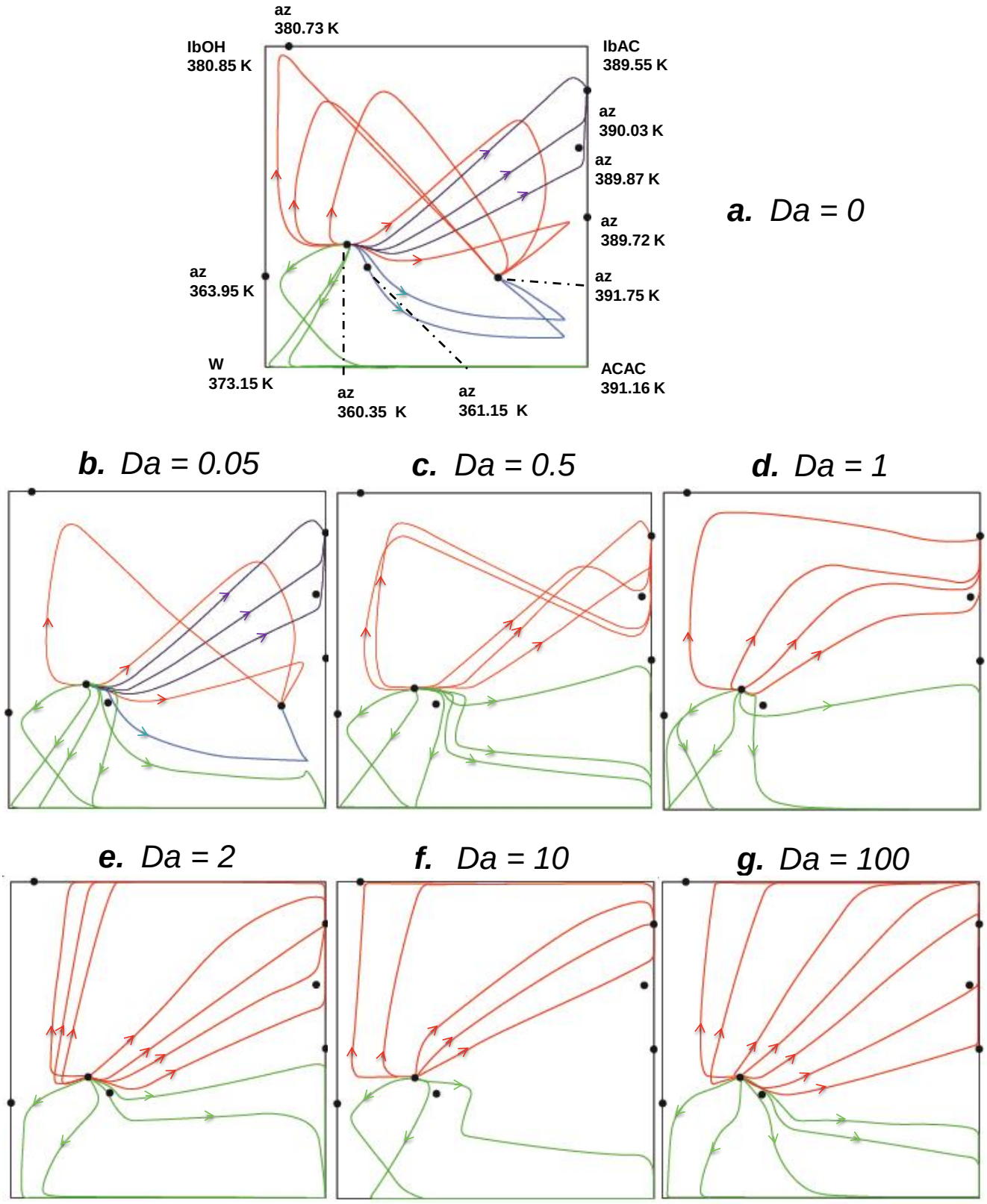

Figure 3.3. Reactive residue curve maps for the system ACAC - IbOH - IbAC - W at 101.3 kPa, for different values of Damhköler number, in the transformed composition scale.

Normally, industrial RD columns operate under kinetically controlled regimes (1< Da < +∞) with residence times at the reactive stages of around 2-5 min, and with a total residence time in the column of ~2 hr [66]. Despite the fact that the Da changes stage to stage within the RD column, a single value was selected to assess the feasibility of IbAC production via RD. In this case, a RRCM for a Da = 2 was used for the preliminary conceptual design, and an initial reactants ratio of ACAC:IbOH = 0.9 was assumed as the feed stream. This Da value is in concordance with experimentally observed for industrial reactive distillation units [66].

The material balance of a RD column was depicted in the RRCM constructed with a Da = 2, as presented in Figure 3.4. The balance corresponds to a straight-line connecting feed, bottoms and top streams of the RD column. As observed, using a feed (F) with a slight excess of IbOH, it would be possible to operate a column with almost pure IbAC as bottoms (i.e. product B), and with the ternary azeotrope as distillate (Product D). The top product is heterogeneous, so the aqueous phase can be removed to overcome equilibrium limitations. As the aqueous phase is mainly contaminated with IbOH, this also highlights the importance of using a slight excess of alcohol in the feed stream.

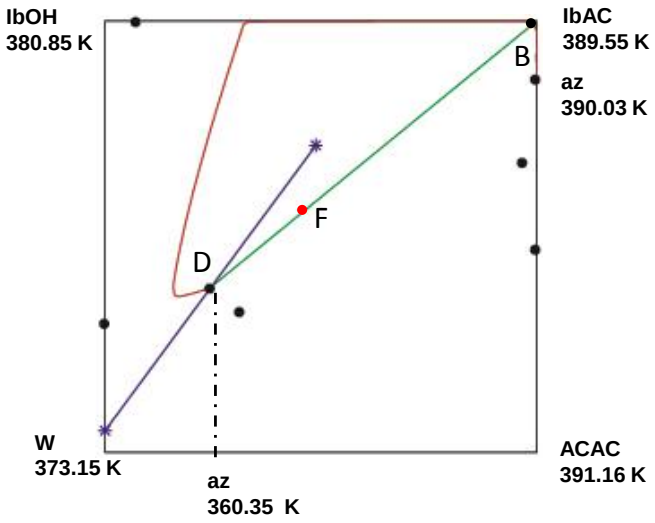

Figure 3.4. RRCM in transformed compositions for a Da = 2. (—) reactive residue curve. (—) RD material balance (—) tie line of the distillate product. (*) Decanter products

Figure 3.5 presents the selected reactive residue curve for Da = 2 in a mole-base diagram. Here it is also presented the chemical equilibrium composition for every

possible quaternary mixture that because of being a reversible reactive mixture with no inert components, this equilibrium condition has a saddle shape.

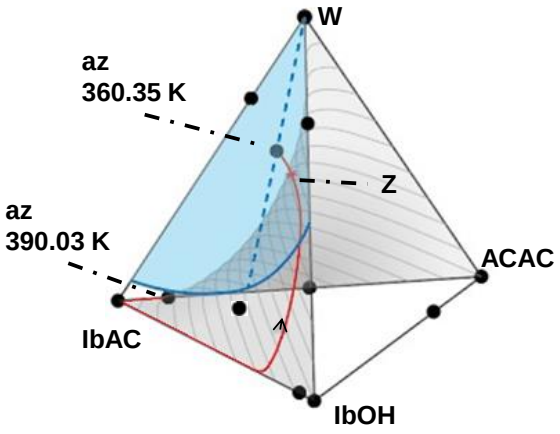

Figure 3.5. Mole-Base Composition Diagram. Saddle surface represents chemical equilibrium conditions at reference temperature (365,15 K), (—) Reactive Residue curve at Da=2. (—) partial miscibility ternary dome. (---) Tie line.

As above mentioned, the location of the unstable node within the immiscibility region indicates that the potential top product of the RD column will generate two liquid phases, with almost pure water that can be removed as distillate. The point **Z** in Figure 3.5 represents the intersection of the reactive residue curve with the chemical equilibrium saddle. As noticed, most part of the reactive residue curve line lies below the chemical equilibrium surface where reaction moves towards the products, thus improving reaction conversion. This part of the residue curve corresponds to the higher bubble temperatures enabling a faster kinetics. Therefore, this preliminary analysis indicates that most stages of the column have to be reactive, and those would have to be located in the stripping section of the RD column as it has being previously verified [67].

The small section of the reactive residue curve above the saddle surface indicates the need for a non-reactive rectifying region to accomplish water separation and to avoid retuning to the reactants. Now, taking into account that the location of reactants inlet stage is guided by their volatility, IbOH (T_b = 380.8 K) would enter near the bottom of the column, and ACAC (T_b = 391.2 K) would access on top of the reactive zone. Here is important to point out the key role of the non-reactive rectifying section above the reactive stages. This section would help to reduce the ACAC drag into the condenser as it might be lost in the aqueous phase. Also, the presence of ACAC on the distillate could inhibit the liquid-liquid splitting that helps improving water removal.

Based upon this analysis the preliminary operating conditions of the potentially feasible RD configuration were obtained, and they are summarized in Table 3.1. As observed the composition of the IbAC product (i.e. > 99% wt.) nearly fulfills urethane grade specifications [68, 69].

Table 3.1. Preliminary operating conditions of a RD column for IbAC production as estimated form the conceptual design

Design variable	Value
Feed Molar ratio.	ACAC:IbOH = 0.9
Condenser temperature	298.15 K
Distillate product (previous to decanter)	Heterogeneous azeotrope IbOH (x =0.275) IbAC (x =0.351) W (x =0,374) (in wt. %).
Aqueous phase product (After decanter)	IbOH (x =0.009) IbAC (x = 9.2e-4) W (x = 0.990) (in wt. %).
Organic phase product (After decanter)	IbOH (x =0.376) IbAC (x =0.484) W (x = 0.140).
Bottom product	IbAC (in wt .%) 0.005 % ACAC, 1.2e-4 % IbOH, 0.995 % IbAC, 3.5e-16 % W
Reflux mixture	Azeotropic organic phase
Reactive zone location	Lower half of the Column
IbOH feed location	Bottom of reactive zone
ACAC feed location	Top of reactive Zone
Da	2

3.4.2. Simulation and optimization results

From the conceptual design it was verified that the reactive system is strongly influenced by the highly non-ideal equilibrium and by the reaction kinetics. Then, to confirm the feasibility of the implementation of a RD column for IbAC, a further exploration of the process was carried out by rigorous simulation. Base case conditions were defined according to preliminary estimations of the conceptual design. The main adjustable variables of the process corresponds to: IbOH:ACAC feed molar ratio, organic split reflux (i.e. fraction of the organic phase removed as distillate), feed to bottom ratio, number of reactive and non-reactive stages, and location of the feed stages. As the target of the RD process is to ensure high conversion of the limiting reagent (i.e. ACAC), this variable was used to assess the impact of each variable of the

column performance. Also, as pure IbAC is a saddle node, the IbAC purity in the bottom stream was assessed during the analysis. Figures C1 to C3 in the annexes C present the influence of the assessed variables on the reaction conversion.

The effect of the molar feed ratio on the reaction conversion and IbAC purity is described in Figure C1. Here, the intensification capacity of the RD process is verified, as conversions above 99% are achieved under the different molar ratios. Nevertheless, the minimum is observed when using the equimolar feed ratio, and as expected, almost complete conversion is achieved when using IbOH excess. Interestingly, the IbAC purity is largely affected when using excess of reactants, either ACAC or IbOH.

Figure C2 presents the effect of removing part of the organic phase from the decanter within the distillate. It is represented as the removed fraction with respect to the total flowrate of the organic phase. As expected, the highest conversion and IbAC purity is obtained when only the aqueous phase is removed as distillate product. Regarding the bottom to feed (B:F) ratio, Figures C3 and C4 present its effect on the conversion, purity of IbAC in the bottom stream, heat duty, and the amount of IbAC lost in the distillate stream. It is observed that high conversion and product purity (99,5% in wt.) is achieved with relatively low B:F ratio (under 0.22). However, at this values the system presents the maximum loses of IbAc in the distillate stream, and requiring larger heat duties.

Using preliminary parameters presented in Table 3.1 and the results from the sensitivity analysis, the range of operating conditions were narrowed for further optimization. The corresponding base case conditions are summarized in Table 3.2, and Figure 3.6 presents the configuration of the simulated RD column. Reactants purchase price were taken from the International Trade Center [70] using an average value for acetic acid of 500 $/ton and 900 $/ton isobutanol, as for the product sales prices a value of 1300 $/ton was used for urethane grade [68, 69]. The energy costs were calculated using references values available in Aspen Plus V10, i.e. 2.12e-7 $/kJ and 2.2e-6 $/kJ for cooling and heating utilities, respectively. Catalyst price was taken from the manufacturer, i.e. 150 $/dry kg [65]. After running the metaheuristic optimization, only 50 generations and 70 individuals were required to achieve the optimal conditions that maximized economic potential while reducing reactants losses. Table 3.2 also summarizes the results of the optimized configuration, and Figure 3.6 presents the corresponding temperature and composition profiles. Additional results are summarized in Tables 3.3 and 3.4.

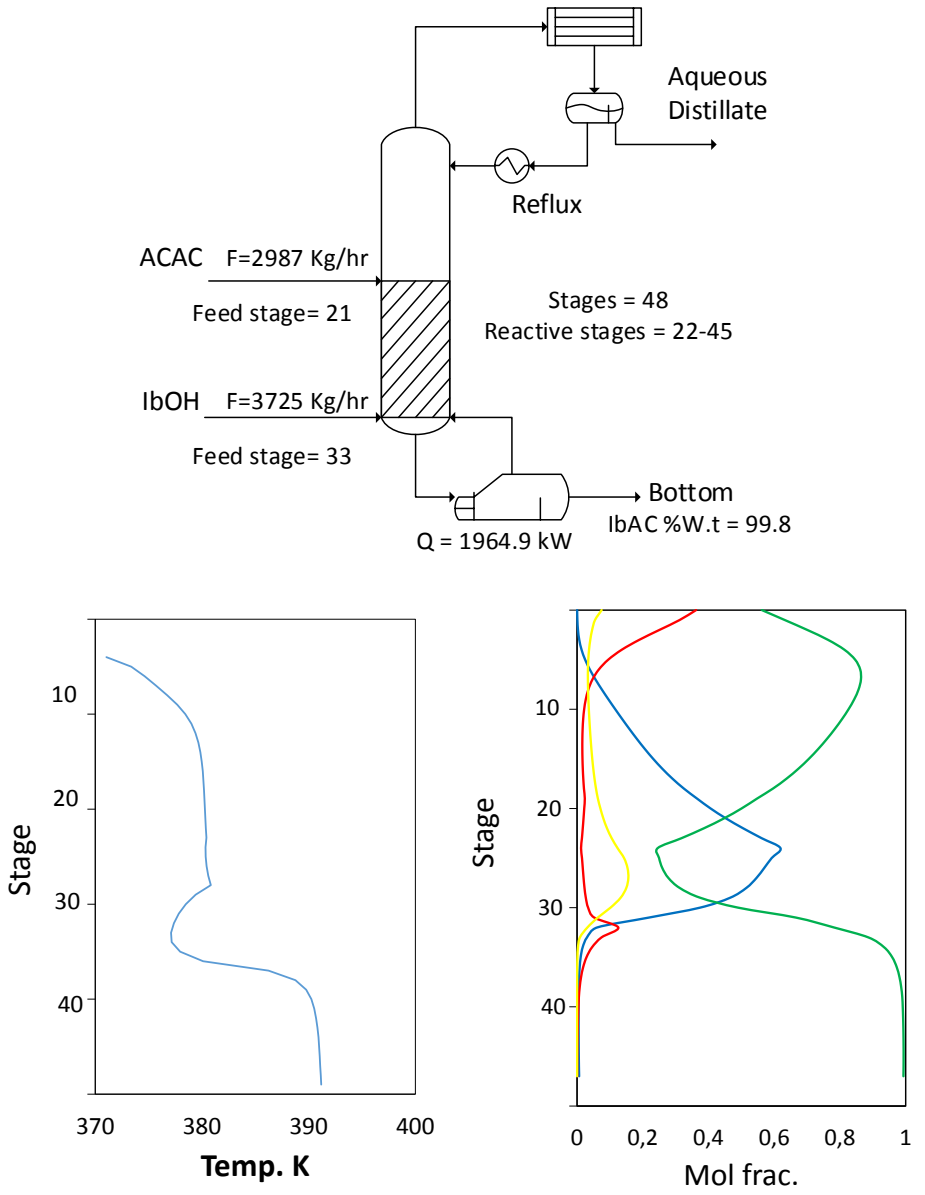

Figure 3.6. Configuration of the optimal RD column, and operating temperature and composition profiles . (—) ACAC, (—) IbOH, (—) IbAC, (—) W.

Table 3.2. General characteristics of the reactive distillation column for the base case and the optimized configuration.

Equipment variables		
Design variable	**Value**	
	Base Case	**Optimized Configuration**
Stages	40	48
Reactive stages	20-40	22-45
Feed stages	20 and 40	21 and 33
Bottom to feed ratio	0.25	0,215
Pressure	101 Kpa	101 Kpa
Total pressure drop	5 Kpa	5 Kpa

Streams conditions		
ACAC molar Flow Kmol/h	47.37	49.74
IbOH molar Flow Kmol/h	52.63	50,25
ACAC:IbOH molar feed ratio	0.90	0,98
Hold-Up	0,033 m^3	
Catalyst load	780 Kg/m^3	

Table 3.3. Main results of the reactive distillation column for the base case and the optimized configuration.

General Results		
	Base Case	**Optimized Configuration**
	Stream Results	
Aqueous Distillate	**Mass Frac./mass Flow (Kg/h)**	
ACAC	0.042 / 34.88	5.2e-5 / 0.048
IbOH	0.005 / 4.855	0.035 / 21.68
IbAC	0.008 / 7.286	0.005 / 5.327
W	0.943 / 779.1	0.96 / 895.9
Bottom Product	**Mass Frac./mass Flow (Kg/h)**	
ACAC	0.023 / 137.8	1e-4 / 0.998
IbOH	0.101 / 598.1	0.001 / 6.018
IbAC	0.871 / 5161	0.998 / 5771.4
W	0.004 / 22.46	7e-15 / 4e-11
	Equipment results	
Stage 1 Temp. °C	104.8	97.6
Bottom Temp °C	109.16	118.09
Reboiler duty KW	1832.1	1964.9
Condenser duty KW	1889.8	2000.8

Table 3.4. Main performance indicators of the reactive distillation column for the base case and the optimized configuration.

General Results		
	Base case	**Optimized Configuration**
ACAC conversion	93.92	99.96
IbOH Conversion.	84.54	98.96
Energy intensity $\left(\frac{kW}{Kg_{IbAC}}\right)$	0.81	0.77
Mass intensity $\left(\frac{kg_{react}}{kg_{IbAC}}\right)$	1.33	1.16
Productivity $\left(\frac{kg_{Ibac}}{m^3 * h}\right)$	306.18	328.72
Production cost $\left(\frac{USD}{ton}\right)$	994.62	978.98

As observed, this final configuration and operating conditions match well with predictions from the conceptual design, verifying the usefulness of the preliminary

RRCM approach. Also, reactants were almost completely converted and a high purity of the IbAC was obtained resembling the specification of a urethane grade product. This optimization also reduced the production costs even though the size of the optimized column is larger thus having larger capital costs. It is also observed that there is a better utilization of the reactants, reducing waste and loses and the corresponding energy consumption.

Finally, the cost distribution involved in the isobutyl acetate production via RD is presented in the figure 3.7. As expected the main costs corresponds to reactants purchase, particularly IbOH which is more expensive and used in excess. This indicates that there is a possibility to improve the process performance by focusing on the recovery of the lost isobutanol in the aqueous outlet stream, or by using a more active catalysts (e.g. homogeneous methanesulfonic acid). Nevertheless, the process seems economically feasible as production costs corresponds to nearly 75% of the selling price. Also, the final cost distribution is similar to that observed in the productions of most chemical commodities.

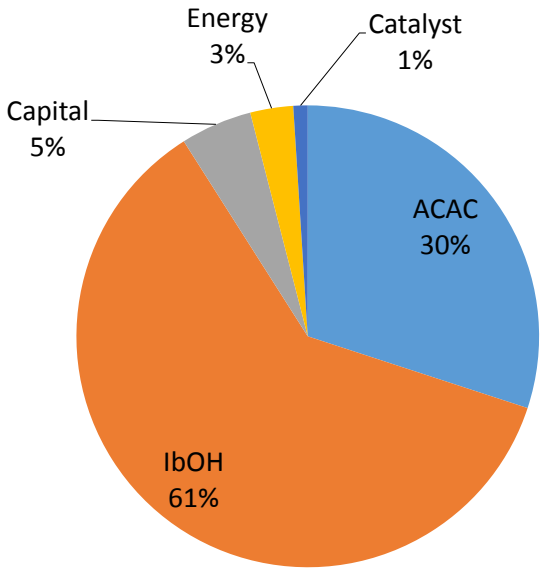

Figure 3.7. Costs distribution during isobutyl acetate production via RD

3.5. Conclusions

In this work, a conceptual design methodology based upon reactive residue curve maps (RRCM) analysis was implemented for the production of isobutyl acetate via reactive distillation. The process involved the heterogeneously catalyzed esterification

of isobutanol with acetic acid. The design methodology was based upon validated phase equilibria and kinetic models. The RRCM analysis provided the identification of the process operating conditions that enables the desired reactants conversion and product separation. Based upon the conceptual design results, a preliminary reactive distillation column configuration was constructed and simulated. This configuration was assessed and further analyzed to identify the key variables to obtain maximum conversions and high isobutyl acetate purities. Once identified, these variables were subjected to optimization using a metaheuristic algorithm to reduce the capital and energy costs, maximizing conversion and product purity. Finally, a reactive distillation column with 48 stages was configured to produce 30,000 t/yr. of urethane-grade isobutyl acetate, and the correspondig production costs were maintained below 1 USD/kg. Acetic acid conversion was nearly complete, and the IbOH conversion was around 99% taking into account that some alcohol is lost within the aqueous distillate stream. The obtained results of the optimized configuration were well predicted by the conceptual analysis verifying the usefulness of the used methodologies. Some performance indicators under optimal conditions corresponded to: energy intensity of 0.77 kW/kg_{IbAC}, mass intensity of 1.16 $kg_{Reactant}$/kg_{IbAC}, productivity of 328.7 kg_{IbAC}/m^3h, and production cost of 0.98 USD/kg_{IbAC}. These values can be further used for comparison with other intensified technologies of for the operation with different catalysts.

3.6. References

1. European Union. 2006. Registration, Evaluation, Authorization and Restriction of Chemicals: REACH. 18.12.2006. https://eur-lex.europa.eu/legal-content/EN/TXT/?uri=CELEX%3A02006R1907-20140410 (Consulted May 13, 2019).

2. EPA. 2016. Toxic Substances Control Act (TSCA) amended by the Frank R. Lautenberg Chemical Safety for the 21st Century Act. 22.06.2016. https://www.congress.gov/114/plaws/publ182/PLAW-114publ182.pdf (Consulted May 13, 2019).

3. Brar, S. K., Sarma, S. J., Pakshirajan, K. (Eds.) 2017. Platform Chemical Biorefinery - Future Green Industry. Elsevier, Amsterdam, Netherlands. DOI: 10.1016/C2014-0-02394-5

4. Takkellapati, S., Li, T., Gonzalez, M. A. 2018. An overview of biorefinery-derived platform chemicals from a cellulose and hemicellulose biorefinery. Clean Technol. Environ. Policy 20: 1615–1630. DOI: 10.1007/s10098-018-1568-5

5. De Jong, E., Higson, A., Walsh, P., Wellisch, M. 2011. Bio-based Chemicals Value Added products from Biorefineries. IEA Bioenergy – Task 42: 2020: 01.

6. De Jong, E., Stichnothe, H., Bell, G., Jørgensen, H. 2020. Bio-based Chemicals A 2020 Update. IEA Bioenergy – Task 42 Biorefinery.

7. E4tech, RE-CORD and WUR. 2015. From the Sugar Platform to biofuels and biochemicals. Final report for the European Commission, contract No. ENER/C2/423-2012/SI2.673791. https://ec.europa.eu/energy/sites/ener/files/documents/EC%20Sugar%20Platform%20final%20report.pdf (Consulted May 13, 2019).

8. Alder, C., Hayler, J. D., Henderson, R., Redman, A., Shukla, L., Shuster L., Sneddon, H. 2016. Updating and further expanding GSK's solvent sustainability guide. Green Chem. 18: 3879-3890. DOI: 10.1039/C6GC00611F

9. Byrne, F., Jin, S., Paggiola, G., Petchey, T., Clark, J., Farmer, T., Hunt, A., McElroy, R., Sherwood, J. 2016. Tools and techniques for solvent selection: green solvent selection guides. Sustain. Chem. Process 4 (7): 1-24. DOI: 10.1186/s40508-016-0051-z

10. Patidar, P., Mahajani, S. 2012. Esterification of fusel oil using reactive distillation – Part I: Reaction kinetics. Chem. Eng. J. 207–208: 377-387. DOI: 10.1016/j.cej.2012.06.139

11. Montoya, **N.,** Durán, J., Córdoba, F., Gil, I., Trujillo, C., Rodríguez, G. 2016. Colombian fusel oil. Ing. Invest. 36: 21–27. DOI: 10.15446/ing.investig.v36n2.52369.

12. Jordison, T. L., Lira, C. T., Miller, D. J. 2015. Condensed-Phase Ethanol Conversion to Higher Alcohols. Industrial and Engineering Chemistry Research. 54 (44): 10991-11000. DOI: 10.1021/acs.iecr.5b02409

13. Phillips, S.; Aden, A., Jechura, J., Dayton, D., Eggeman, T. 2007. Thermochemical Ethanol via Indirect Gasification and Mixed Alcohol Synthesis of Lignocellulosic Biomass. Technical Report NREL/TP-510-41168. National Renewable Energy Laboratory. Golden, Co., USA. https://www.nrel.gov/docs/fy07osti/41168.pdf (Consulted May 13, 2019).

14. Brown, R. C. (Ed.) 2011. Thermochemical Processing of Biomass: Conversion into Fuels, Chemicals and Power. John Wiley & Sons, Ltd. NY, USA. DOI: 10.1002/9781119417637

15. Pang, J., Zheng, M., Zhang, T. 2019. Synthesis of ethanol and its catalytic conversion. Advances in Catalysis 64: 89-191. DOI: 10.1016/bs.acat.2019.08.001

16. Rosales-Calderon, O., Arantes, V. 2019. A review on commercial-scale high-value products that can be produced alongside cellulosic ethanol. Biotechnol. Biofuels 12, 240 DOI: 10.1186/s13068-019-1529-1

17. Moncada, J., Posada, J., Ramírez, A. 2017. Comparative early stage assessment of multiproduct biorefinery systems: An application to the isobutanol platform. Bioresour. Technol. 241: 44–53. DOI: 10.1016/j.biortech.2017.05.074

18. Butamax, 2016. The Biofuel of the Future. https://www.butamax.com/the-bio-isobutanol-advantage/higher-value-biofuel/ (Consulted May 13, 2019).

19. Eikmanns, B.J., Blombach, B. 2014. Isobutanol. In: (Bisaria, V. S., Kondo, A. Eds.) Bioprocessing of Renewable Resources to Commodity Bioproducts. John Wiley & Sons pp 327- 352. DOI: 10.1002/9781118845394.ch12.

20. Ryan, C. 2019. An overview of Gevo's biobased isobutanol production process. GEVO. https://gevo.com/wp-content/uploads/2019/11/Gevo-WP_Isobutanol.1.pdf (Consulted May 13, 2020).

21. REACH. Isobutyl Acetate. Substance Information. European Chemicals Agency. https://echa.europa.eu/substance-information/-/substanceinfo/100.003.406 (Consulted May 13, 2019).

22. Opdyke, D. L. J. 1978. Isobutyl acetate. Food Cosmet. Toxicol. 16: 795-796. DOI: 10.1016/S0015-6264(78)80119-9

23. Falcke, H., Holbrook, S., Clenahan, I., López, A., Sanalan, T., Brinkmann, T., Roth, J., Zerger, B., Roudier, S., Delgado, L. 2017. Best Available Techniques (BAT) Reference Document for the Production of Large Volume Organic Chemicals; EUR 28882 EN; Publications Office of the European Union, Luxembourg. DOI: 10.2760/77304

24. Ramli, N. A., Rahman, R. A., Ngadi, N., Samah, R. A. 2017. Optimisation of fermentation conditions for isobutanol production by saccharomyces cerevisiae using response surface methodology. CET 56: 301-306. DOI: 10.3303/CET1756051

25. Atsumi S., Hanai, T. Liao, J. C. 2008. Non-fermentative pathways for synthesis of branched-chain higher alcohols as biofuels. Nature 451 (7174): 86–89. DOI: 10.1038/nature06450

26. Xiao, Y., Feng, X. Varman, A., He, L., Yu, H., Tang, Y. 2012. Kinetic Modeling and Isotopic Investigation of Isobutanol Fermentation by Two Engineered Escherichia coli Strains. Ind. Eng. Chem. Res. 51 (49): 15855-15863. DOI: 10.1021/ie202936t

27. Lan, E. I., Liao, J. C. 2013. Microbial synthesis of n-butanol, isobutanol, and other higher alcohols from diverse resources. Bioresour. Technol. 135, 339–349. DOI: 10.1016/j.biortech.2012.09.104

28. Minty, J. J., Singer, M. E., Scholz, S. A., Bae, C. H., Ahn, J. H., Foster, C. E., Liao, J. C., Lin, X. N. 2013. Design and characterization of synthetic fungal-bacterial consortia for direct production of isobutanol from cellulosic biomass. Proc. Natl. Acad. Sci. 110: 14592–14597. DOI: 10.1073/pnas.1218447110

29. Gak, E., Tyurin, M., Kiriukhin, M. 2014. Genome tailoring powered production of isobutanol in continuous CO_2/H_2 blend fermentation using engineered acetogen biocatalyst. J. Ind. Microbiol. Biotechnol. 41 (5): 763-781. DOI: 10.1007/s10295-014-1416-5

30. Tao, L., Tan, E., McCormick, R., Zhang, M., Aden, A., He, X., Zigler, B. 2014. Techno-economic analysis and life-cycle assessment of cellulosic isobutanol and

comparison with cellulosic ethanol and n-butanol. Biofuel. Bioprod. Biorefin. 8: 30–48. DOI: 10.1002/bbb.1431

31. Siripong, W., Wolf, P., Kusumoputri T. P., Downes J. J., Kocharin, K., Tanapongpipat, S., Runguphan, W. 2018. Metabolic engineering of Pichia pastoris for production of isobutanol and isobutyl acetate. Biotechnol Biofuels. 11: 1-16. DOI: 10.1186/s13068-017-1003-x

32. Bauer, F., Hulteberg, C. 2014. Isobutanol from glycerine – A techno-economic evaluation of a new biofuel production process. Appl. Energy 122: 261-268. DOI: 10.1016/j.apenergy.2014.02.037

33. Subramanian, N., Adeyinka, A., Spivey, J. J. 2013. Catalytic conversion of syngas to i-butanol - Synthesis routes and catalyst developments: A review. Catalysis 26: 161-178. DOI: 10.1039/9781782620037-00161

34. Sahu, A., Pandit, A. B. 2019. Facile Synthesis of Homogeneous Catalyzed Esterification of Medium-Chain-Length Fatty Acids and Kinetic Study. Ind. Eng. Chem. Res. 58 (49): 22212-22224. DOI: 10.1021/acs.iecr.9b05034

35. Sahu, A., Pandit, A. B. 2019. Kinetic Study of Homogeneous Catalyzed Esterification of a Series of Aliphatic Acids with Different Alcohols. Ind. Eng. Chem. Res. 58 (8): 2672-2682. DOI: 10.1021/acs.iecr.8b04781

36. Chin S. Y., Azizan N., Ahmad M. A. A., Kamaruzaman M. R. 2019. Ion Exchange Resins Catalysed Esterification for the Production of Value Added Petrochemicals and Oleochemicals. In: (Inamuddin, I., Rangreez T. A., Asiri A. M. Eds.) Applications of Ion Exchange Materials in Chemical and Food Industries. Springer, Cham. DOI: 10.1007/978-3-030-06085-5_4

37. Fattahi, N., Triantafyllidis, K., Luque, R., Ramazani, A. 2019. Zeolite-Based Catalysts: A Valuable Approach toward Ester Bond Formation. Catalysts 9: 758. DOI: 10.3390/catal9090758

38. Izci, A., Bodur, F. 2007. Liquid-phase esterification of acetic acid with isobutanol catalyzed by ion-exchange resins. React. Funct. Polym. 67: 1458–1464. DOI: 10.1016/j.reactfunctpolym.2007.07.019

39. Altıokka, M. R., Çıtak, A. 2003. Kinetics study of esterification of acetic acid with isobutanol in the presence of amberlite catalyst. Appl. Catal. Gen. 239: 141–148. DOI: 10.1016/S0926-860X(02)00381-2

40. Izci, A., Uyar, E., Izci, E. 2008. Determination of Adsorption and Kinetic Parameters for Synthesis of Isobutyl Acetate Catalyzed by Amberlite Ir-122. Chem. Eng. Commun. 196: 56–67. DOI: 10.1080/00986440802303293

41. Muñoz, R., Montón, J. B., Burguet, M. C., de la Torre, J. 2006. Separation of isobutyl alcohol and isobutyl acetate by extractive distillation and pressure-swing distillation: simulation and optimization. Sep. Purif. Technol. 50: 175–183. DOI: 10.1016/j.seppur.2005.11.022

42. Patidar, P., Mahajani, S. 2013. Esterification of fusel oil using reactive distillation Part II: Process Alternatives. Ind. Eng. Chem. Res. 52 (47): 16637-16647. DOI: 10.1021/ie401553z

43. Korkmaz, S., Salt, Y., asanoglu, A., Ozkan, S., Salt, I., Dincer, S. 2009. Pervaporation membrane reactor study for the esterification of acetic acid and isobutanol using polydimethylsiloxane membrane. Appl. Catal. A: Gen. 366 (1): 102-107. DOI: 10.1016/j.apcata.2009.06.037

44. Korkmaz, S., Salt, Y., Dincer, S. 2011. Esterification of acetic acid and isobutanol in a pervaporation membrane reactor using different membranes. Ind. Eng. Chem. Res. 50: 11657-11666. DOI: 10.1021/ie200086h

45. Cho, S. J., Shin, J. S., Choi, S. H., Lee, E. S., Park, S. J. 2014. Optimization study for pressure swing distillation process for the mixture of isobutyl-acetate and isobutyl-alcohol system. Korean Chem. Eng. Res. 52: 307-313. DOI: 10.9713/kcer.2014.52.3.307

46. Chen, L., Ye, Q., Feng, S., Zhang, H., Wang, N., Cen, H., Fan, Y. 2020. Investigation about energy-saving for the isobutyl acetate synthesis in a reactive divided-wall column via vapor recompression heat pump. Chem. Eng. Process. Process Intensif. 147: 107783. DOI: 10.1016/j.cep.2019.107783

47. Steiningeweg, S., Gmehling, J. 2002. n-Butyl Acetate Synthesis Via Reactive Distillation: Thermodynamic Aspects, Reaction Kinetics, Pilot-Plant Experiments And Simulation Studies. Ind. Eng. Chem. Res. 41 (22): 5483-5490 DOI: 10.1021/ie020179h

48. Gonzales, D., Bastidas, P., Rodriguez, G., Gil, I. 2017. Design alternatives and control performance in the pilot scale production of isoamyl acetate via reactive distillation. Chem. Eng. Res. Des. 123: 347-350. DOI: 10.1016/j.cherd.2017.05.028.

49. Tang, Y., Huang, H., Chien, I. 2003. Design of a complete ethyl acetate reactive distillation system. J. Chem. Eng. Japan. 36 (11): 1352-1363 DOI: 10.1252/jcej.36.1352.

50. Martinez, A.F., Sanchez, C.A., Orjuela, A., Rodriguez, G. 2020. Isobutyl acetate production by reactive distillation. Non-reactive phase equilibrium and topological analysis. Fluid Phase Equilibr. 516: 112612. DOI: 10.1016/j.fluid.2020.112612

51. Orjuela, A., Santaella, M., Molano, P. 2016. Process Intensification by Reactive Distillation. In: (Segovia-Hernández, J. G., Bonilla, A., Eds.) Process intensification in chemical Engineering, Springer International Publishing, Switzerland 2016. DOI: 10.1007/978-3-319-28392-0_6.

52. Martinez, A. F., Sanchez, C. A., Orjuela, A., Gil, I. D., Rodriguez, G. 2020. Kinetic study on the catalytic esterification of acetic acid with isobutanol over Amberlyst 15. Chem. Eng. Res. Des. In revision.

53. D. Barbosa, Doherty, M. 1988. The simple distillation of homogeneous reactive mixtures, Chem. Eng. Sci. 43: 541–550. DOI: 10.1016/0009-2509(88)87015-5

54. Venimadhavan, G., Buzad, G., Doherty, M. F., Malone, M. F. 1994. Effect of Kinetics on Residue Curve maps for Reactive Distillation. AIChE J. 40 (11): 1814-1824. DOI: 10.1002/aic.690401106.

55. Orjuela, A., Kolah, A., Hong, X., Miller, D., Lira, C. 2012. Diethyl Succinate Synthesis by Reactive Distillation. Sep. Purif. Technol. 88: 151-162. DOI: 10.1016/j.seppur.2011.11.033

56. Zhang C, Wan H, Xue L, Guan G. 2011. Investigation on isobaric vapor liquid equilibrium for acetic acid+water+(n-propyl acetate or iso-butyl acetate). Fluid Phase Equilibr. 305 (1): 68–75. DOI: 10.1016/j.fluid.2011.03.006

57. Burguet, M. C.; Monton, J. B.; Munoz, R.; Wisniak, J.; Segura, H. J. 1996. Polyazeotropy in Associating Systems: The 2-Methylpropyl Ethanoate + Ethanoic Acid System. J. Chem. Eng. Data. 41: 1191-1195. DOI: 10.1021/je960159k

58. Matthew J., Okasinski., Doherty M.F. Design Method for Kinetically Controlled, Staged Reactive Distillation Columns. Ind. Eng. Chem. Res. (1998) Vol. 37 pp. 2821-2834.

59. Cash, J. R., Karp, A.H. 1990. A variable order Runge-Kutta method for initial value problems with rapidly varying right-hand sides. ACM T. Math. Software, 16: 201-222. DOI: 10.1145/79505.79507

60. Press, W. Teukolsky, S. A., Vetterling, W. T., Flannery, B. P. 2007. Numerical Recipes: The Art of Scientific Computing, Cambridge University Press, New York, NY United States. DOI: 10.5555/1403886

61. W. Song, R.S. Huss, M.F. Doherty & M.F. Malone. Discovery of a reactive azeotrope. Nature (1997). Vol 338 pg 661-663.

62. Kolah, A., Asthana, N. S., Vu, D. T., Lira, C. T., Miller, D. J. 2008. Triethyl Citrate Synthesis by Reactive Distillation. Ind. Eng. Chem. Res. 47 (4): 1017-1025. DOI: 10.1021/ie070279t

63. Behrens, M., Olujic, Z., Jansens, P. J. 2008. Liquid Holdup in Catalyst-Containing Pockets of a Modular Catalytic Structured Packing. Chem. Eng. Technol. 31 (11): 1630-1637. DOI: 10.1002/ceat.200800236

64. Yang, X. S. (Ed) 2010. Nature-Inspired Metaheuristic Algorithms. 2nd Edition, Luniver Press. UK. DOI: 10.5555/1893084

65. DUPONT. AMBERLYST™ 15DRY Polymeric Catalyst, available in: https://www.dupont.com/content/dam/dupont/amer/us/en/water-solutions/public/documents/en/45-D00927-en.pdf (Consulted May 13, 2019).

66. Shah, M., Kiss, A. A., Zondervan, E., de Haan, A. 2012. Influence of liquid back mixing on a kinetically controlled reactive Distillation process. Chem. Eng. Sci. 68: 184–191. DOI: 10.1016/j.ces.2011.09.027

67. Bessling, B., Schembercker, G., Simmrock. K.H. 1997. Design of Processes with Reactive Distillation Line Diagrams. Ind. Eng. Chem. Res. 36:3032-3042. DOI: 10.1021/ie960727p

68. DOW. 2012. Isobutyl Acetate, Urethane Grade. Available in: https://www.dow.com/en-us/pdp.isobutyl-acetate-urethane-grade.85031z.html (Consulted May 13, 2019).

69. EASTMAN. 2015. Isobutyl Acetate Sales Specifications. Available in: https://www.eastman.com/supplemental/salespecs/71000132.pdf (Consulted May 13, 2019).

70. INTERNATIONAL TRADE CENTER. 2019. Acetic acid and Isobutanol Sales price. Available in: https://www.trademap.org/Index.aspx (consulted January 15, 2020).

4. FINAL CONCLUSIONS

The present work developed a complete study of the reactive distillation process for production of Isobutyl acetate.

Initially, a suitable modeling of the phase equilibrium of the quaternary mixture was accomplished by correlating experimental-obtained and reported data. Particularly, liquid-liquid phase equilibrium for the ternary system Acetic Acid - Isobutanol - Water were measured at different temperatures. Combining the measured data with literature reports, a set of regressed parameters were obtained for the NRTL-HOC thermodynamic model. The obtained model accurately represents the reactive and non-reactive phase equilibria as the topological structures were validated, and can be used for process design purposes. Afterwards, a kinetic model for the heterogeneously catalyzed (i.e. Amberlyst 15) esterification between acetic acid and isobutanol was fitted to experimental measurements. This was done by correlating the experimental kinetic data using a pseudo-homogeneous mole-fraction based model, and incorporating an experimentally evaluated chemical equilibrium constant. The kinetic model fitted reasonably well the experimental data, and it can also be used for further process modeling, and to assess different intensification alternatives in the production of isobutyl acetate.

Finally, using the previously obtained phase equilibria and kinetic models, an industrial reactive distillation process for the production of urethane-grade isobutyl acetate was obtained. This was developed by mean of a conceptual design using a reactive residue curve map approach, followed by further rigorous simulation and optimization. The optimization was carried out using an effective meta-heuristic algorithm and it was possible to minimize energy and materials intensity, reducing reactants loses and maximizing isobutyl acetate productivity under reduced costs. This project verified that isobutyl acetate production can be feasibly produced using a reactive distillation process.

5. Annexes A.

Phase equilibrium and topological analysis for the system acetic acid + isobutanol + isobutyl acetate + water

Table A1. Antoine parameters for vapor pressure calculation of pure components*.

Parameter**	Component			
	ACAC	**IbOH**	**H_2O**	**IbAC**
C_1	53,27	121,78	73,649	72,31
C_2	-6304,5	-10504	-7258,2	-6944,3
C_3	0	0		
C_4	0	0		
C_5	-4,2985	-13,921	-7,3037	-7,298
C_6	8,8865E-18	1,6898E-17	4,1653E-06	3,7892E-06
C_7	6	6	2	2

* $\ln(P) = C_1 + \frac{C_2}{T+C_3} + C_4 T + C_5 \ln(T) + C_6 T^{C_7}$ (P in N/m^2, T in K)

** Taken from Aspen Plus V.10 Databank.

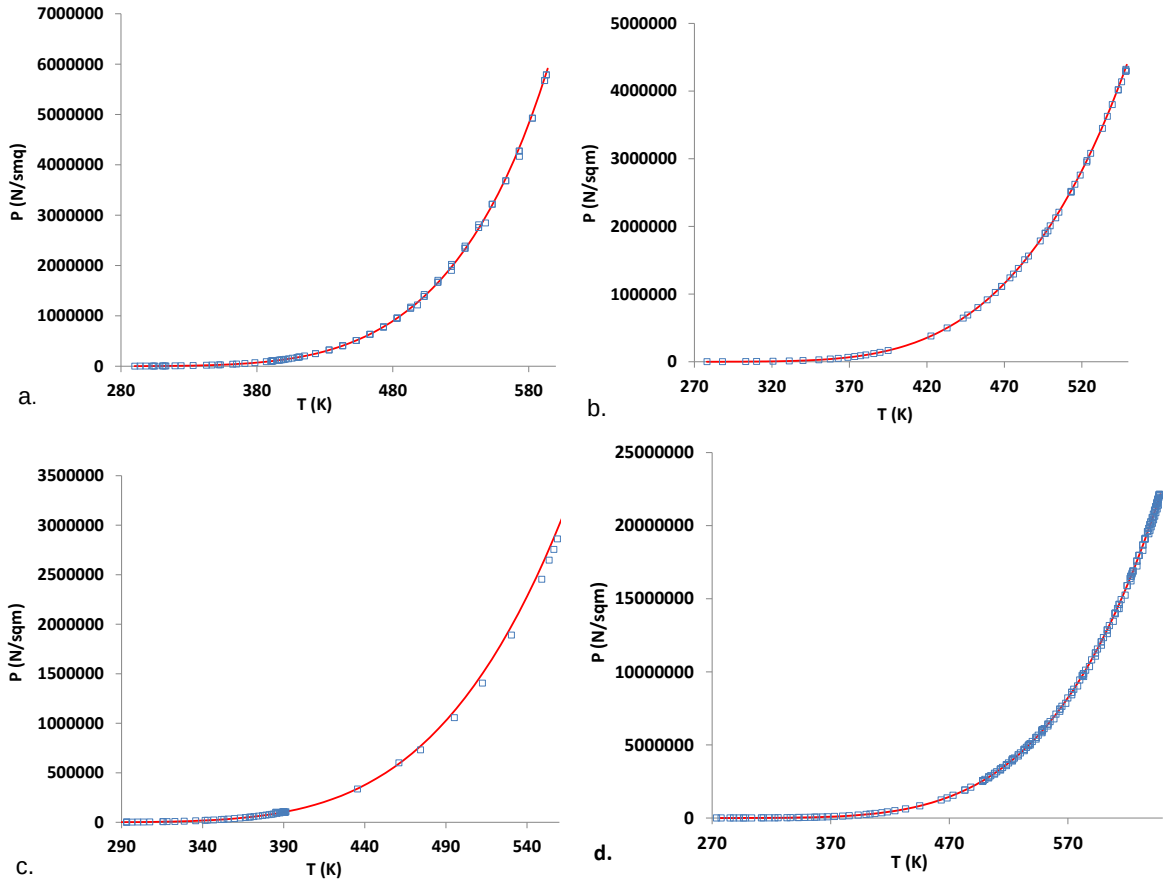

Figure A1. Experimental and calculated pure vapor pressure diagram for (a.) Acetic acid [1] (b.) Isobutanol [2-3] (c.) Isobutyl acetate [4-5] (d.) water, (□) experimental vapor pressure, (—), calculated vapour pressure using Antoine parameters presented in Table A1.

Table A2: Solvation and association parameters for Isobutyl acetate [13]

	Acetic acid	Isobutanol	Water	Isobutyl acetate
Acetic acid	4,5	2,5	2,5	2
Isobutanol	-	1,9	1,55	1,3[a]
Water	-		1,7	1,3
Isobutyl acetate	-	-	-	0.53

a. The Isobutanol - Isobutyl acetate parameter was estimated using the value of several alcohols with their corresponding acetate. [6-7]

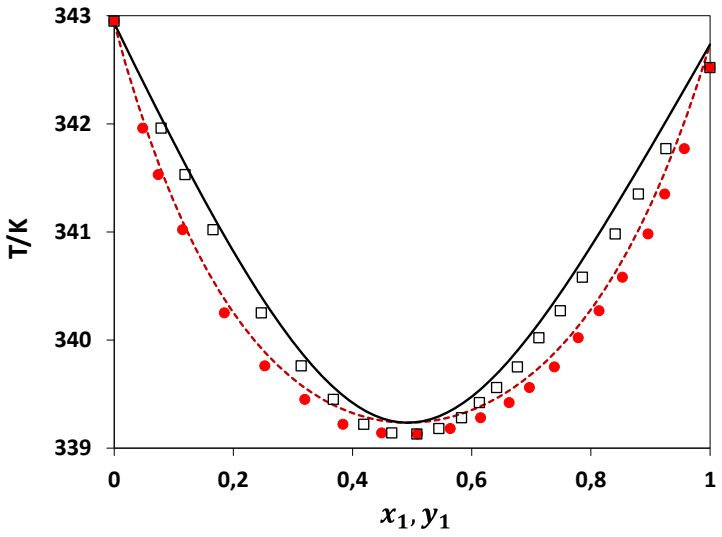

Figure A2. Experimental and calculated $T - x - y$ diagram of the system Isobutanol (1) + Isobutyl acetate (2) at 20 Kpa: (•), experimental liquid phase; (□), experimental Vapor phase; (—), calculated vapour phase with NRTL model with retrieved parameters; (---), calculated liquid phase with NRTL model with retrieved parameters. Experimental information from [4].

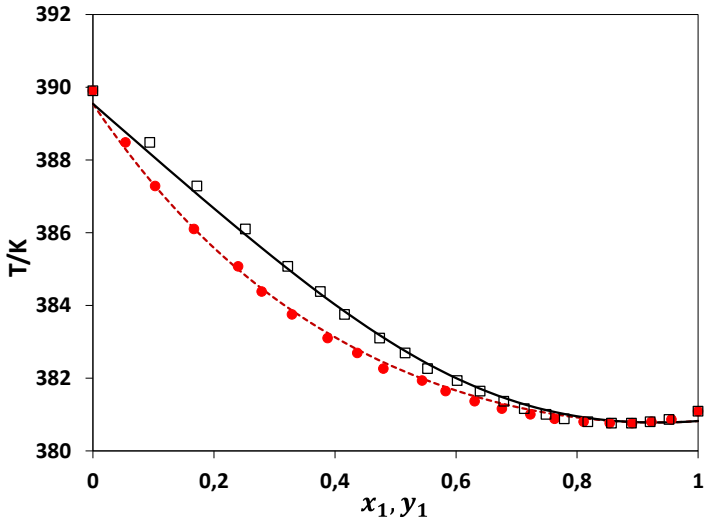

Figure A3. Experimental and calculated $T - x - y$ diagram of the system Isobutanol (1) + Isobutyl acetate (2) at 101,3 Kpa: (•), experimental liquid phase; (□), experimental Vapor phase; (—), calculated vapour phase with NRTL model with retrieved parameters; (---), calculated liquid phase with NRTL model with retrieved parameters. Experimental information from [4].

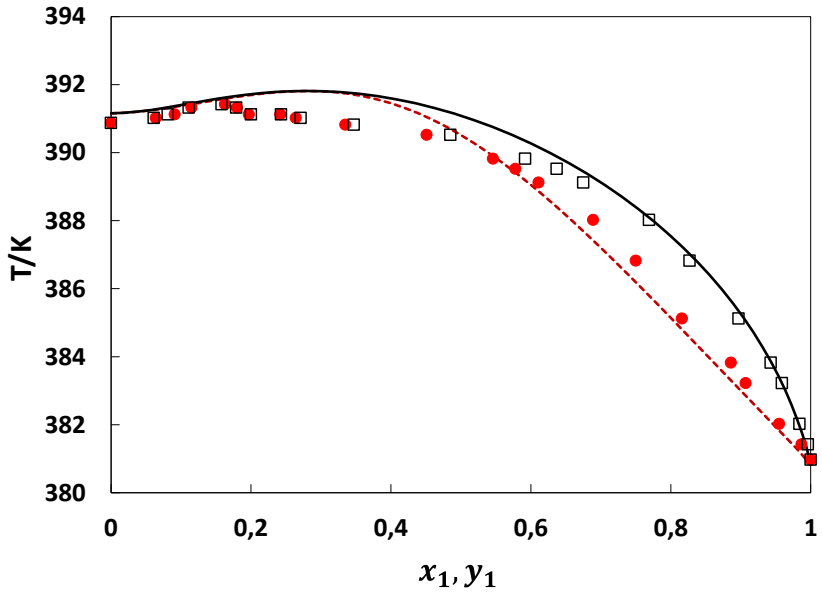

Figure A4. Experimental and calculated $T - x - y$ diagram of the system Isobutanol (1) + Acetic acid (2) at 101,3 Kpa: (•), experimental liquid phase; (□), experimental Vapor phase; (—), calculated vapour phase with NRTL model with retrieved parameters; (---), calculated liquid phase with NRTL model with retrieved parameters. Experimental information from [8].

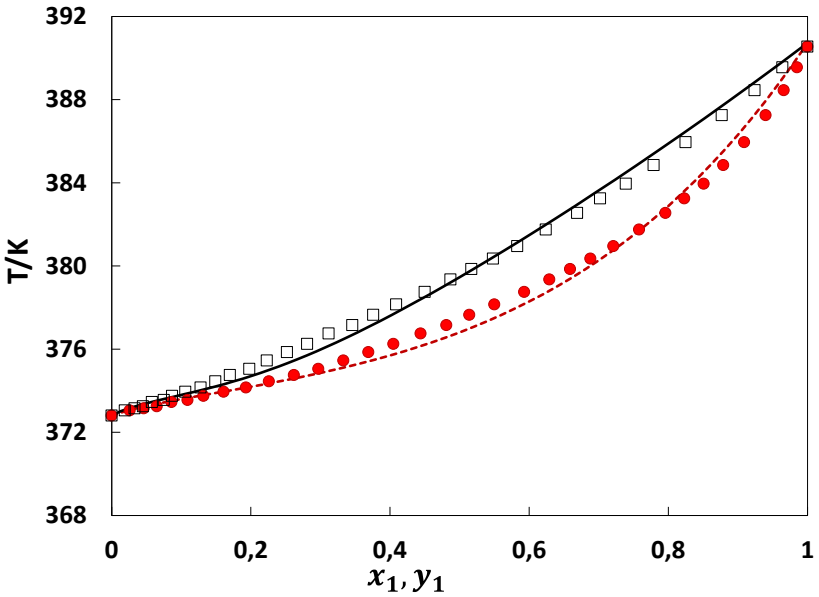

Figure A5. Experimental and calculated $T - x - y$ diagram of the system Acetic acid (1) + Water (2) at 100 Kpa: : (•), experimental liquid phase; (□), experimental Vapor phase; (—), calculated vapour phase with NRTL model with retrieved parameters; (---), calculated liquid phase with NRTL model with retrieved parameters. Experimental information from [14]

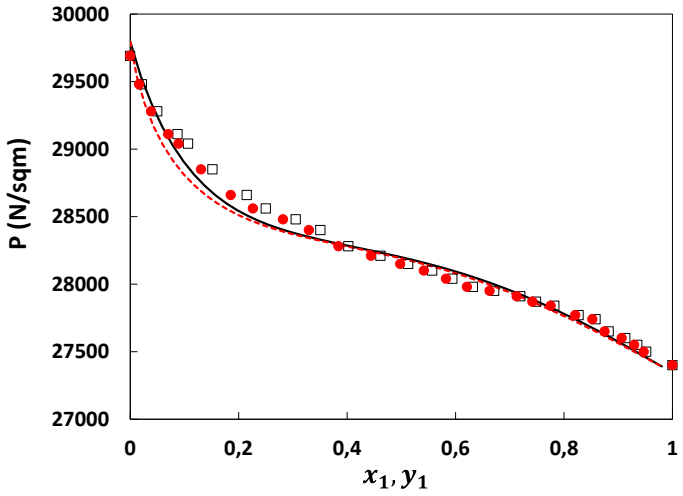

Figure A6. Experimental and calculated $P - x - y$ diagram of the system Acetic acid (1) + Isobutyl acetate (2) at 353,15 K: (•), experimental liquid phase; (□), experimental Vapor phase; (—), calculated vapour phase with NRTL model with retrieved parameters; (---), calculated liquid phase with NRTL model with retrieved parameters. Experimental information from [9].

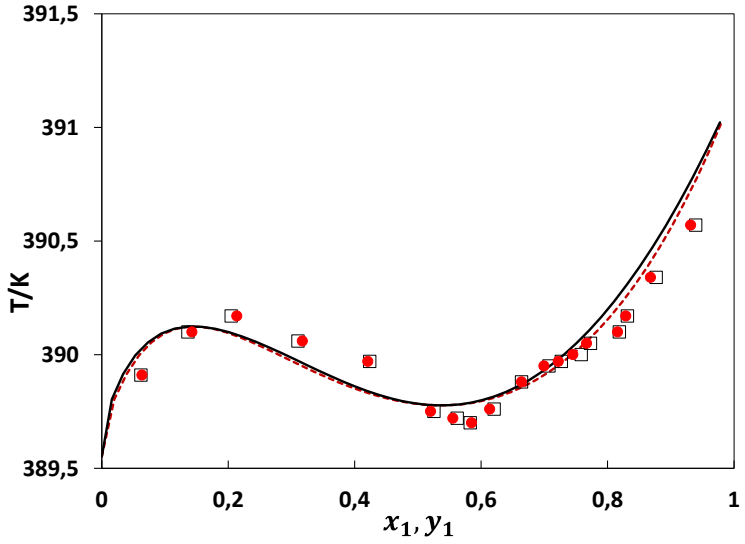

Figure A7. Experimental and calculated $T - x - y$ diagram of the system Acetic acid (1) + Isobutyl acetate (2) at 101,3 Kpa: (•), experimental liquid phase; (□), experimental Vapor phase; (—), calculated vapour phase with NRTL model with retrieved parameters; (---), calculated liquid phase with NRTL model with retrieved parameters. Experimental information from [10].

EXPERIMENTAL AND CALCULATED BINARY VAPOR-LIQUID-LIQUID EQUILIBRIUMS.

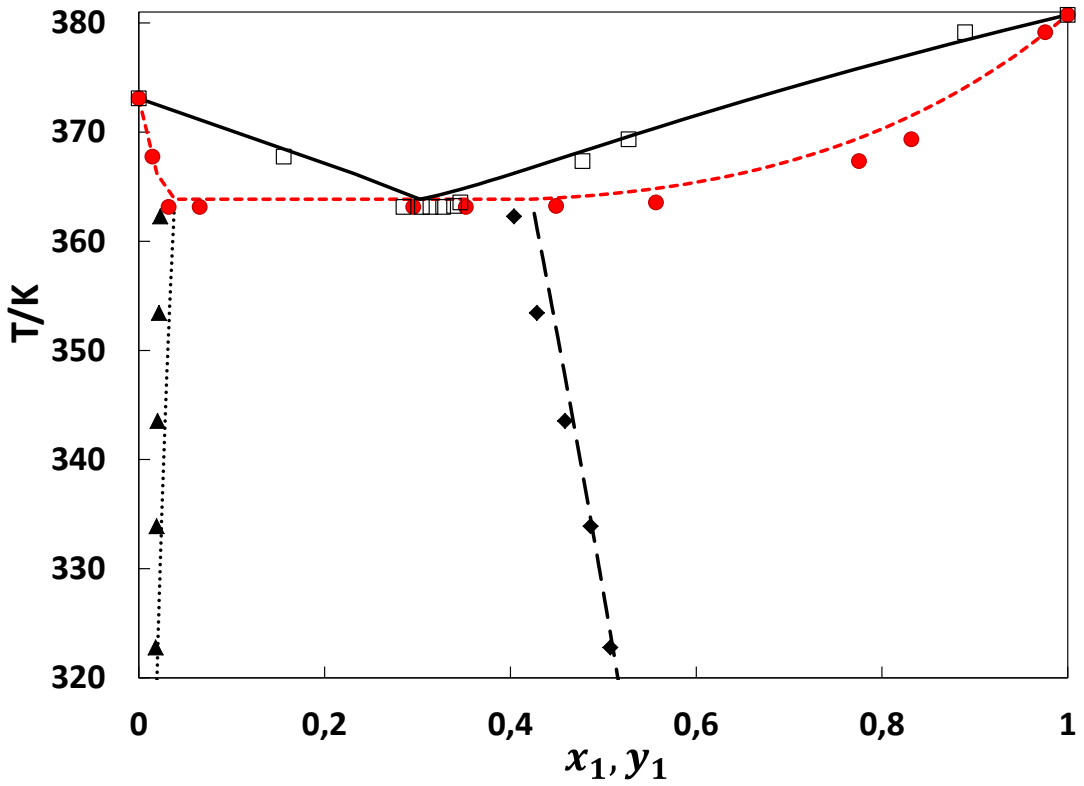

Figure A8. Experimental and calculated $T - x - y$ diagram of the system Isobutanol (1) + Water (2) at 101 Kpa: (○), experimental liquid phase; (□), experimental Vapor phase; (—), calculated vapour phase with NRTL model with retrieved parameters; (---), calculated liquid phase with NRTL model with retrieved parameters; (---), calculated organic liquid phase with NRTL model with retrieved parameters.; (•••), calculated aqueous liquid phase with NRTL model with retrieved parameters Experimental information from [11-12].

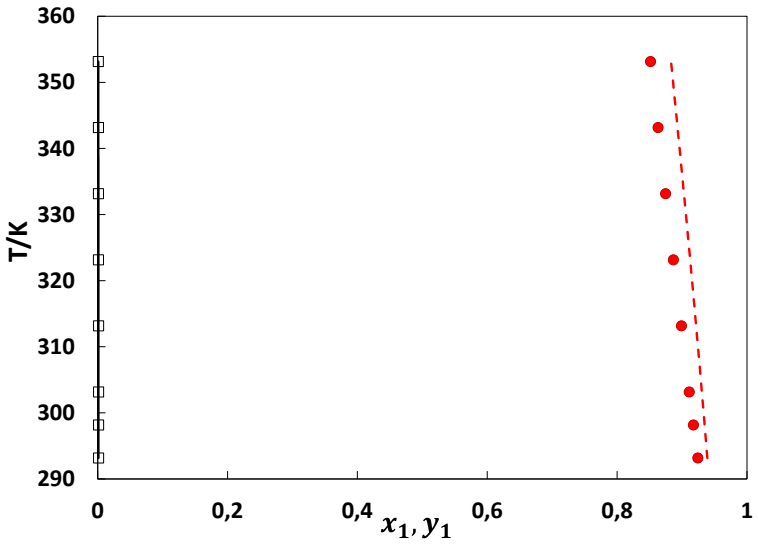

Figure A9. Experimental and calculated $T - x - x$ diagram of the system Isobutyl Acetate (1) + Water (2) at 101,3 Kpa: (○), experimental organic liquid phase; (□), experimental aqueous liquid phase; (—), calculated organic liquid phase with NRTL model with retrieved parameters; (---), calculated aqueous liquid phase with NRTL model with retrieved parameters. Experimental information from [13].

EXPERIMENTAL AND CALCULATED TERNARY LIQUID-LIQUID EQUILIBRIUMS.

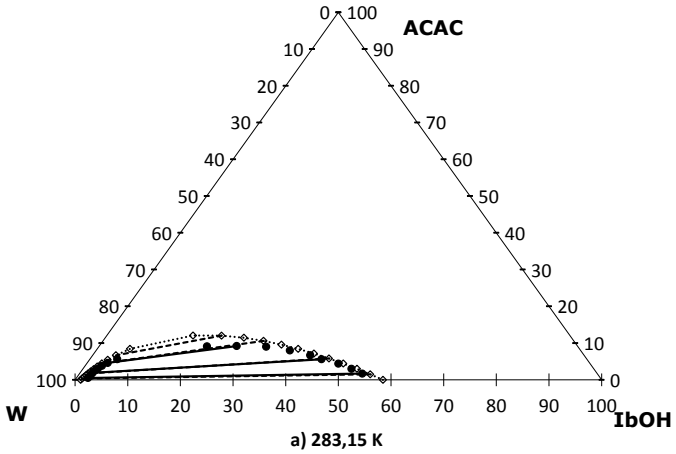

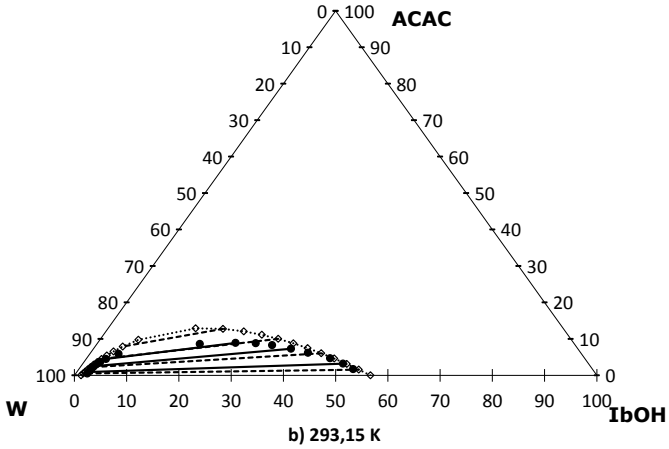

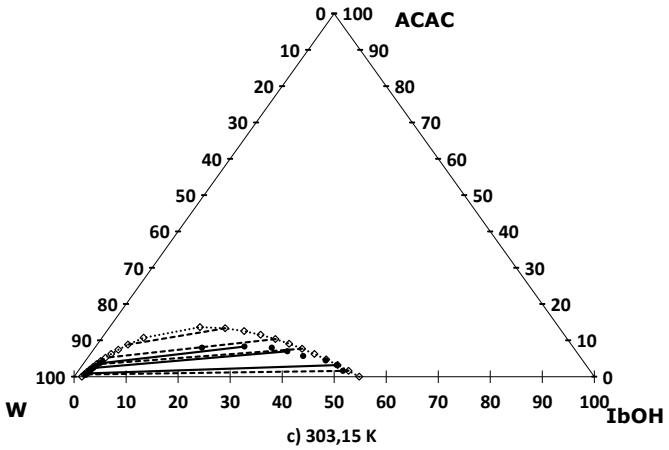

Figure A10. Ternary diagrams for mixtures of IbOH+ACAC+W at different temperatures. (a). 283,15 K; (b). 293,15 K; (c). 393,15 K. (•) experimental information; (—) experimental tie line; (••• ◊) binodal curve; (---) model tie line. Experimental information developed in laboratory.

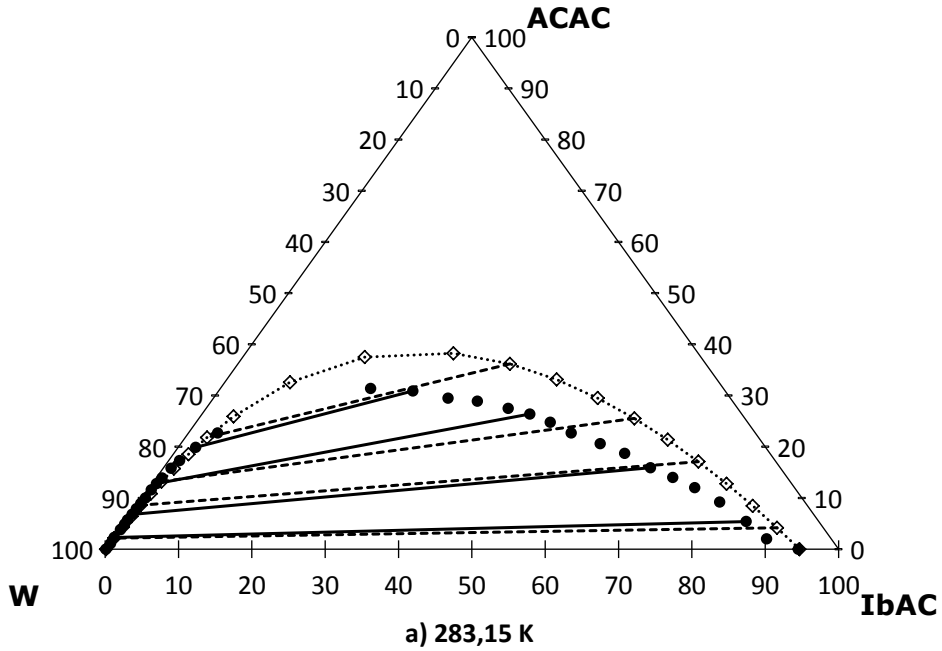

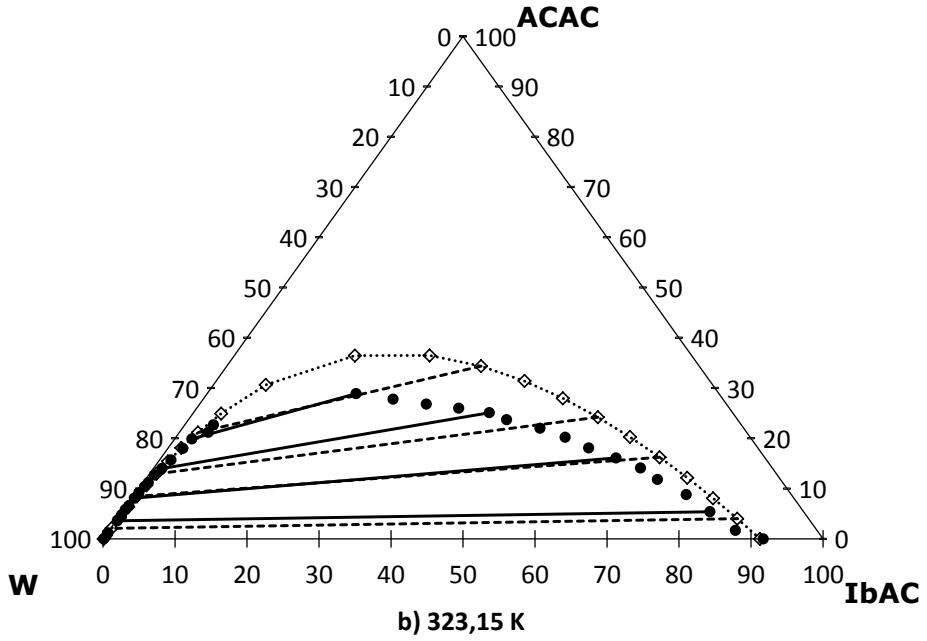

Figure A11. Ternary diagrams for mixtures of IbAC+ACAC+W at different temperatures. (a). 283,15 K; (b). 323,15 K; (•) experimental information; (—) experimental tie line; (••• ◊) binodal curve; (---) model tie line. Experimental information taken from [14].

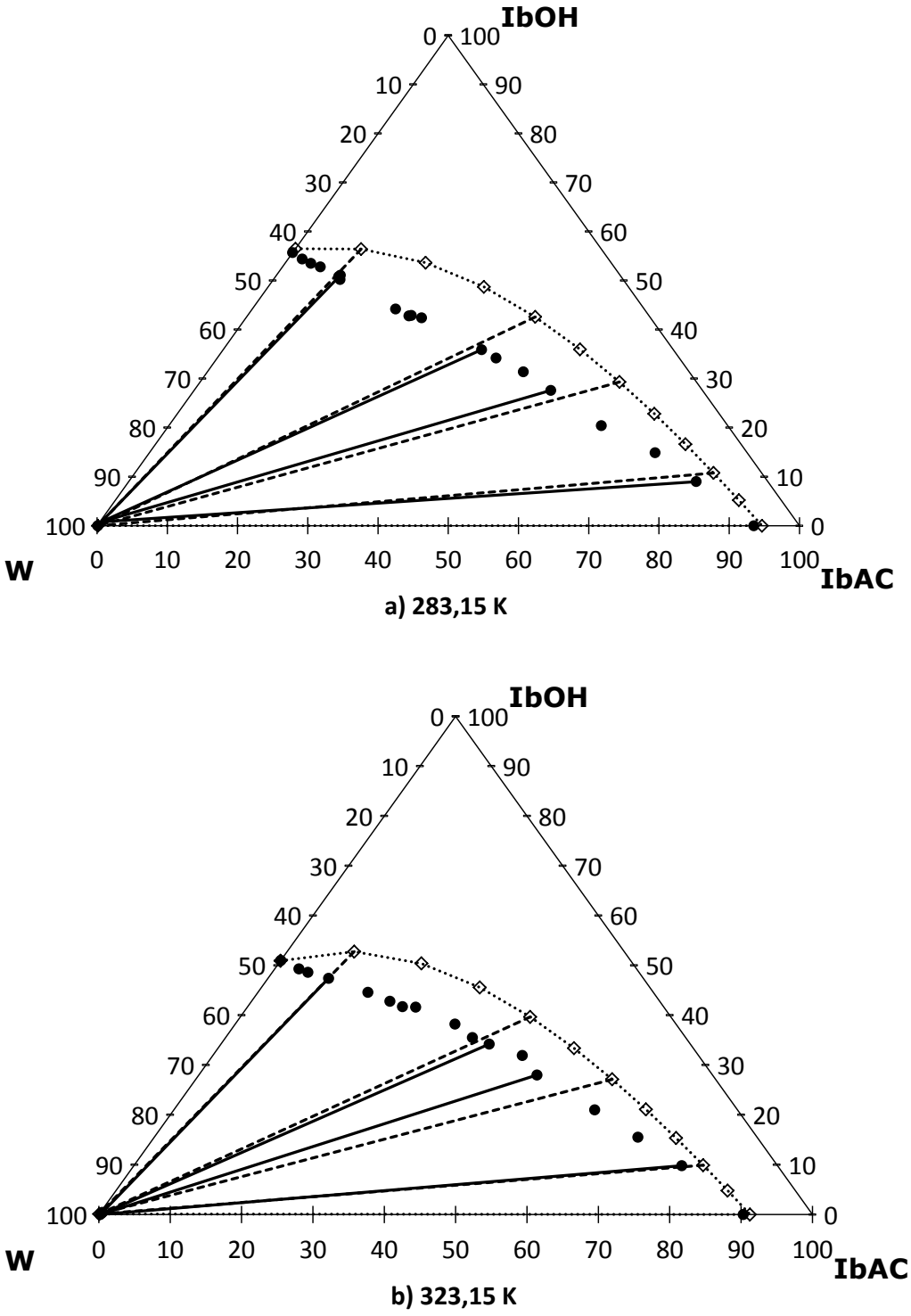

Figure A12. Ternary diagrams for mixtures of IbOH+IbAC+W at different temperatures. (a). 283,15 K; (b). 323,15 K; (•) experimental information; (—) experimental tie line; (••• ◊) binodal curve; (---) model tie line. Experimental information taken from [15].

CALCULATED TERNARY RESIDUE CURVE MAPS

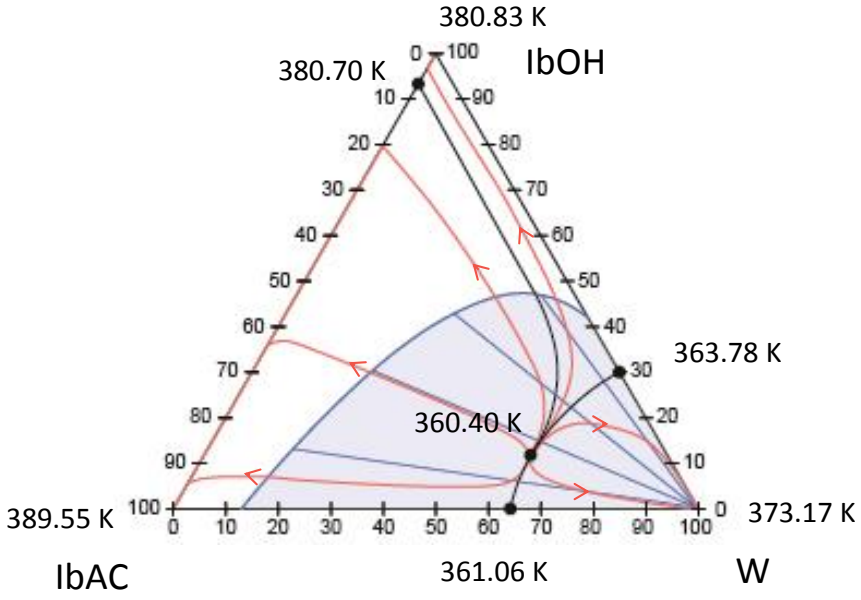

Figure A13. Ternary Residue Curve Map for mixtures of IbOH+IbAC+W; (•) Azeotropes; (—) Distillation boundary; (—) Residue Curve; (—) Immiscibility region and tie lines.

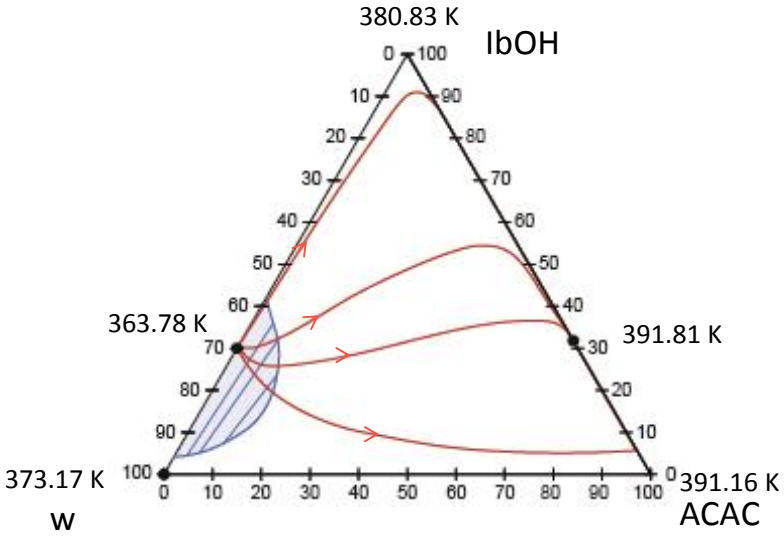

Figure A14. Ternary Residue Curve Map for mixtures of IbOH+ACAC+W; (•) Azeotropes; (—) Distillation boundary; (—) Residue Curve; (—) Immiscibility region and tie lines.

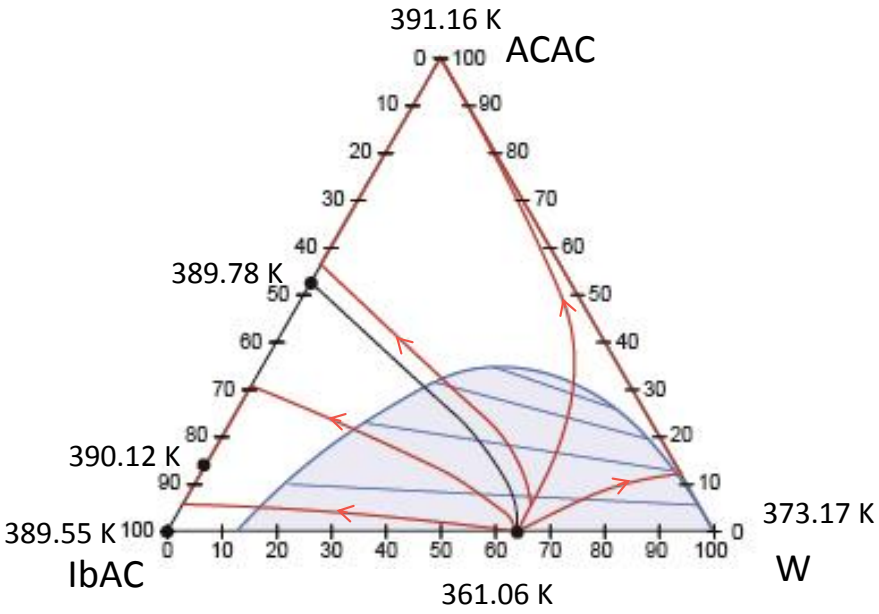

Figure A15. Ternary Residue Curve Map for mixtures of ACAC+IbAC+W; (•) Azeotropes; (—) Distillation boundary; (—) Residue Curve; (—) Immiscibility region and tie lines.

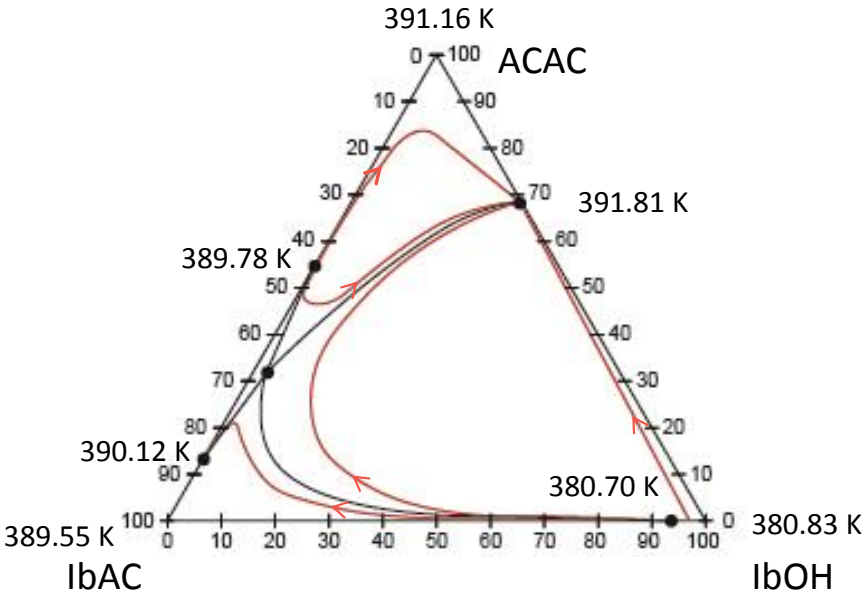

Figure A16. Ternary Residue Curve Map for mixtures of IbOH+IbAC+ACAC; (•) Azeotropes; (—) Distillation boundary; (—) Residue Curve.

5.1. References

1. Krichevskii, I. P.; Efremova, G. D.; Pryanikova, R. O.; Polyakov, E. W.Khim. Prom-st. (Moscow), 1961, 37, 54.Temperature: 298.14 K - 573.18 K

2. Ambrose, D.; Townsend, R. Thermodynamic Properties of Organic Oxygen Compounds IX. The Critical Properties and Vapor Pressures Above Five Atmospheres of Six Aliphatic Alcohols. J. Chem. Soc., 1963, 54, 3614-3625.

3. Brown, I.; Fock, W.; Smith, F. The thermodynamic properties of solutions of normal and branched alcohols in benzene and n-hexane. J. Chem. Thermodyn., 1969, 1, 273.

4. J.B. Montón, R. Muñoz, M.C. Burguet, J. de la Torre, Isobaric vapor–liquid equilibria for the binary systems isobutyl alcohol+isobutyl acetate and tert-butyl alcohol+tert-butyl acetate at 20 and 101.3kPa, Fluid Phase Equilibria. 227 (2005) 19–25. doi:10.1016/j.fluid.2004.10.022.

5. Ma, P.; Fang, Z.; Zhang, J.; Ruan, Y. Determination of Critical Constants, Saturated Vapor or Liquid Densities and Vapor Pressures of Six Organic Compounds. Gaoxiao Huaxue Gongcheng Xuebao, 1992, 6, 112-117.

6. C. Zhang, H. Wan, L. Xue, G. Guan, Investigation on isobaric vapor liquid equilibrium for acetic acid+water+(n-propyl acetate or iso-butyl acetate), Fluid Phase Equilibria. 305 (2011) 68–75. doi:10.1016/j.fluid.2011.03.006.

7. J.M.P. J. P. O'Connell, R.V.O. C. A. Eckert, Computer calculations for multicomponent vapor-liquid equilibria, AIChE J. 13 (1967) 238. doi:10.1002/aic.690130306.

8. Amezaga, S. A.; Biarge, J. F. An. Quim., 1973, 69, 587 Liquid-vapor equilibrium in systems formed by acetic acid and propyl, isopropyl, isobutyl, sec-butyl, and tert-butyl at 760 mm.

9. Burguet, M. C.; Monton, J. B.; Munoz, R.; Wisniak, J.; Segura, H. J. Chem. Eng. Data, 1996, 41, 1191-1195 Polyazeotropy in Associating Systems: The 2-Methylpropyl Ethanoate + Ethanoic Acid System.

10. Zhang C, Wan H, Xue L, Guan G. Investigation on isobaric vapor liquid equilibrium for acetic acid+water+(n-propyl acetate or iso-butyl acetate). Fluid Phase Equilibria. junio de 2011;305(1):68–75.

11. Zong, Z. L.; Yang, X.H.; Zheng, X. Y. J. Determination and correlation of vapor-liquid equilibria of alcohol solutions. Chem. Eng. Jpn., 1983, 16, 1. https://doi.org/10.1252/jcej.16.1.

12. Zhang, J.; Zhang, Y.; Fu, J.; Wang, X. Prediction of Partially Miscible System by VLE Data. Chemical Engineering (China), 1986, No. 4, 53-57.

13. Bomshtein, A. L.; Trofimov, A. N.; Gotlib, V. A.; Serafimov, L. A. Liquid-liquid phase equilibrium in isobutyl acetate-water and isobutyl acetate-water-acetic acid systems at normal temperature. Zh. Prikl. Khim. (Leningrad), 1978, 51, 440-442.

14. Cháfer A, Lladosa E, de la Torre J, Burguet MC. Study of liquid–liquid equilibrium of the systems isobutyl acetate+acetic acid+water and isobutyl alcohol+acetic acid+water at different temperatures. Fluid Phase Equilibria. octubre de 2008;271(1–2):76–81.

15. Cháfer A, de la Torre J, Monton JB, Lladosa E. Liquid–liquid equilibria of the systems isobutyl acetate+isobutyl alcohol+water and isobutyl acetate+isobutyl alcohol+glycerol at different temperatures. Fluid Phase Equilibria. marzo de 2008;265(1–2):122–8.

6. Annexes B.

Kinetic study on the catalytic esterification of acetic acid with isobutanol over Amberlyst 15

Table B1. Experimental conditions during the exploration of external mass transfer limitations. catalyst was used without sieving.

Experiment Number	ACAC:IbOH feed Ratio	Reaction Temperature (K)	catalyst Loading (% wt.)	Stirring Speed (RPM)
1	1:1	365	0.75	600
2	1:1	365	0.75	800
3	1:1	365	0.75	1000

Table B2. Experimental conditions for the internal mass preliminary tests.

Exp. Number	catalyst diameter (μm)	MESH sieve number	Reaction Temperature (K)	catalyst Loading (%wt)	Stirring Speed (RPM)	ACAC:IbOH feed Ratio
1	500<φ	35				
2	425<φ	40				
3	300<φ	50	365	0.75	1000	1:1
4	250<φ	60				
5	Φ<250	Max				

Table B3. Conditions during kinetic experiments

Exp. Number	Reaction Temperature (K)	catalyst Loading (%wt)	ACAC:IbOH feed Ratio
1	363.15	1.5	1:1
2	363.15	0.25	1:1
3	363.15	0.75	1:2
4	363.15	0.75	2:1
5	343.15	0.75	1:1
6	353.15	0.75	1:1
7	363.15	0.75	1:1
8	373.15	0.75	1:1

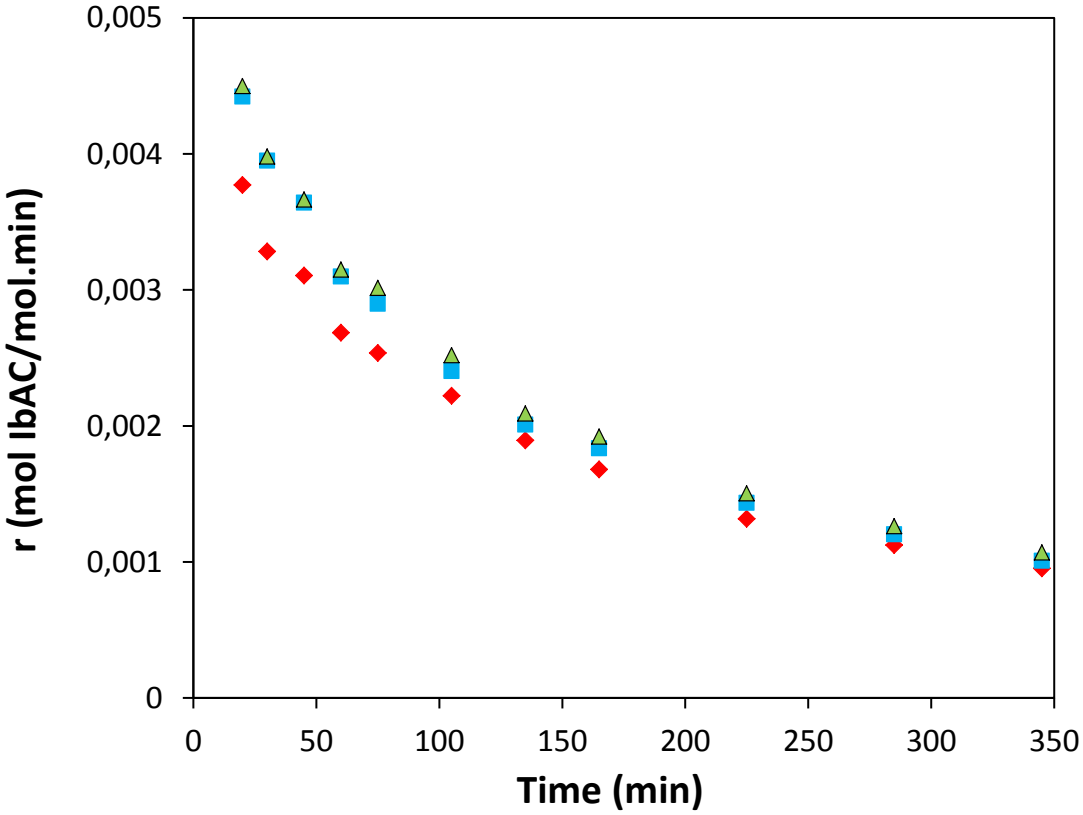

Figure B1. Esterification rate of reaction during experiments run at three different stirring rates (600, 800 ad 1000 RPM's). Feed molar ratio, 1:1; Temperature, 363.15 K; catalyst loading equivalent to sulfuric acid at 0.75% wt. (♦) 600 RPM. (■) 800 RPM. (▲) 1000 RPM.

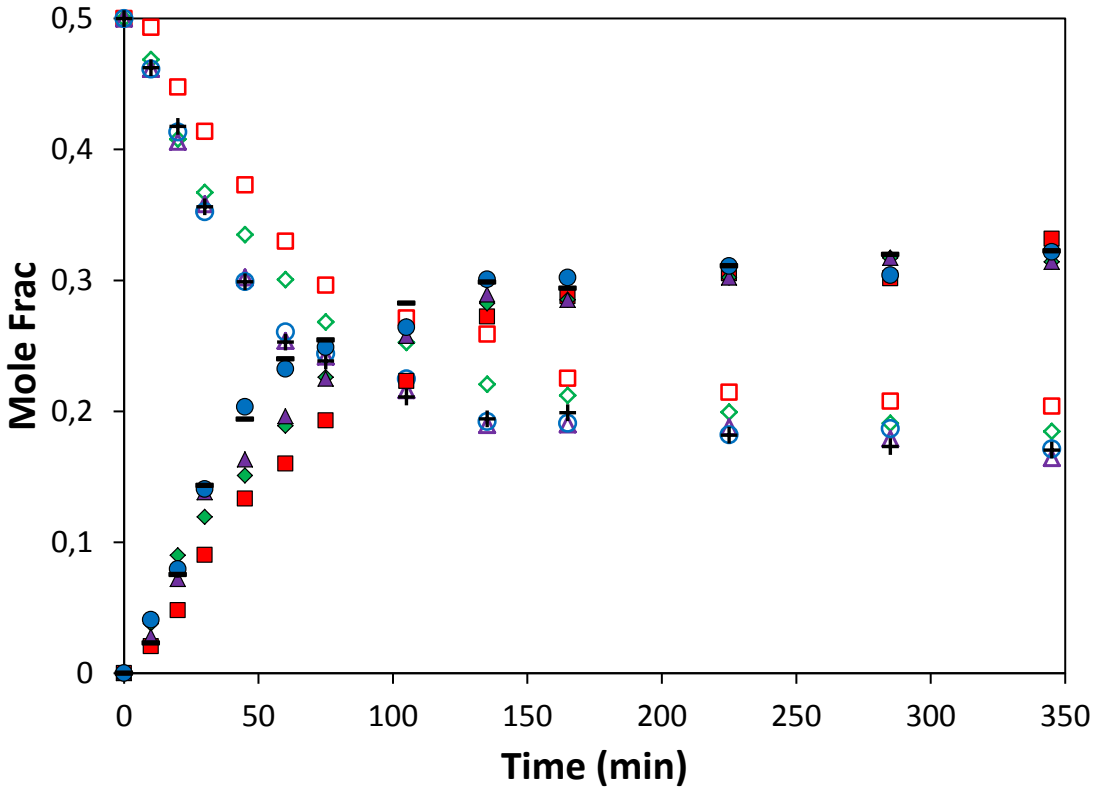

Figure B2. Esterification of acetic acid with Isobutanol using Amberlyst 15 as Catalyst, using different catalyst particle diameters (30, 40, 50, 60 and 100 MESH size). The reaction conditions where: Feed molar ratio, 1:1; Temperature, 363.15 K; Catalyst loading 0.75% wt. equivalent to Sulfuric Acid. (□) ACAC - 30 MESH. (◊) ACAC -40 MESH. (△) ACAC - 50 MESH. (○) ACAC - 60 MESH. (**+**) ACAC - 100 MESH. (■) IbAC - 30 MESH. (♦) IbAC - 40 MESH. (▲) ACAC - 50 MESH. (●) ACAC - 60 MESH. (**-**) ACAC - 100 MESH.

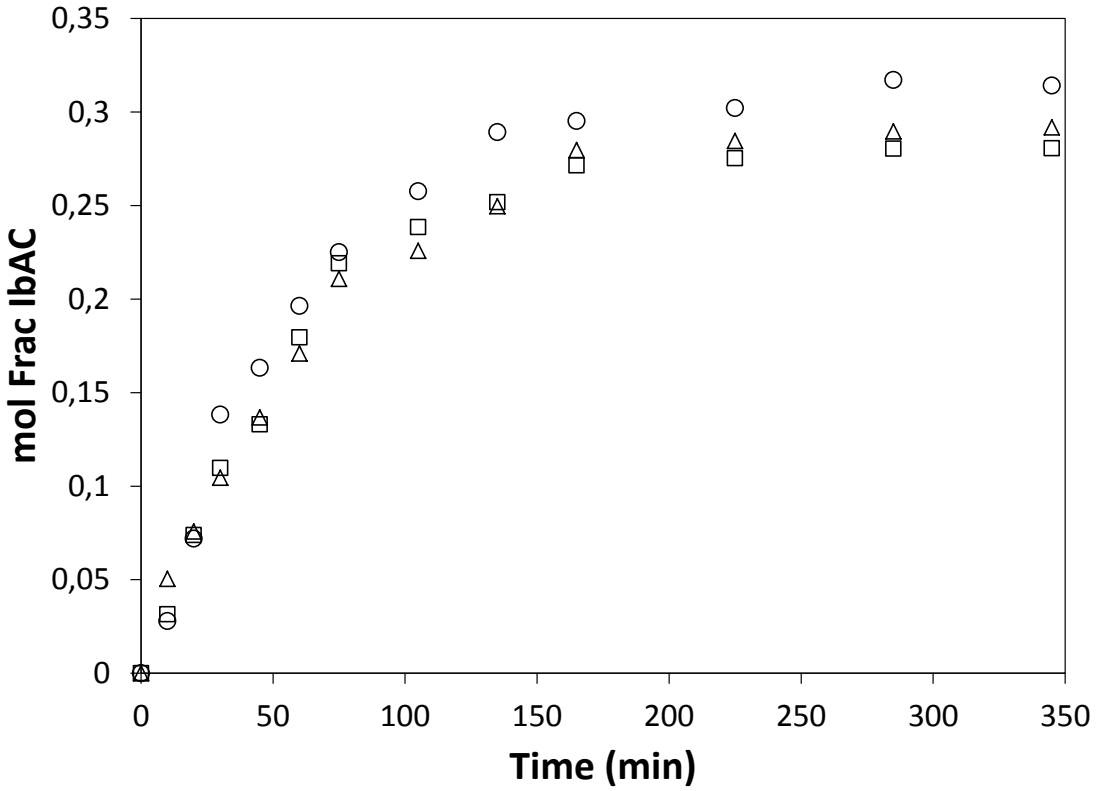

Figure B3. Esterification of acetic acid with Isobutanol using Amberlyst 15 as catalyst, at three different feed molar ratios (ACAC:OH 1:1; 2:1; 1:2). Temperature, 363.15 K; catalyst loading equivalent to sulfuric acid at 0.75% wt. (○) ACAC:IbOH - 1:1. (□) ACAC:IbOH - 2:1. (Δ) ACAC:IbOH - 1:2.

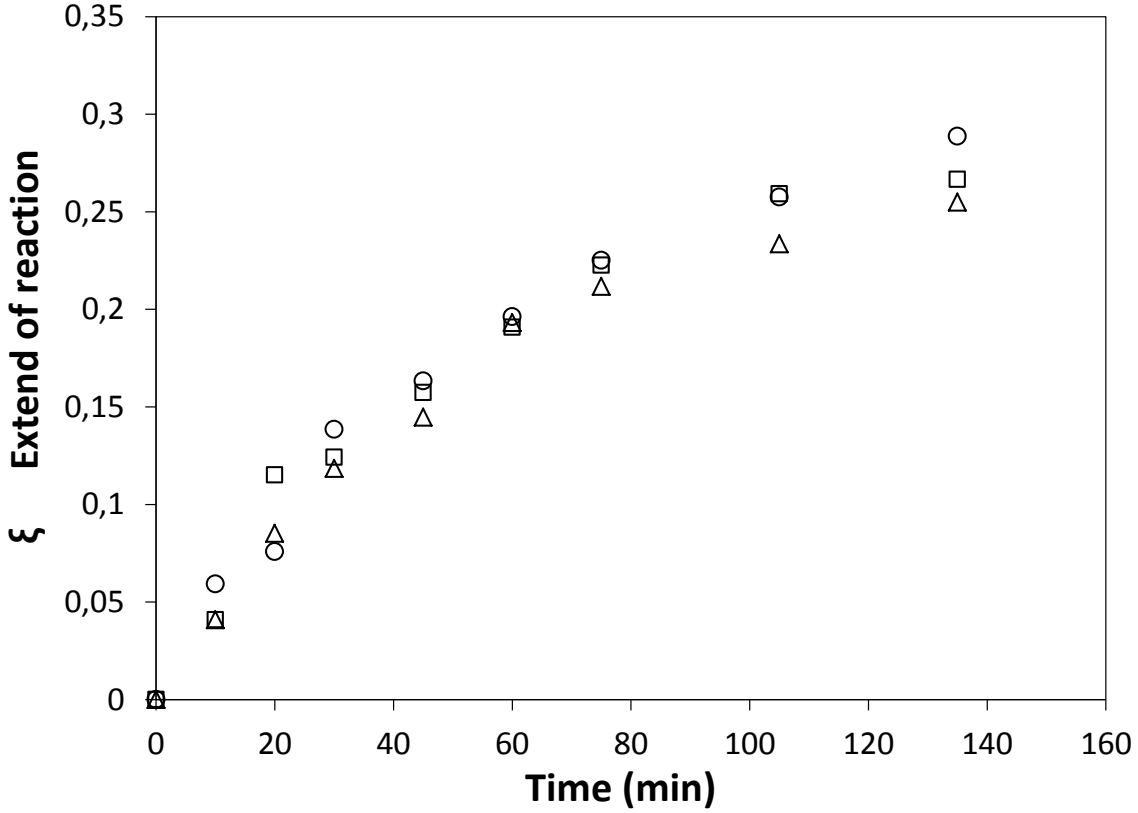

Figure B4. Extend of reaction in the esterification of acetic acid with Isobutanol using Amberlyst 15 as catalyst, at three different feed molar ratios (ACAC:OH 1:1; 2:1; 1:2). Temperature, 363.15 K; catalyst loading equivalent to sulfuric acid at 0.75% wt. (○) ACAC:IbOH - 1:1. (□) ACAC:IbOH - 2:1. (∆) ACAC:IbOH - 1:2.

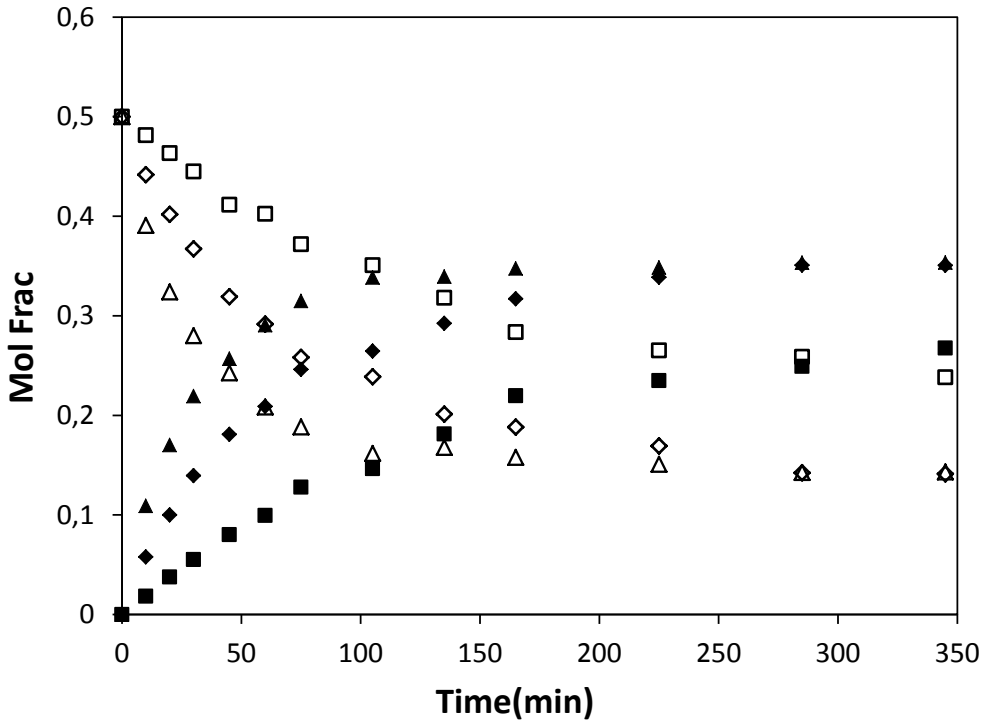

Figure B5. Esterification of acetic acid with Isobutanol using Amberlyst 15 as catalyst, at three different catalyst loadings equivalent to sulfuric acid at 0.25%, 0.75%, and 1.5% Wt. Feed molar ratio 1:1; Temperature, 363.15 K; (■) IbAC – 0.25%; (♦) IbAC – 0.75%; (▲) IbAC – 1.5%; (□) ACAC – 0.25%; (◊) ACAC – 0.75%; (Δ) ACAC – 1.5%.

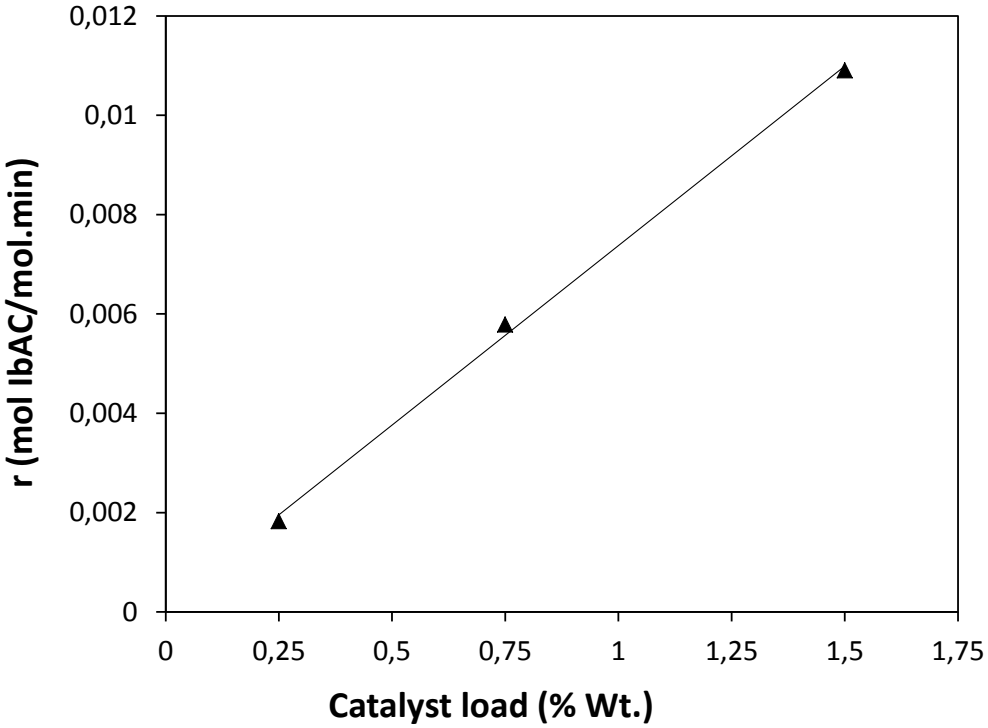

Figure B6. Reaction rate at ten minutes for reactions 1, 2 and 7. Feed molar ratio, 1:1; Temperature, 363.15 K.

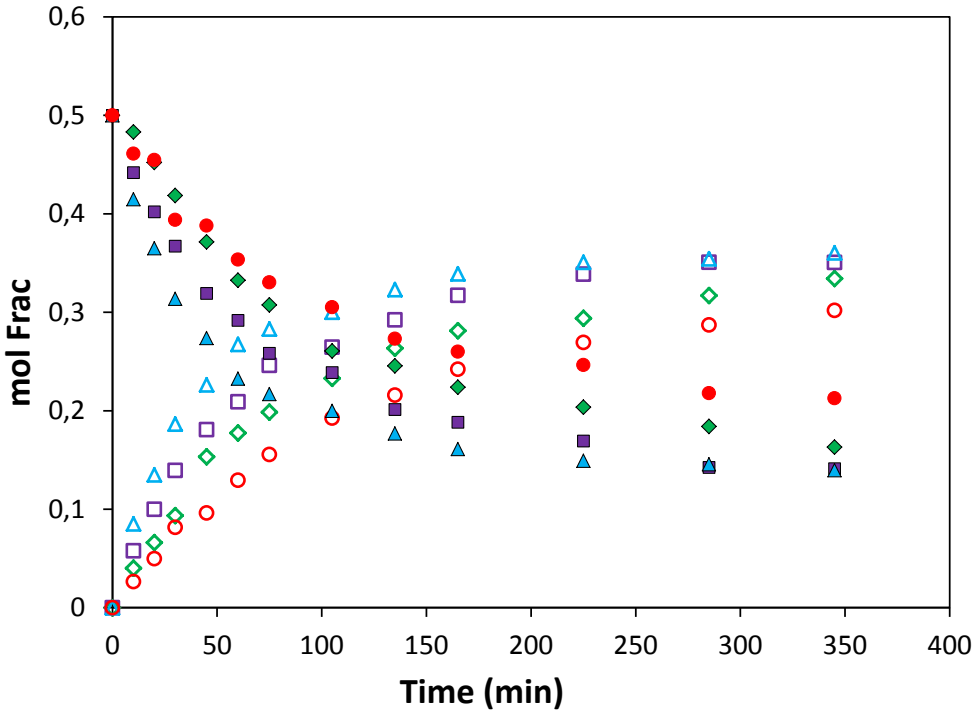

Figure B7. Esterification of acetic acid with Isobutanol using Amberlyst 15 as catalyst, at four different Temperatures (343.15 K; 353.15 K; 363.15 K; 373.15 K). Molar feed ratio, 1:1; Catalyst loading equivalent to sulfuric acid at 0.75% wt.; Filled markers ACAC at (●) 343.15K; (♦) 353.15 K; (■) 363.15 K; (▲) 373.15 K. Void markers IbAC at (○) 343.25 K; (◊) 353.15 K; (□) 363.15 K; (△) 373.15 K.

In the following plots are presented the kinetic profiles obtained during the whole set of experiments of Table S3, and the corresponding model adjustment.

Exp 1.

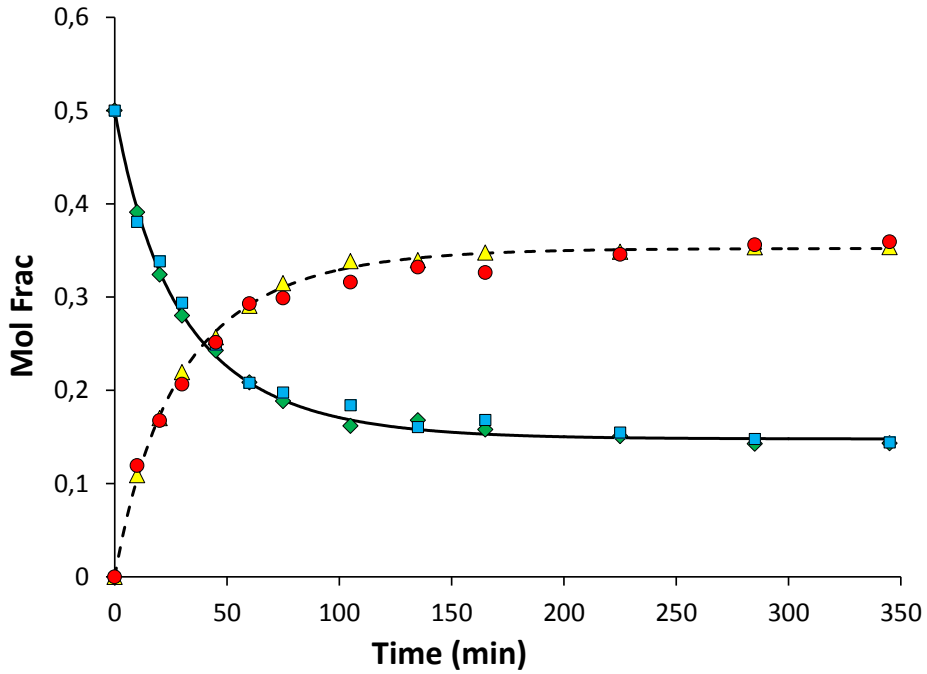

Figure B8. Esterification of acetic acid with Isobutanol using Amberlyst 15 as catalyst. Temperature, 363.15K; Feed molar ratio, 1:1; catalyst loading equivalent to sulfuric acid at 1.5% wt.; (♦) exp ACAC; (■) exp. IbOH; (▲) exp. IbAC; (●) exp. W; (—) Model ACAC/IbOH; (---) Model IbAC/W.

Exp.2

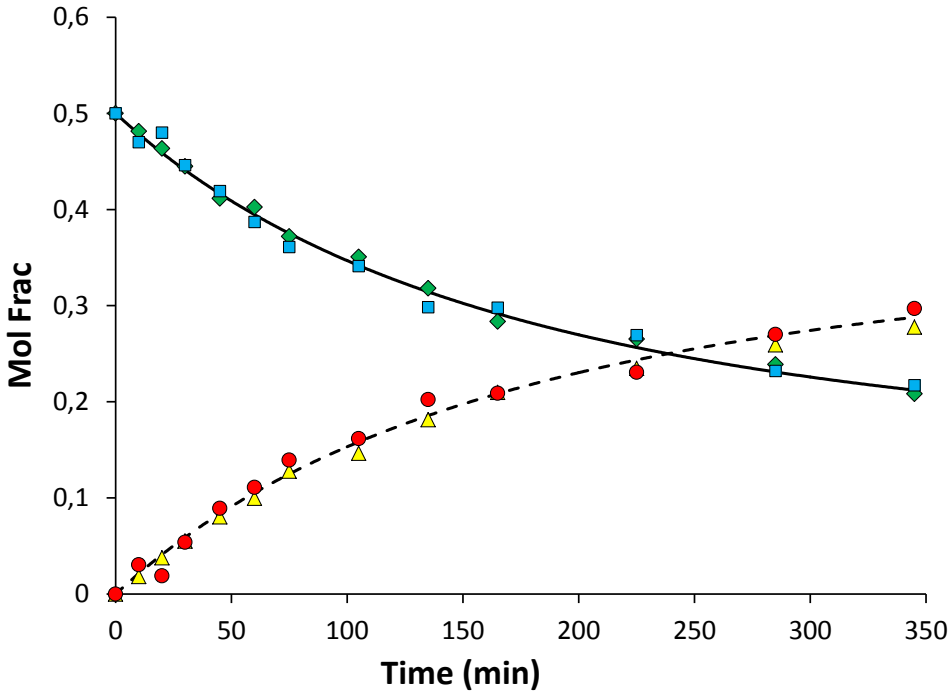

Figure B9. Esterification of acetic acid with Isobutanol using Amberlyst 15 as catalyst. Temperature, 363.15K; Feed molar ratio, 1:1; catalyst loading equivalent to sulfuric acid at 0.25% wt.; (♦) exp ACAC; (■) exp. IbOH; (▲) exp. IbAC; (●) exp. W; (—) Model ACAC/IbOH; (---) Model IbAC/W.

Exp. 3

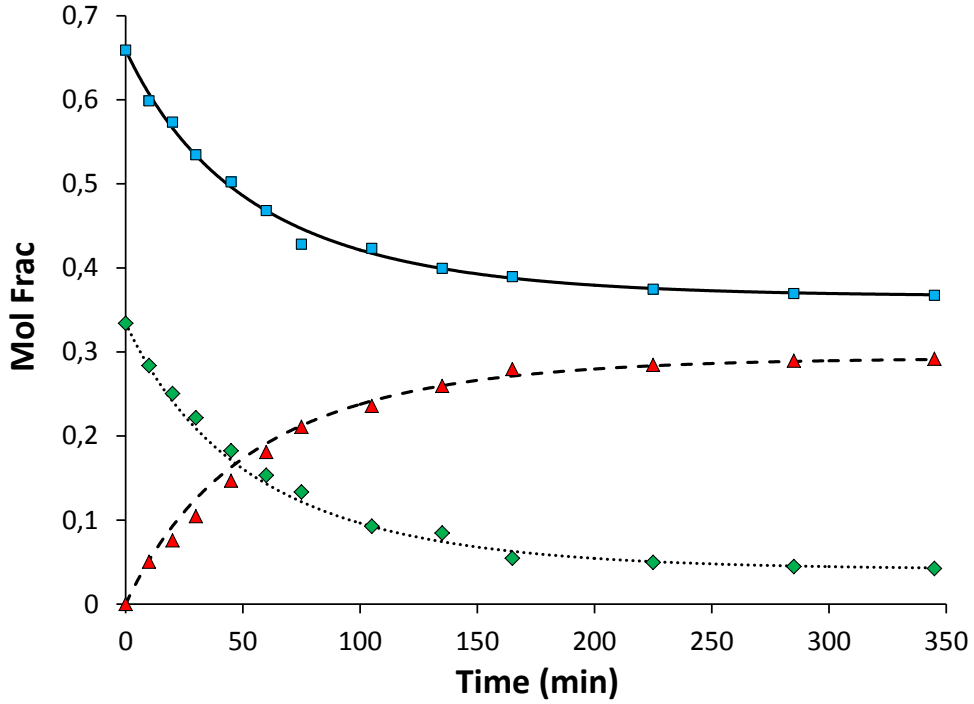

Figure B10. Esterification of acetic acid with Isobutanol using Amberlyst 15 as catalyst. Temperature, 363.15K; Feed molar ratio Acid:alcohol 1:2; catalyst loading equivalent to sulfuric acid at 0.75% wt.; (♦) exp ACAC; (■) exp. IbOH; (▲) exp. IbAC; (—) Model ACAC; (•••) Model IbOH; (---) Model IbAC/W.

Exp.4

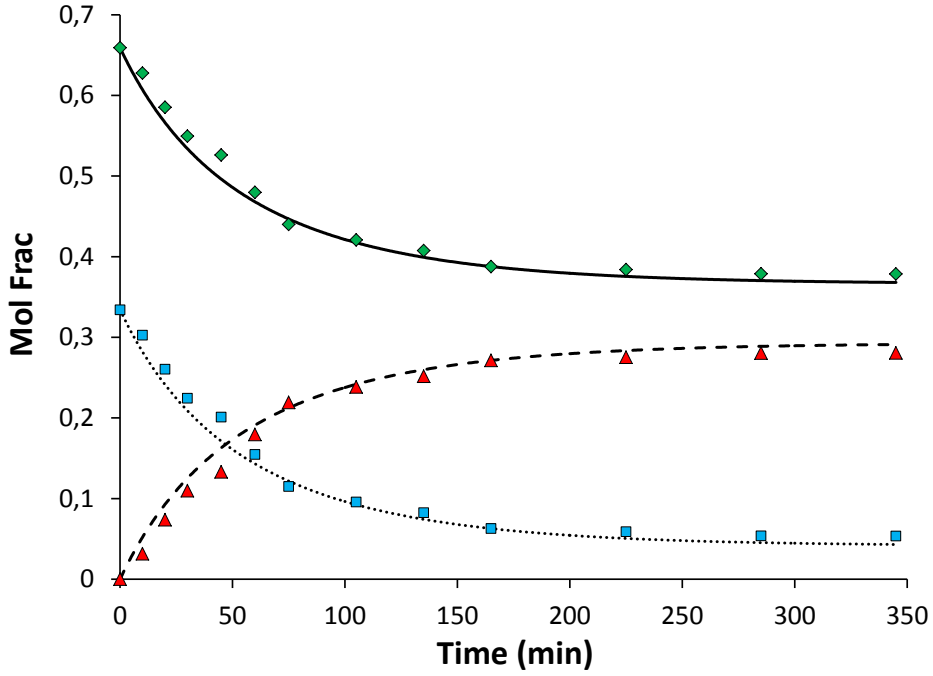

Figure B11. Esterification of acetic acid with Isobutanol using Amberlyst 15 as catalyst. Temperature, 363.15K; Feed molar ratio acid:alcohol 2:1; catalyst loading equivalent to sulfuric acid at 0.75% wt.; (♦) exp ACAC; (■) exp. IbOH; (▲) exp. IbAC; (—) Model ACAC; (•••) Model IbOH; (---) Model IbAC/W.

Exp. 5

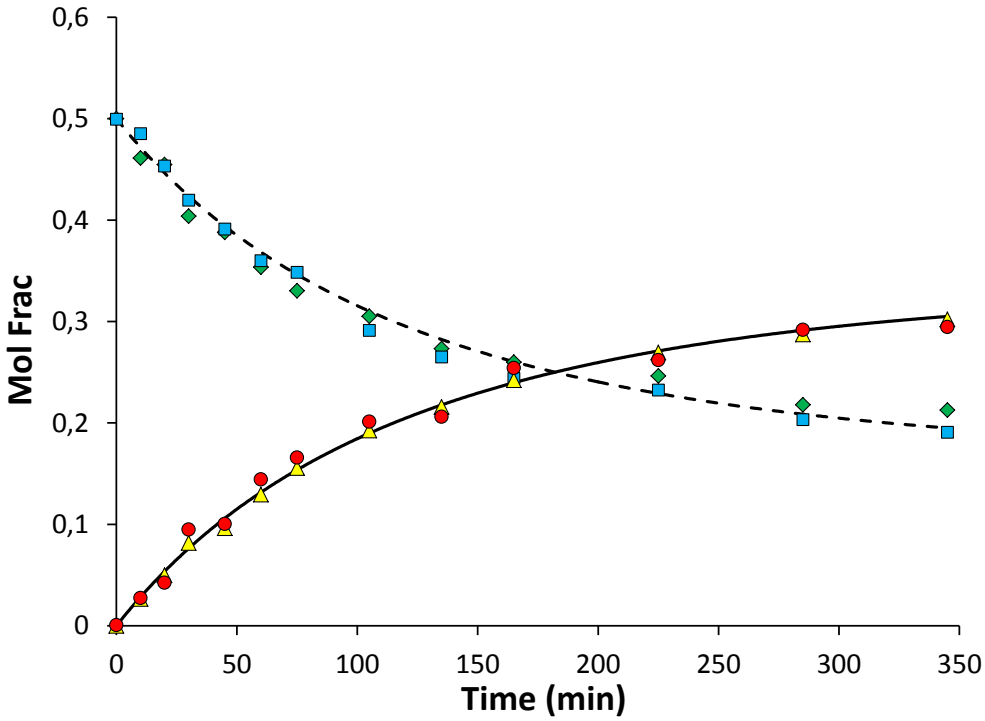

Figure B12. Esterification of acetic acid with Isobutanol using Amberlyst 15 as catalyst. Temperature, 343.15K; Feed molar ratio, 1:1; catalyst loading equivalent to sulfuric acid at 0.75% wt.; (♦) exp ACAC; (■) exp. IbOH; (▲) exp. IbAC; (●) exp. W; (—) Model ACAC/IbOH; (---) Model IbAC/W.

Exp. 6

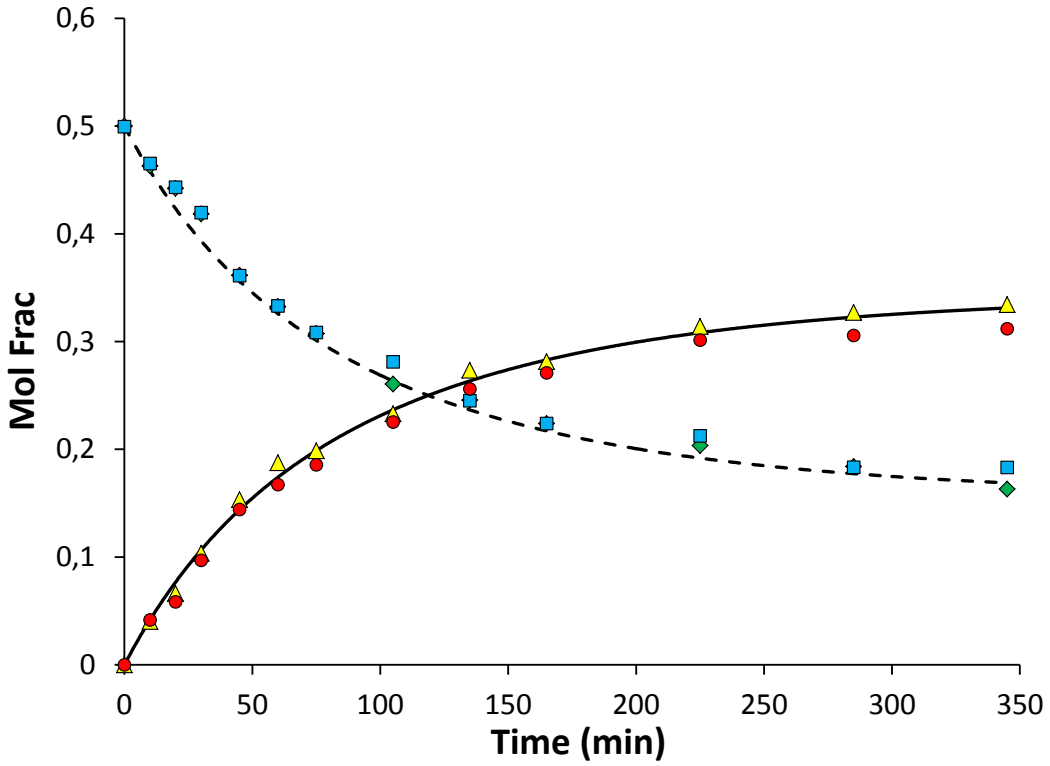

Figure B13. Esterification of acetic acid with Isobutanol using Amberlyst 15 as catalyst. Temperature, 353.15K; Feed molar ratio, 1:1; catalyst loading equivalent to sulfuric acid at 0.75% wt.; (♦) exp ACAC; (■) exp. IbOH; (▲) exp. IbAC; (●) exp. W; (—) Model ACAC/IbOH; (---) Model IbAC/W.

Exp. 7

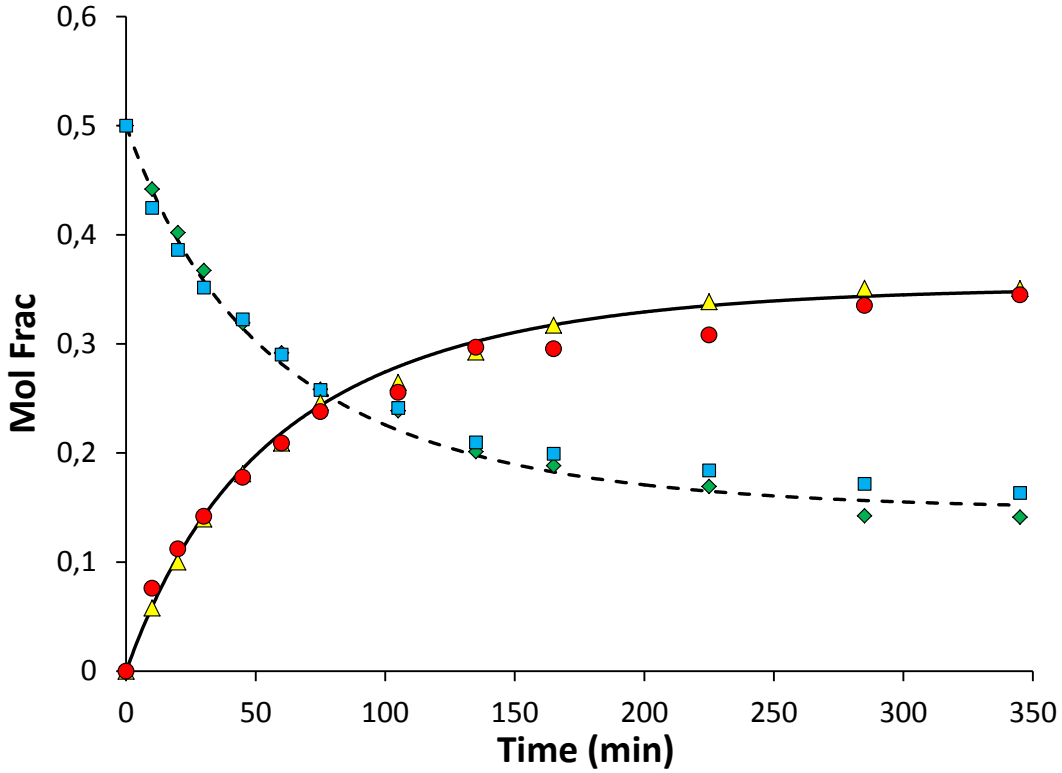

Figure B14. Esterification of acetic acid with Isobutanol using Amberlyst 15 as catalyst. Temperature, 363.15K; Feed molar ratio, 1:1; catalyst load equivalent to sulfuric acid at 0.75% wt.; (♦) exp ACAC; (■) exp. IbOH; (▲) exp. IbAC; (●) exp. W; (—) Model ACAC/IbOH; (---) Model IbAC/W.

Exp. 8

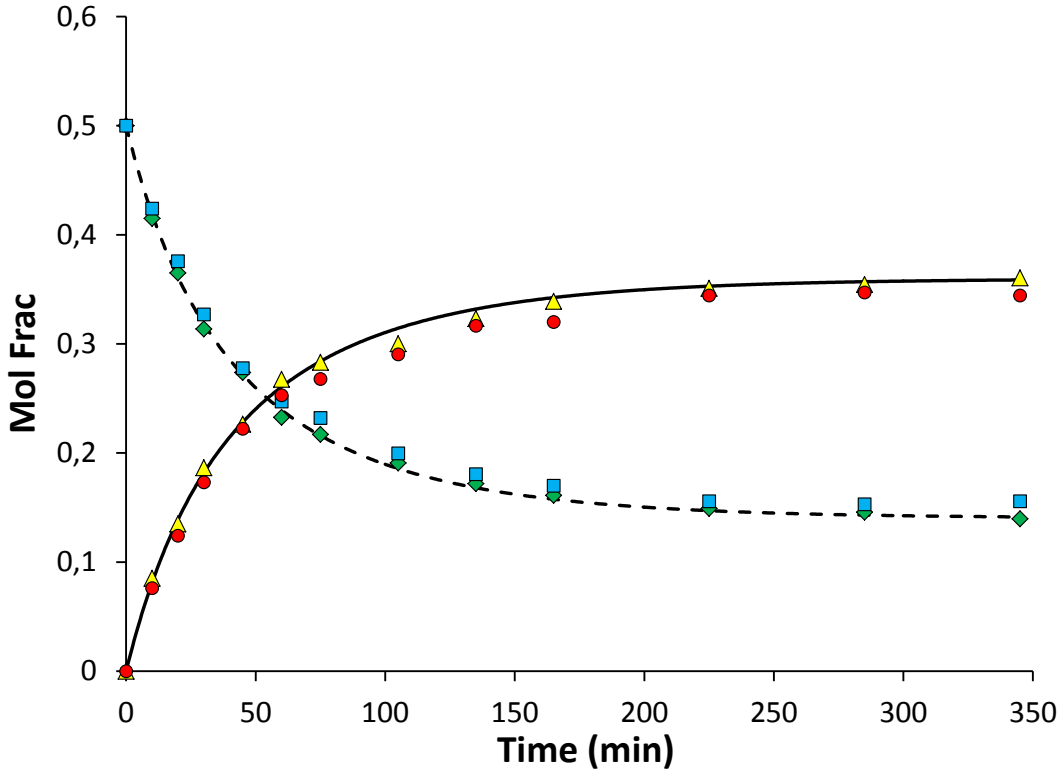

Figure B15. Esterification of acetic acid with Isobutanol using Amberlyst 15 as catalyst. Temperature, 373.15K; Feed molar ratio, 1:1; catalyst loading equivalent to sulfuric acid at 0.75% wt.; (♦) exp ACAC; (■) exp. IbOH; (▲) exp. IbAC; (●) exp. W; (─) Model ACAC/IbOH; (---) Model IbAC/W.

7. Annexes C.

Isobutyl acetate by reactive distillation. Conceptual design and simulation

NRTL-HOC-Antoine Parameters

$$ln(\gamma_{ij}) = \frac{\sum_{j=1}^{n} x_j \tau_{ji} G_{ji}}{\sum_{k=1}^{n} x_k G_{ki}} + \sum_{j=1}^{n} \frac{x_j G_{ij}}{\sum_{k=1}^{n} x_k G_{kj}} \left(\tau_{ij} - \frac{\sum_{m=1}^{n} x_m \tau_{mj} G_{mj}}{\sum_{k=1}^{n} x_k G_{kj}} \right)$$

$$\tau_{ij} = A_{ij} + \frac{B_{ij}}{T}$$

$$G_{ij} = \exp(-\alpha_{ij} \tau_{ij})$$

Table C1. Reported binary interaction parameters of NRTL equation [1].

Component		Binary interaction parameters				
i	j	A_{ij}	A_{ji}	B_{ij} (K)	B_{ji} (K)	$C_{ij} = \alpha_{ij}$
ACAC	IbOH	7.20005	-4.43801	-2195.15	1366.33	0.47
ACAC	IbAC	1.8059	-0.9455	-666.5556	584.0002	0.3
IbOH	IbAC	-2.7472	-0.0272	1099.7379	74.6936	0.3
IbOH	W	-1.74621	0.97442	667.127	875.726	0.357937
IbAC	W	-2.2213	8.8038	1012.1378	-866.8213	0.2
ACAC	W	-1.9763	3.3293	609.8886	-723.888.1	0.3

Table C2: Reported solvation and association parameters for HOC equation [1]

	Acetic acid	Isobutanol	Water	Isobutyl acetate
Acetic acid	4.5	2.5	2.5	2
Isobutanol	-	1.9	1.55	1.3
Water	-		1.7	1.3
Isobutyl acetate	-	-	-	0.53

Table C3. Reported Antoine parameters for vapor pressure calculation of pure components* [1]

Parameter**	Component			
	ACAC	**IbOH**	**H_2O**	**IbAC**
C_1	53.27	121.78	73.649	72.31
C_2	-6304.5	-10504	-7258.2	-6944.3
C_3	0	0		
C_4	0	0		
C_5	-4.2985	-13.921	-7.3037	-7.298
C_6	8.8865E-18	1.6898E-17	4.1653E-06	3.7892E-06
C_7	6	6	2	2

* $\ln(P) = C_1 + \frac{C_2}{T+C_3} + C_4 T + C_5 \ln(T) + C_6 T^{C_7}$ (P in N/m^2, T in K)

** Taken from Aspen Plus V.10 Databank.

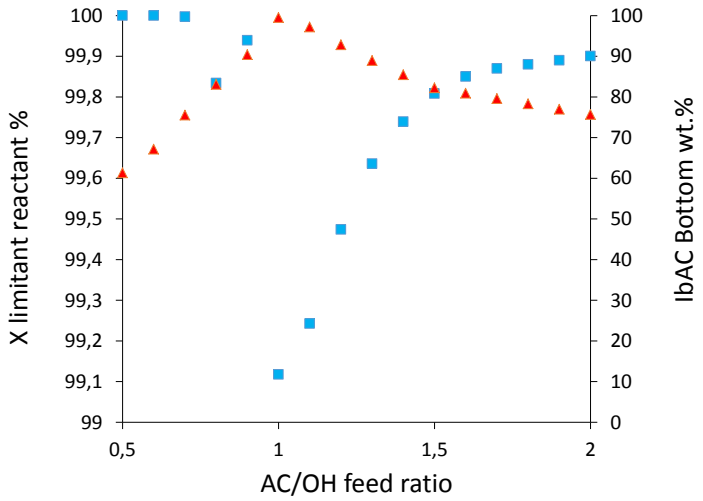

Figure C1. Effect of reactant molar ratio. (■) limiting reactant conversion, (▲) IbAC mass fraction in the bottom stream**.**

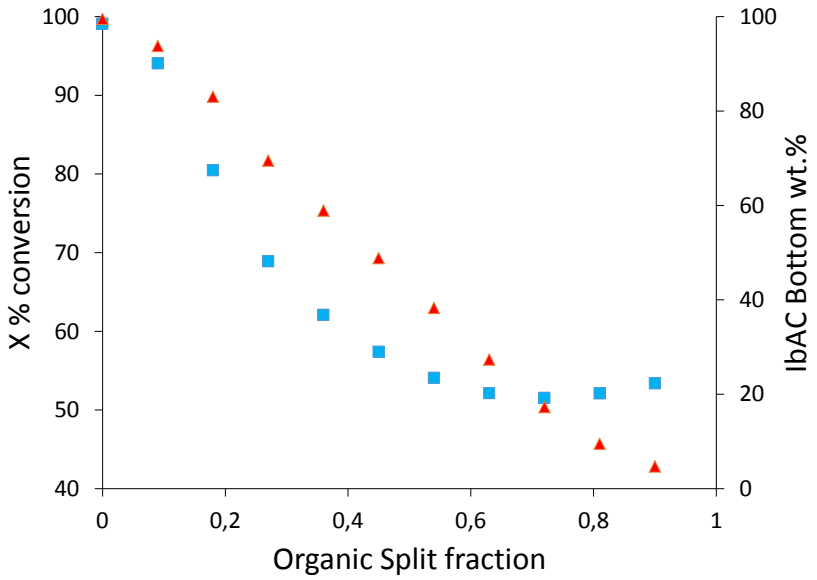

Figure C2. Effect of the organic stream split fraction. (■) conversion, (▲) IbAC mass fraction in the bottom stream**.**

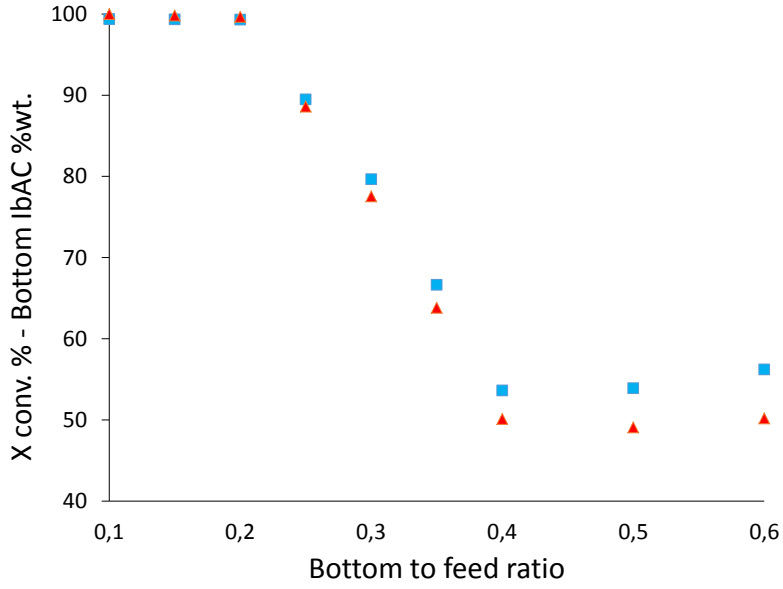

Figure C3. Effect of bottom to feed ratio. (■) conversion, (▲) IbAC mass fraction in the bottom stream**.**

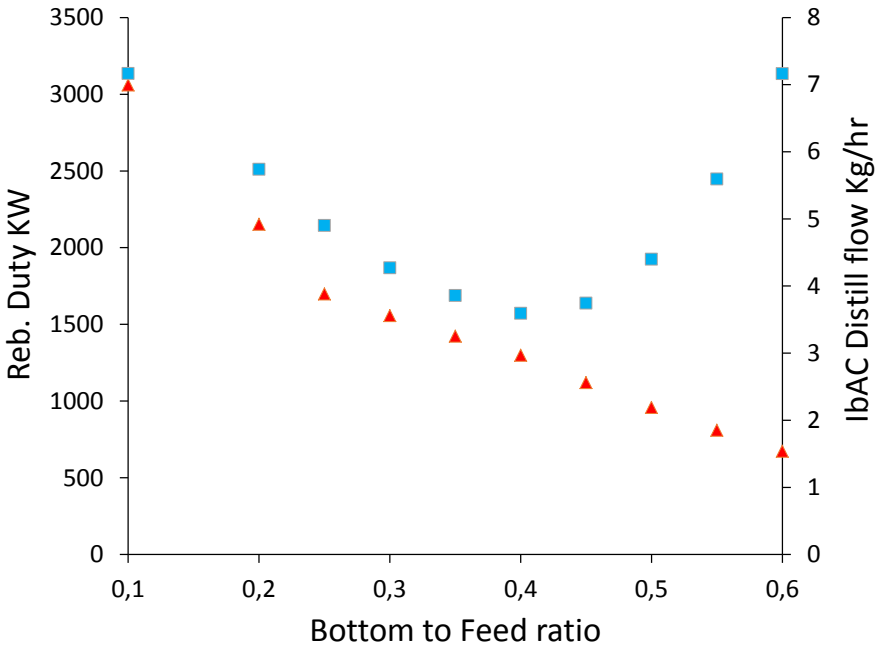

Figure C4. Effect of bottom to feed ratio. (▲) Reboiler heat duty (kW), (■) IbAC mass flow in the distillate stream**.**

7.1. References

1. Martinez, A.F., Sanchez, C.A., Orjuela, A., Rodriguez, G. 2020. Isobutyl acetate production by reactive distillation. Non-reactive phase equilibrium and topological analysis. Fluid Phase Equilibr. 516: 112612. DOI: 10.1016/j.fluid.2020.112612